IS-T--1412

DE91 018168

Received
SEP 0 9

# Reduced Molybdenum Oxidation States in Hydrodesulfurization Catalysis by Chevrel Phases

by Mark Eugene Ekman

PHD thesis submitted to Iowa State University

Ames Laboratory, U. S. DOE

Iowa State University

Ames, Iowa 50011

Date Transmitted: July 1991

Prepared for the U. S. Department of Energy

Under contract no. W-7405-eng-82.

MASTER

DISTRIBUTION OF THIS DOCUMENT IS UNLIMITED

DISCLAIMER

This report was prepared as an account of work sponsored by an agency of the United States Government. Neither the United States Government nor any agency thereof, nor any of their employees, makes any warranty, express or implied, or assumes any legal liability or responsibility for the accuracy, completeness, or usefulness of any information, apparatus, product, or process disclosed, or represents that its use would not infringe privately owned rights. Reference herein to any specific commercial product, process, or service by trade name, trademark, manufacturer, or otherwise does not necessarily constitute or imply its endorsement, recommendation, or favoring by the United States Government or any agency thereof. The views and opinions of authors expressed herein do not necessarily state or reflect those of the United States Government or any agency thereof.

DISCLAIMER

Portions of this document may be illegible in electronic image products. Images are produced from the best available original document.

# DISCLAIMER

This report was prepared as an account of work sponsored by an agency of the United States Government. Neither the United States Government nor any agency thereof, nor any of their employees, makes any warranty, express or implied, or assumes any legal liability or responsibility for the accuracy, completeness or usefulness of any information, apparatus, product, or process disclosed, or represents that its use would not infringe privately owned rights. Reference herein to any specific commercial product, process, or service by trade name, trademark, manufacturer, or otherwise, does not necessarily constitute or imply its endorsement, recommendation, or favoring by the United States Government or any agency thereof. The views and opinions of authors expressed herein do not necessarily state or reflect those of the United States Government or any agency thereof.

This report has been reproduced directly from the best available copy.

AVAILABILITY:

To DOE and DOE contractors: Office of Scientific and Technical Information
P.O. Box 62
Oak Ridge, TN 37831

prices available from: (615) 576-8401
FTS: 626-8401

To the public: National Technical Information Service
U.S. Department of Commerce
5285 Port Royal Road
Springfield, VA 22161

# Reduced molybdenum oxidation states in hydrodesulfurization catalysis by Chevrel phases

Mark Eugene Ekman

Under the supervision of Glenn L. Schrader
From the Department of Chemical Engineering
Iowa State University

The catalytic activities of reduced (relative to $Mo^{4+}$) molybdenum sulfides, known as Chevrel phases, have been evaluated for thiophene and benzothiophene hydrodesulfurization (HDS) and 1-butene hydrogenation (HYD). These materials have been found to have HDS activities comparable to, or greater than, model unpromoted and cobalt-promoted $MoS_2$ catalysts; in contrast, Chevrel phases exhibit low activities for 1-butene HYD.

X-ray powder diffraction and laser Raman spectroscopy analysis of the used (10 hours of thiophene reaction) catalysts indicated that the bulk structures were stable under reaction conditions. XPS analysis demonstrated that reduced molybdenum oxidation states were present at the surface, compared to the $Mo^{4+}$ state of $MoS_2$ catalysts.

The effect of the oxidation state of molybdenum on the catalytic HDS of thiophene was investigated using a series of lead–lutetium Chevrel phases with compositions of $Lu_{1.2x}PbMo_6S_8$ for $0 \leq x \leq 0.2$, and $Lu_{1.2x}Pb_{1-x}Mo_6S_8$ for $0.2 < x \leq 1$. These same materials were used to evaluate the chemisorption of $O_2$ and NO as probe molecules of catalytically active sites. The maximum rate of thiophene

HDS was observed for catalysts having reduced formal oxidation states (compared to $MoS_2$). The chemisorption of $O_2$ and NO could be related to HDS activity and the formal oxidation state of molybdenum: the same reduced molybdenum species which exhibited the greatest activity for thiophene HDS also display the greatest uptake of $O_2$ and NO.

An infrared reflection–absorption spectroscopy (IRRAS) cell, capable of obtaining spectra under conditions ranging from atmospheric pressure to ultra-high vacuum conditions, was designed, assembled, and tested. A cosine-emitter gas doser was designed and evaluated by observing the response of a mass spectrometer to pulses of CO, He, and Kr. The analysis of a poly(methyl methacrylate) (PMMA) layer deposited with various thicknesses on a silicon–copper thin film structure was used to demonstrate the operation of the completed system. The gas doser was found to operate in an ''on/off'' manner without affecting the system background pressure. Comparable results to previous IRRAS studies were obtained for the analysis of the thin film structures, indicating the successful completion of the system.

# TABLE OF CONTENTS

# GENERAL INTRODUCTION

## Introduction

Hydroprocessing techniques for the removal of sulfur (hydrodesulfurization), nitrogen (hydrodenitrogenation), and metals (hydrodemetallization) from petroleum feedstocks, as well as liquids derived from coal, oil shale, and tar sands, have been of increasing importance ever since fossil fuels have been used as an energy source. More stringent environmental standards require reductions in the emission of sulfur and nitric oxides, produced by the combustion of sulfur- or nitrogen-containing fuels, which lead to the formation of acid rain. Other catalysts which are used in subsequent refining steps (*e.g.*, precious metals for catalytic reforming) are severely poisoned by sulfur and metals. In addition, shorter supplies of "clean" petroleum feedstocks have created the need to more efficiently process crude oil residua containing larger amounts of sulfur, nitrogen and metals.

Hydrodesulfurization (HDS) is among the most important applications of hydroprocessing [1]. In 1990, approximately 60.5 million barrels of oil per day were

refined worldwide [2], virtually all of which underwent HDS, making HDS one of the largest chemical processing techniques currently practiced.

HDS reactions are of the following type:

$$\text{organosulfur compound} + H_2 \longrightarrow \text{desulfurized products} + H_2S$$

HDS reactions are essentially irreversible under industrially applied conditions [1]. These conditions include temperatures ranging from 300 to 500°C and pressures of 30 to 200 atm. Catalysts based on transition metal sulfides are used. During HDS, extra hydrogen is consumed, due to hydrogenation (HYD) of unsaturated hydrocarbon products. This side reaction is undesirable since it leads to the loss of expensive hydrogen.

HDS technology for light petroleum feeds (low-boiling components) has been well established, with the major objectives being the improvement of the properties of gasoline formed in catalytic cracking, and the pretreatment of feedstocks for catalytic reforming to prevent poisoning of the sulfur-sensitive metals. HDS of heavier petroleum fractions (higher boiling components) is much more difficult and gives products such as diesel and jet fuels, heating oils, and residual fuel oils. The literature of HDS chemistry and technology has been extensively reviewed (*e.g.*, [1,3–19]).

Significant quantities of sulfur are present in petroleum and coal in varying amounts, depending on its source location. Petroleum contains between 0.05 to

6.0 wt% sulfur [20], while coal contains 0.4 to 5.3 wt% sulfur, of which 0.2 to 2.0% is organically bound sulfur [21]. Representative sulfur-containing organic compounds found in petroleum feeds are shown in Table 1, listed in approximate order of decreasing HDS activity [3]. The thiols and disulfides are more easily desulfurized than the thiophenic compounds. Thiophenic species comprise up to 84% of sulfur-containing compounds found in the middle and high boiling petroleum fractions [22]. Alternative fuel sources, such as coal, oil shale, and tar sands, contain thiophenic compounds as the predominant organosulfur species as well [23]. Accordingly, the thiophenic compounds, particularly thiophene, have been the most widely used organosulfur compounds in HDS investigations.

Commercial catalysts applied in HDS have evolved from those developed in Germany in the 1920's for the hydrogenation of coal and coal-derived liquids [3–4]. In early work, it was quickly discovered that cobalt (Co), nickel (Ni), molybdenum (Mo), and tungsten (W) sulfides and their mixtures were the "most active–least expensive" transition metal sulfides [24]. These catalysts are generally prepared from molybdenum (or tungsten) oxides supported on high surface area alumina ($\gamma$–$Al_2O_3$). The addition of cobalt (or nickel) to the molybdenum catalysts greatly enhances their catalytic activity; therefore, these metals are often referred to as promoters. Recently, the addition of a secondary promoter, such as phosphorus [25], has been reported to improve the catalyst activity and selectivity, and to provide greater strength and thermal stability to the alumina support [26–27].

Table 1. Common sulfur containing compounds in petroleum [3]

| Compound class | Structure |
|---|---|
| Thiols (mercaptans) | RSH |
| Disulfides | RSSR′ |
| Sulfides | RSR′ |
| Thiophenes | 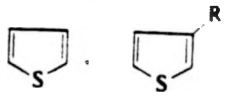 |
| Benzothiophenes | 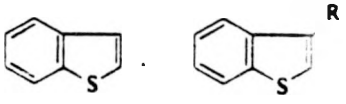 |
| Dibenzothiophenes | 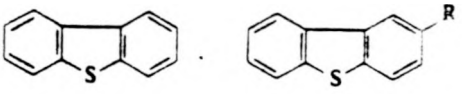 |
| Benzonaphthothiophenes | 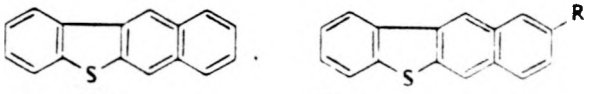 |
| Benzo[*def*]dibenzothiophenes | 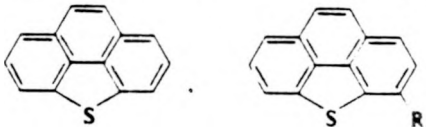 |

The oxidic precursor of the catalyst is transformed into the working HDS catalyst by a sulfiding procedure, which may consist of treatment in a mixture of $H_2$ and $H_2S$, $H_2$ and thiophene, or $H_2$ and a liquid feed of sulfur-containing molecules. These catalysts have been widely used for over 60 years, and are currently found in every refinery in the world [28]. Although these materials are best known for their HDS applications, they have also found use in hydrodenitrogenation (HDN),

hydrodeoxygenation (HDO), hydrodemetallization (HDM), the reaction of CO and $H_2$ to form alcohols, and emission control catalysis [19,28–29].

## Conventional HDS Catalysts

### $MoS_2$ phase

Industrial developments which have occurred in HDS catalysts have been based largely on trial and error experiments rather than on a fundamental understanding of the nature of the active phase and factors governing its formation [16]. Despite extensive research, it has been difficult to establish even the form in which the elements are present in the active state of HDS catalysts. However, there is general agreement in the literature that the operating catalyst is nearly completely sulfided to form a $MoS_2$ phase and sulfides of the promoter atoms. During sulfiding and actual HDS, the conditions are highly reducing with $H_2S$ always present. Thermodynamics predict that molybdenum should be present as $MoS_2$, cobalt as $Co_9S_8$, and nickel as $Ni_3S_2$ [19]. The presence of this $MoS_2$ phase has been demonstrated by various techniques such as X-ray photoelectron spectroscopy (XPS) [30–32], extended X-ray absorption fine structures (EXAFS) analysis [33–34], X-ray diffraction [35], and laser Raman spectroscopy [36].

The alumina support contributes no fundamental catalytic property to the system; its contribution has been described as allowing for a more effective use of metals (through dispersion) and ease of production and handling [28]. Therefore, unsupported

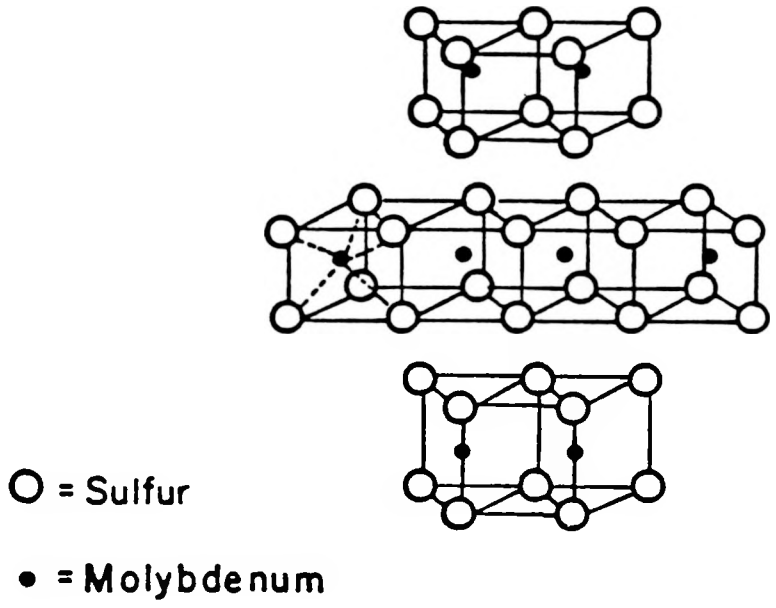


Figure 1. Structure of $MoS_2$

$MoS_2$–based catalysts have been investigated as more simple models of the complex supported materials. Unsupported $MoS_2$–based materials have been found to be active HDS catalysts and to exhibit properties similar to supported catalysts [9].

The anisotropic layer structure of $MoS_2$ is illustrated in Figure 1. Each molybdenum atom is coordinated to six sulfur atoms, which together form a centered trigonal prism. These prisms share edges, resulting in an infinite two dimensional layer. The layers are stacked and held together by weak van der Waals forces between the adjacent sulfur atoms of each layer. This arrangement provides for edge surfaces and basal plane surfaces with distinct geometries. The basal plane surface is a nearly close-

packed arrangement of sulfur atoms, while the edge planes expose both sulfur and molybdenum.

**Role of the promoter**

Information concerning the structure of the catalytically active phase incorporating the promoter has been more difficult to obtain. In the sulfidic form, cobalt may be present in tetrahedral sites in the $\gamma$–$Al_2O_3$ surface, as $Co_9S_8$ crystallites on the support, and as cobalt ions adsorbed onto the surface of $MoS_2$ crystallites (the Co–Mo–S phase) [37]. A schematic representation of the different forms in which cobalt ions can be present in a cobalt-promoted Mo/$\gamma$–$Al_2O_3$ catalyst is presented in Figure 2. Depending on the relative concentrations of cobalt and molybdenum [38] and on the pretreatment [39], a sulfided catalyst contains a relatively large amount of either $Co_9S_8$ or the Co–Mo–S phase.

Several models have been proposed for the active phase and structure of Co–Mo/$\gamma$–$Al_2O_3$ HDS catalysts. One of the first, the "monolayer" model, was conceived by Lipsch and Schuit [40], and has been refined by Schuit and Gates [41]. Its underlying feature is the supposed formation of an epitaxial monolayer of $MoO_3$ on the $\gamma$–$Al_2O_3$ surface. Cobalt promoter ions are present both in the $\gamma$–$Al_2O_3$ lattice and at the surface as $Co_3O_4$. Upon reduction and sulfidation, the ideal monolayer structure is supposed to remain intact, resulting in the formation of $Mo^{5+}$ sites. Subsequent sulfur removal leads to the formation of single and dual $Mo^{3+}$ sites, which are believed to be the active HDS centers.

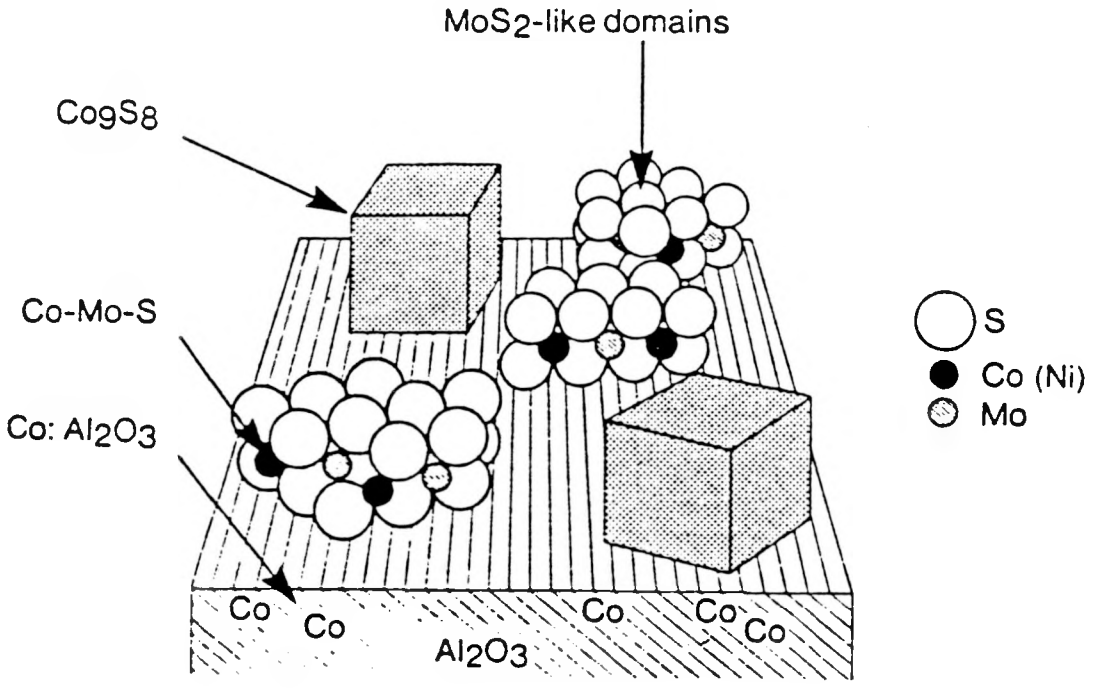


Figure 2. Schematic representation illustrating the different phases present on a typical cobalt-promoted alumina-supported catalyst [15]

In another model, the addition of promoters has been attributed to an increase in the number of molybdenum sites at the catalyst surface. By altering the texture of the catalyst, the promoter creates more active sites without being involved in the catalysis itself. This ''pseudo-intercalation'' or ''dissociation'' model was proposed by Voorhoeve and Stuiver [42] and extended by Farragher and Cossee [43]. Voorhoeve and Stuiver [42] proposed that nickel or cobalt atoms can be intercalated anywhere between alternating $MoS_2$ layers. Farragher and Cossee [43] suggested that the promoter is located only at the edges of the $MoS_2$ crystals, in between alternate layers of

$MoS_2$. The role of the promoter ions was thought to induce a surface reconstruction of the edges of the $MoS_2$ layers, leading to the exposure of single or dual $Mo^{3+}$ ions.

A different model has been proposed by Delmon [44]. In the ''contact synergy'' or ''remote control'' model, the promotional effect is due to two separate contacting sulfide phases, $Co_9S_8$ and $MoS_2$, thought to lead to a synergism in catalytic activity. The exact nature of this contact was not known. It has been suggested that spill-over hydrogen produced by $Co_9S_8$ would create reduced centers on the $MoS_2$ surface, creating the catalytically active sites [45]. This model is supported by the fact that a synergistic effect is also observed in mixtures of separate crystallites of $Co_9S_8$ and $MoS_2$ [46].

Topsøe *et al.* [37] have reported the existence of a cobalt–molybdenum–sulfide (Co–Mo–S) phase on both unsupported and supported cobalt-promoted HDS catalysts. This phase is believed to be the most catalytically significant phase present, based on a linear correlation between the amount of cobalt in the Co–Mo–S phase and thiophene HDS [38]. They concluded that the promoter ions are not located between $MoS_2$ layers (''pseudo-intercalation'' model), but in the $MoS_2$ layers in the plane of the molybdenum cations [47]. Therefore, the Co–Mo–S phase is considered to be a $MoS_2$-like material in which promoter atoms occupy crystallite edge positions [48].

Harris [49–50] and Harris and Chianelli [51–52] have proposed an ''electronic'' model for HDS catalysts based on SCF–X$\alpha$ scattered wave method molecular orbital calculations for $MS_6^{n-}$ ($M$ = first- and second-row transition metals) and $M'MoS_9^{n-}$

($M'$ = first-row transition-metal promoters V–Zn) clusters. They assumed that such complexes are representative of the environment of the metal cations at the catalyst surface. In their model, several electronic factors are related to catalytic activity, such as the number of electrons in the highest occupied molecular orbital (HOMO), the degree of covalency of the metal–sulfur bond, and the metal–sulfur bond strength. These factors were incorporated into an activity parameter, $A_2$, shown to correlate with dibenzothiophene HDS. Their calculations indicate that promoters, such as cobalt or nickel, donate electrons to molybdenum, reducing the formal oxidation state of molybdenum relative to $Mo^{4+}$ in $MoS_2$. Copper, a metal which poisons the activity of $MoS_2$-based catalysts, formally oxidizes molybdenum relative to $Mo^{4+}$. These relationships are illustrated in Figure 3.

A completely different model was proposed by Prins *et al.* [53–55]. They observed that cobalt and nickel sulfides supported on carbon exhibited higher thiophene HDS activities than that of carbon-supported $MoS_2$. They suggested that cobalt or nickel sulfide might act as the catalyst instead of as the promoter. Accordingly, $MoS_2$ should be regarded as a support for the cobalt sulfide phase, enabling the cobalt sulfide to be optimally dispersed. Enhanced activity due to the addition of phosphorus as a secondary promoter has also been explained as increased dispersion of the cobalt phase [56–57].

In summary, most models proposed can explain many of the reported experimental results, but no one model is consistent with all the experimental evidence

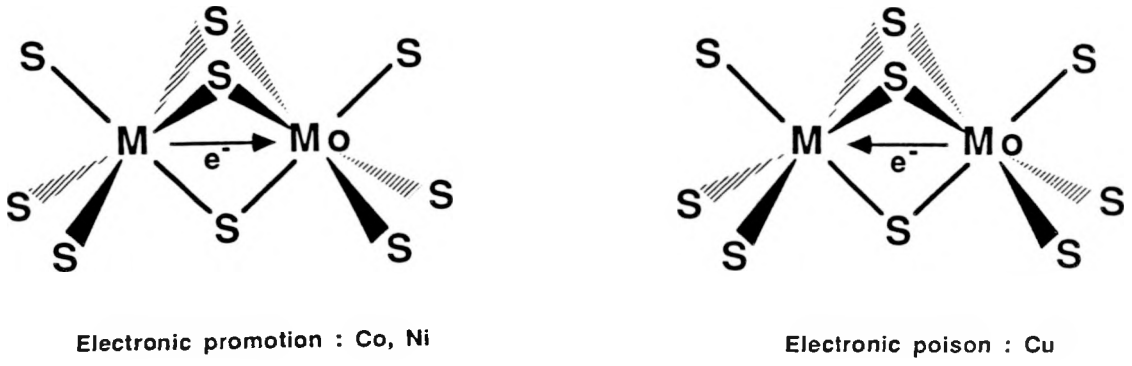


Figure 3. Schematic representation of electron transfer associated with promotion by Co and Ni or poisoning by Cu [28]

found in the literature. This situation exists because there is a lack of conclusive evidence regarding the degree of dispersion of the $MoS_2$ phase or knowledge of the precise promoter concentration at the interface of the $MoS_2$ surface [28]. However, there is general (but not unanimous) agreement that promotion requires interaction between molybdenum (or tungsten) 4*d* electrons and cobalt (or nickel) 3*d* electrons, which result in a net charge transfer and an increase in the number of electrons in the HOMO of $MoS_2$. This results in either an active site which is more active than an

unpromoted site (electronic promotion), or the stabilization of more active sites (structural promotion) [28].

**Active sites**

The precise nature of the catalytically active sites is not known. However, it is generally believed that coordinatively unsaturated sites (CUS), created by the introduction of anion (sulfur) vacancies on molybdenum ions during reduction and sulfidation, are the active sites for HDS [42,58–59]; and that these sites may be titrated by the use of suitable probe molecules.

Tauster *et al.* [60] reported that the chemisorption of $O_2$ varied linearly with HDS activity for unsupported $MoS_2$ catalysts. Based on these results, they proposed that $O_2$ selectively titrated the catalytically active HDS sites. Since then, the use of $O_2$ and other probe molecules (*e.g.*, NO and CO) have been extensively investigated.

The literature does not provide a universal relationship between chemisorption data and catalytic activity; nor does it specify the nature of the adsorption or catalytically active sites. However, it has been established that probe molecules, such as $O_2$, NO, or CO, titrate only a small fraction (approximately 5–10%) of the total available molybdenum CUS [61]. Based on the low degree of catalyst surface coverage by probe molecules, it has been proposed that only a select group of surface molybdenum CUS with some special properties are able to chemisorb suitable probe molecules. These properties are thought to include, among others, the oxidation state of molybdenum [61].

Studies of the chemisorption of $O_2$ and NO on reduced and sulfided supported molybdenum catalysts were interpreted by Hall *et al.* [62–64] as adsorption on $Mo^{2+}$ centers. Related investigations of the chemisorption of $O_2$, NO, and CO on unpromoted and promoted HDS catalysts have also resulted in the postulation that reduced molybdenum species (relative to $Mo^{4+}$) are responsible as the catalytically active sites for HDS reactions (*e.g.*, [65–67]).

Other analytical methods have detected the presence of catalytically important reduced molybdenum oxidation states as well. Techniques such as XPS [68–71], EXAFS [72], and electron paramagnetic resonance (EPR) [73–75] have detected the presence of molybdenum species more deeply reduced than $Mo^{4+}$, and have associated these reduced species with the catalytically active HDS sites.

In addition to the molecular orbital calculations of Harris [49–50] and Harris and Chianelli [51–52] discussed above, Duben [76] has provided theoretical support indicating that reduced molybdenum oxidation states are involved as the active sites in HDS catalysts. Using simple Hückel theory, he concluded that $Mo^{3+}$ would be the most effective molybdenum species for carbon–sulfur bond breaking and for easy removal of the surface bound sulfur atom required to regenerate the active site.

Despite intensive research efforts, the complexity of typical industrial HDS catalysts, and even the uncertainties associated with unsupported $MoS_2$-based materials, has made identification of catalytically important reduced molybdenum species difficult. Due to the presence of a large amount of $MoS_2$ (or related phases with predominantly

$Mo^{4+}$ oxidation states) in these catalysts, the role of more highly reduced molybdenum has been difficult to establish. In addition, the extent to which the molybdenum chemistry can be altered is limited by the abundance of $MoS_2$.

## Chevrel Phases

### Introduction

Recently, the catalytic properties of reduced (relative to $Mo^{4+}$) molybdenum chalcogenides, known as Chevrel phases, have been reported [77–85]. Chevrel phases have been shown to have thiophene and benzothiophene HDS activities comparable to, or greater than, model $MoS_2$ or Co–Mo–S catalysts. In addition, these materials have exhibited very low activity for 1-butene HYD and for the formation of cracking products, making them rather selective catalysts.

Chevrel *et al.* [86] reported the initial synthesis and characterization of this now extensive class of materials. A significant amount of experimental and theoretical work has been devoted to these materials in an attempt to understand their unusual superconducting properties. Comprehensive reviews of Chevrel phases have been provided [87–94].

Chevrel phases have the general formula $M_xMo_6Z_8$ ($M$ = ternary metal; $Z$ = sulfur, selenium, or tellurium; $0 \leq x \leq 4$). The ternary metal $M$ can be any of approximately 40 different metals. In addition, it is possible to partially substitute Nb, Ta, Re, Ru, or Rh for molybdenum, and to partially replace the chalcogen with Cl, Br,

I, or O. When *M* is a large cation, such as Pb or Sn, a second component, such as a rare earth (*RE*) metal, may be incorporated to produce a series of compounds with nominal formulas $RE_xM_{1-x}Mo_6Z_8$.

The Chevrel phases are often grouped into classes according to their structural properties, most notably the size of the ternary metal cation. "Small" cation (*e.g.*, Cu, Ni, Co) compounds exhibit a range of continuously varying concentration of the ternary metal, within specific limits (*e.g.*, $1.5 \leq x \leq 4.0$ for $Cu_xMo_6S_8$). For "large" cation (*e.g.*, Pb, Sn, *RE*) materials, there is very little to no concentration range of the ternary metal. These materials are referred to as small and large cation compounds, respectively.

**Chevrel phase structure**

The structural basis of the Chevrel phases is the $Mo_6Z_8$ building block or cluster. This cluster consists of a distorted octahedron of tightly packed molybdenum atoms elongated along the ternary axis, surrounded by a slightly distorted chalcogen cube. These building blocks are interconnected by short, covalent molybdenum–chalcogen bonds to form structures with rhombohedral or triclinic geometries. Each unit is bonded to six other units through these bonds, resulting in a highly stable structure.

This arrangement of the $Mo_6Z_8$ units leaves a certain number of cavities within the chalcogen atom network. The largest of these is approximately cube shaped and is formed by eight chalcogen atoms belonging to eight different $Mo_6Z_8$ units. This cavity

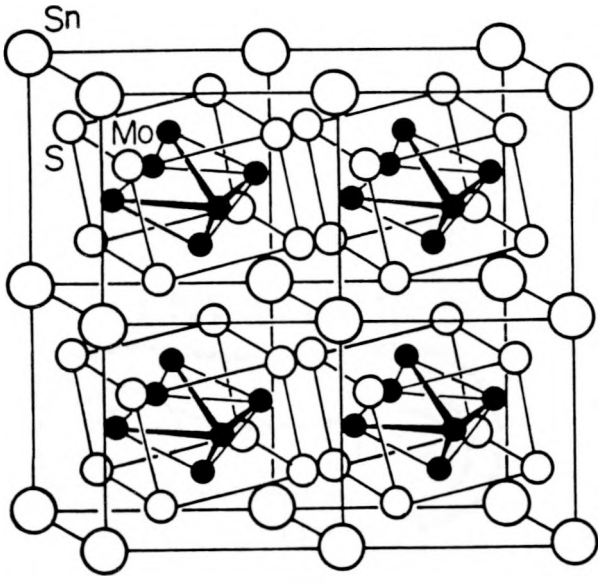


Figure 4. The large cation Chevrel phase structure of $SnMo_6S_8$ [91]

is situated at the origin of the rhombohedral unit cell. Smaller, more irregularly shaped holes are also found within the structure. These cavities are all interconnected and form infinite channels in the form of "zig-zag" chains running in the directions of the rhombohedral axes. Large cations occupy exclusively the large hole at the origin and yield a stoichiometric compound ($x \approx 1$). Small cations simultaneously occupy the small interstices also and lead to a nonstoichiometric compound ($x \geq 1$). Figure 4 and Figure 5 illustrate the structures of representative large and small cation Chevrel phases, respectively.

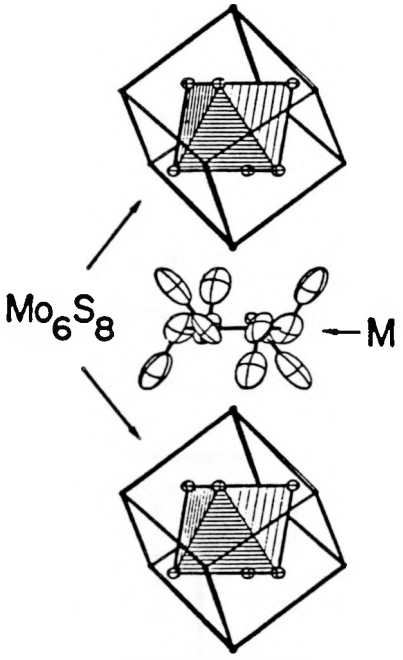


Figure 5. Illustration of the structure of small cation Chevrel phases [95]

**Preparation of Chevrel phases**

Most sulfide Chevrel phases are prepared by the direct combination of the elements or sulfides of the metallic compounds. These solid-state reactions are generally conducted in evacuated fused-silica tubes at temperatures of 1000–1200°C.

Other preparation techniques for the sulfide Chevrel phases have been reported. Improvements in purity can be obtained by high temperature (greater than 1700°C) meltings of the initial reaction products [96]. Small cation materials have been synthesized by electrochemical insertion of the ternary component into the binary $Mo_6S_8$ compound at room temperature [97–98]. Some large cation materials have been

prepared by thermally inserting the ternary element into the $Mo_6S_8$ cluster [99]. Moderately high temperature (470°C) and long reaction times (1–3 weeks) were required. Small cation Chevrel phases have also been prepared by the platinum-catalyzed hydrogen reduction of $MoS_2$ in the presence of the ternary metal at 1000–1050°C [100]. Preparations from the hydrogen reduction (1000°C) of $M_p(NH_4)_qMo_3S_9$ ($M$ = Cu, Pb, La, or Gd) precursors have been reported [101]. Thin solid films of Chevrel phases have been prepared by sputtering (*e.g.*, [102–105]), evaporation [106–107], and chemical vapor transport (CVT) [108] techniques.

**Molybdenum oxidation state**

Compared to the dominant $Mo^{4+}$ state of conventional HDS catalysts, molybdenum exists in a low oxidation state in the Chevrel phases. Assuming a sulfur valence of –2, the formal oxidation state of molybdenum in $Mo_6S_8$ can be calculated as +2.67. The addition of ternary metal cations results in a donation of electrons from the ternary component cations to the molybdenum octahedron, increasing the number of electrons on the molybdenum atoms and resulting in the stabilization of the $Mo_6S_8$ structure [87,90,93,95]. For example, the formal oxidation state of molybdenum in $Cu_{4.0}Mo_6S_8$ is +2, assuming a copper valence of +1. Therefore, by varying the ternary metal or its concentration (or both), the formal oxidation state of molybdenum can be varied continuously between +2 and +2.67.

**Catalytic properties**

The Chevrel phases have been reported to have activities for thiophene and benzothiophene HDS comparable to, or greater than, those of model $MoS_2$ and Co–Mo–S catalysts [77–85]. As a class, the sulfide Chevrel phases have demonstrated the highest thiophene HDS activity, followed by the selenides, and then the tellurides [85].

The HDS activity of the sulfide Chevrel phases can be grouped according to their structural classification, with the large cation compounds being the most active, and the small cation materials being the least active [77–80]. The most active Chevrel phases involve the unusual "promoters" Ho, Pb, and Sn. In contrast, the Chevrel phases containing Ni and Co—the two most common conventional HDS promoters—are among the least active.

The 1-butene HYD activities of the Chevrel phases were found to be much lower than model unpromoted and cobalt-promoted $MoS_2$ catalysts [77–80,83], indicating their high degree of selectivity.

X-ray powder diffraction and laser Raman spectroscopy were used to determine the bulk purity and stability of the Chevrel phases [77–84]. The bulk structures for all of the Chevrel phases were found to be stable under thiophene reaction conditions; there was no loss in crystallinity, and no new phases were formed. Based on XPS investigations [77–80], differences were observed in the stability of the surface molybdenum oxidation states for the specific classes of the Chevrel phases: the

oxidation state of the surface molybdenum atoms of the large cation compounds remained unchanged, but some oxidation was observed for the small cation compounds. The differences in stability were related to the mobilities of the ternary metal cations within the Chevrel phase structures. HDS activity was found to be the highest for the most stable Chevrel phase catalysts.

## Research Objectives

The objectives of this research were two-fold. The primary objective was to achieve a better understanding of the oxidation state and chemical reactivity (selectivity) of the catalytically active sites of HDS catalysts. This investigation involved the preparation, physical characterization, and catalytic activity evaluation of a series of Chevrel phases in comparison with model $MoS_2$-based catalysts.

The second objective of this research was to design, construct, and provide preliminary testing of an infrared reflection–absorption spectroscopy (IRRAS) cell, capable of obtaining spectra under conditions ranging from atmospheric to ultra-high vacuum pressures. This chamber will ultimately be used in the analysis of catalytic thin films and subsequent elucidation of possible reaction mechanisms.

## Explanation of Dissertation Format

This dissertation contains four sections, each written in a form suitable for publication in a technical journal. A general introduction has been included to orient the

reader to the scientific and industrial relevance of this work. An overall summary with recommendations for future research follows Section IV. A reference list is provided at the end of each section. References cited in the general introduction and summary are given at the end of the dissertation.

Section I incorporates original work conducted by the author into a review of previous investigations with Chevrel phases as HDS catalysts (based on [77–80]). This original work consists of the research presented on $La_{1.2}Mo_6S_8$, $Dy_{1.2}Mo_6S_8$, and the lead–lutetium Chevrel phases, including their preparation, characterization, and activity evaluation (for thiophene and benzothiophene HDS, and 1-butene HYD). The research presented in Sections II–IV represent original work conducted by the author.

# SECTION I.

# CHEVREL PHASE HDS CATALYSTS: STRUCTURAL AND COMPOSITIONAL RELATIONSHIPS TO CATALYTIC ACTIVITY (A REVIEW)

# ABSTRACT

The catalytic activities of ''reduced'' molybdenum sulfides, known as Chevrel phases, have been evaluated for hydrodesulfurization of thiophene and benzothiophene and hydrogenation of 1-butene. These materials have been found to have hydrodesulfurization activities comparable to, or greater than, model unpromoted and cobalt-promoted $MoS_2$ catalysts; in contrast, Chevrel phases exhibit low activities for 1-butene hydrogenation. In this section, a general discussion of the relationship between the solid state chemistry of Chevrel phases and their catalytic activity is presented. Structural properties appear to be an important factor: large cation Chevrel phases are the most active and stable materials. It is also likely that the most active phases resist surface oxidation, which may occur if the ternary metal components undergo surface migration. ''Reduced'' molybdenum oxidation states can be associated with the active sites, in direct analogy with conventional catalysts.

# INTRODUCTION

Industrial hydrodesulfurization (HDS) catalysts are typically formed from oxides of molybdenum (or tungsten) and cobalt (or nickel) supported on alumina. During use, the catalysts become sulfided. The historical origin of presently-used HDS catalysts dates from work conducted during the early 1920's in Germany on the hydrogenation of coal and coal-derived liquids [1–2]. Over the past seventy years, much research has been directed toward elucidating catalyst structure, composition, and the nature of the active sites. Most of this work has emphasized the relationship of the active component in industrial catalysts to $MoS_2$-based structures [3–6]. However, characterization of these catalysts remains a challenging aspect of much current research.

A new class of HDS catalysts—''reduced'' molybdenum sulfides known as Chevrel phase catalysts—has been reported previously [7–11]. Considerable evidence has been offered that ''reduced'' molybdenum oxidation states are associated with the active sites on even conventional HDS catalysts [12–13]. Chevrel phases have been shown to have activities comparable to, or exceeding those of, conventional $MoS_2$ or Co–Mo–S materials for thiophene and benzothiophene HDS. In addition, the Chevrel

phases apparently favor desulfurization rather than hydrogenation (HYD), making them selective catalysts. Over twenty Chevrel phases have been examined [7–11,14], including the recent discovery of additional catalytically active compounds. It has also been possible to clarify some aspects of HDS reaction pathways and mechanisms using these catalysts [11,15]. In this section, some of the relationships between catalytic activity and the structural and compositional properties of Chevrel phases are presented.

In 1971, Chevrel *et al.* [16] reported the initial synthesis and characterization of molybdenum chalcogenides referred to as Chevrel phases. The general formula for these compounds is $M_xMo_6Z_8$ where $M$ can be over forty different elements, $x$ ranges from 1 to 4, and $Z$ is usually S, Se, or Te. Much interest developed in these compounds due to their superconducting properties. Literature reviews have been provided by Yvon [17], Chevrel and Sergent [18], Chevrel *et al.* [19], and Peña and Sergent [20]. The basis for the structure of sulfide Chevrel phases is the $Mo_6S_8$ fundamental cubic unit (Figure 1). The sulfur atoms form a slightly distorted cube built around a molybdenum octahedron which is elongated along the ternary axis. The Mo–Mo bond distances are quite short, ranging from 2.65 to 2.80 Å, compared to 2.72 Å for metallic molybdenum. The Mo–Mo intracluster bond distance can be influenced by the addition of ternary metals: if the number of valence electrons is increased by increasing the concentration of the ternary component or by using ternary elements with a higher valence, the Mo–Mo bond distance decreases. This has led to the description of the unique structural character of Chevrel phases as consisting of "little bits of

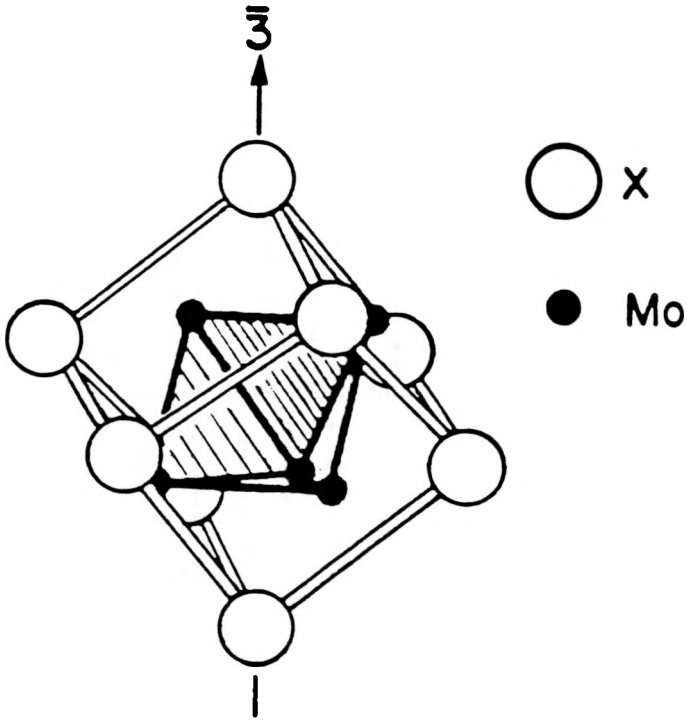


Figure 1. The $Mo_6S_8$ structural unit aligned along the ternary axis [17]

metal.'' The conductivity behavior (poor conductors which can become superconductors at temperatures as high as 15 K) has also been discussed in these terms [19].

The $Mo_6S_8$ structural units may be stacked to form structures with rhombohedral or triclinic geometries. The $Mo_6S_8$ units are interconnected by short, covalent Mo–S bonds of 2.4–2.6 Å. The structures of the Chevrel phases tend to be highly stable because each unit is bonded to six other units through these linkages. The $Mo_6$ clusters interact through Mo–Mo intercluster bonds of 3.1–3.4 Å.

The Chevrel phases can be grouped according to the ternary metal components which influence specific structural properties. The valence state and size of the ternary

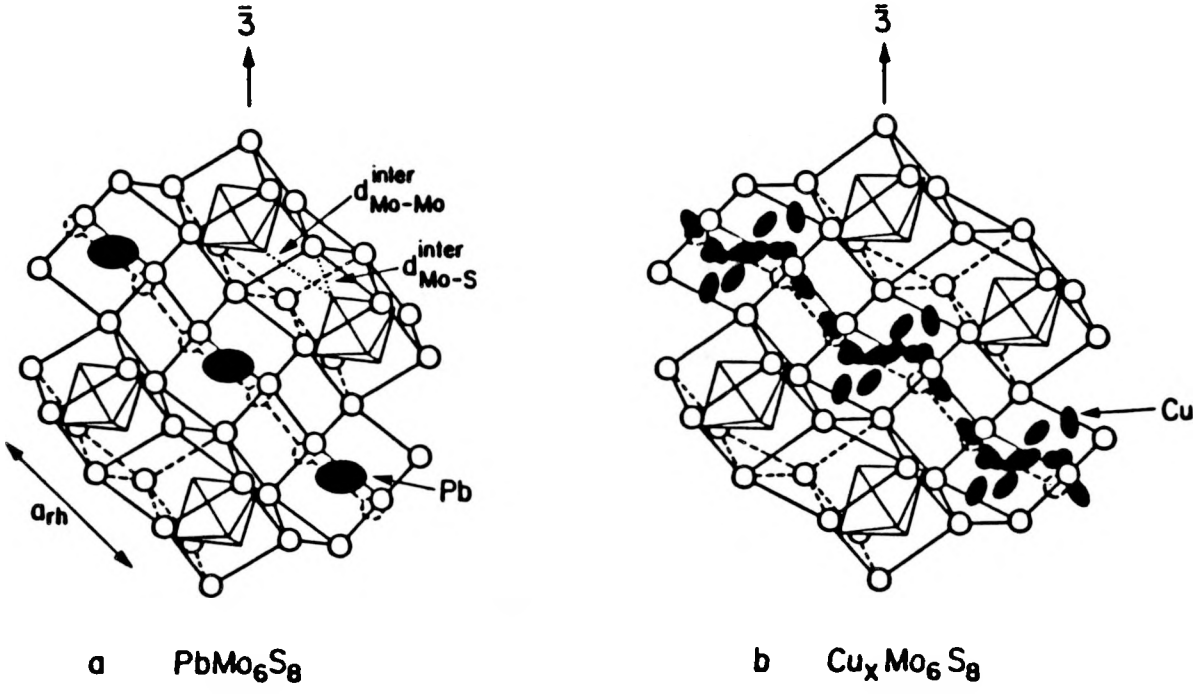


Figure 2. Chevrel phase structure illustrating the arrangement of the ternary metal atoms in (a) $PbMo_6S_8$ (large cation compound), and (b) $Cu_xMo_6S_8$ (small cation compound) [17]

metal are particularly important. The ternary metals are located in "infinite channels" existing along the rhombohedral axes (Figure 2); thermal motion of the ternary atoms is highly anisotropic, with large motion perpendicular to the ternary axis but with very little motion in the parallel direction. Physically, this is interpreted as giving rise to a delocalization of the ternary atoms. However, the extent of the delocalization is primarily dependent on the size of the metal atom (Figure 3). On this basis, Chevrel phases are classified as small cation, intermediate cation, and large cation compounds (Table 1).

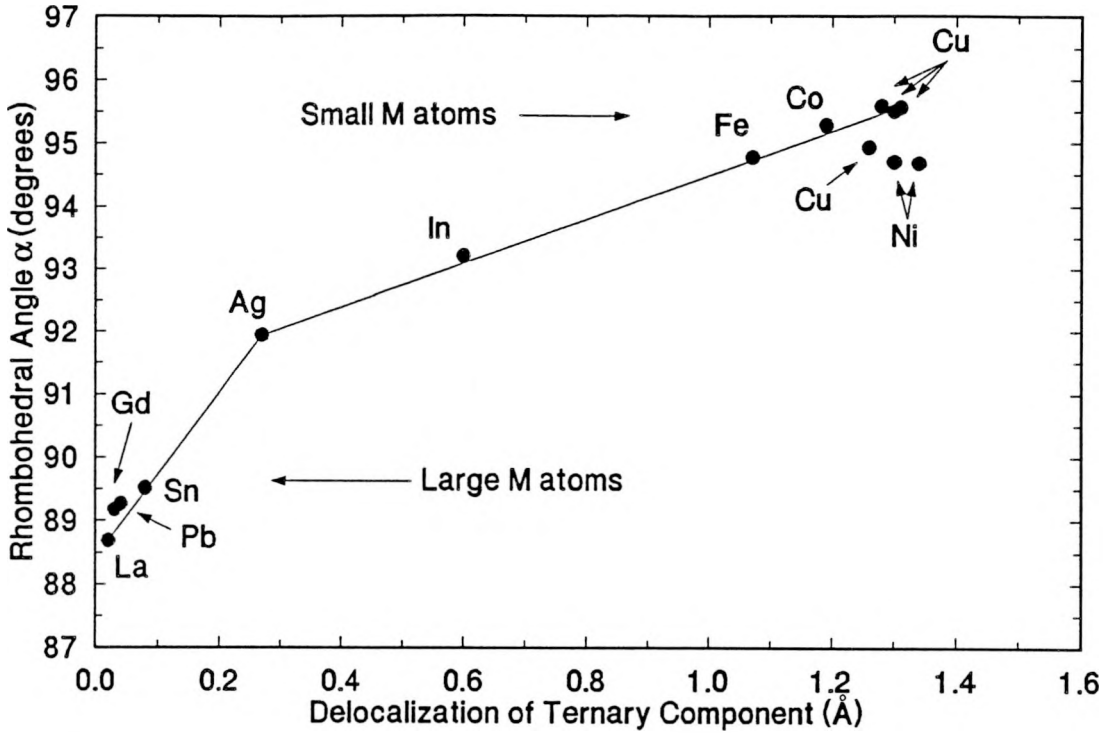


Figure 3. The delocalization of the cation *M* as a function of the rhombohedral angle

The Chevrel phases also demonstrate compositional ranges depending on the size of the cation (Table 1). Small cation ternary metal concentrations (for components such as Cu, Fe, Ni, Co) can varied continuously within specific limits (*e.g.*, $1.6 \leq x \leq 4.0$ for $Cu_xMo_6S_8$). Conversely, the concentration ranges for large cations, such as Ho, Pb, or Sn, is very small or nonexistent. For the light rare earths (*RE*), a composition of $RE_{1.0}Mo_6S_8$ is found, but for the heavy rare earths it is closer to $RE_{1.2}Mo_6S_8$. High purity lead Chevrel phases cannot be prepared at $PbMo_6S_8$; rather, the most pure phases are obtained for $PbMo_{6.2}S_8$. For both lead and tin Chevrel phases, a second ternary metal, such as a rare earth, may be incorporated to produce a series of structurally

Table 1. Sulfur Chevrel phases ($M_xMo_6S_8$)[a]

| Ternary components reported in the literature | |
|---|---|
| Li, Na, K, Mg, Ca, Sr, Ba, Sc, Y, La, Cr, Mn, Fe, Co, Ni, Pd, Cu, Ag, Zn, Cd, Al, In, Tl, Sn, Pb, Ce, Pr, Nd, Sm, Eu, Gd, Tb, Dy, Ho, Er, Tm, Yb, Lu, Th, U, Np, Pu, Am | |
| Examples of small cation compounds | compositional ranges |
| $Cu_xMo_6S_8$ | $1.6 \leq x \leq 4.0$ |
| $Co_xMo_6S_8$ | $1.3 \leq x \leq 2.0$ |
| $Ni_xMo_6S_8$ | $1.3 \leq x \leq 2.0$ |
| Examples of intermediate cation compounds | |
| $AgMo_6S_8$ | |
| $InMo_6S_8$ | |
| Examples of large cation compounds | |
| $HoMo_6S_8$ | |
| $PbMo_6S_8$ | |
| $SnMo_6S_8$ | |

[a]Data from [18,20].

related compounds with a nominal formula $RE_xM_{1-x}Mo_6S_8$. The solid solutions are complete. However, limitations in compositional ranges reflect some restrictions on the extent of rare earth insertion. In some compounds, smaller cations are inserted into channel positions at low concentration, while substitution for the large cation occurs at higher concentration.

The oxidation state of molybdenum in the metal-rich Chevrel phases is low relative to $MoS_2$. Based on simple calculations of formal oxidation states, the $Mo_6S_8$ binary compound has a molybdenum valence of +2.67. Introduction of the ternary

metal decreases the molybdenum oxidation state by the transfer of electrons from the ternary component cations to the molybdenum octahedron. For example, the formal oxidation state of molybdenum in $Cu_{4.0}Mo_6S_8$ can be calculated as $+2$.

The Chevrel phases possess a broad range of possible compositions, structures, and oxidation states. The ability to control these properties make them attractive materials for studying the relationships between catalysis and solid state chemistry.

# EXPERIMENTAL METHODS

## Catalyst Preparation

Several differences have been reported in the literature regarding the formulations required to produce pure, single phase Chevrel materials. For example, $SnMo_6S_8$ has been prepared with stoichiometry of $Sn_xMo_{6-z}S_8$ ($0.9 \leq x \leq 1.1$; $0.2 \leq z \leq 1$), and $PbMo_6S_8$ has been reported with stoichiometry $Pb_xMo_6S_{8-y}$ ($0.85 \leq x \leq 1.05$; $0.8 \leq y \leq 1.2$) [21]. ''Pure'' rare earth compounds have been prepared with compositions of $RE_{1.0}Mo_6S_8$ and $RE_{1.2}Mo_6S_8$ [22]. Studies of single crystals have shown that the ideal stoichiometries $M_{1.0}Mo_6S_8$ (large cation compounds) and $M_xMo_6S_8$ (small cation compounds) exist [23–24]. Polycrystalline samples with compositions deviating from these ''ideal'' values may possibly contain some unidentified impurities.

In this work, homogeneous pure polycrystalline samples were obtained for the rare earth materials at compositions of $RE_{1.2}Mo_6S_8$. Representative small cation materials were prepared as $M_xMo_6S_8$ (involving compositional ranges for some ternary metals such as Co, where $1.5 \leq x \leq 1.9$) [9–10]. Lead and tin compounds can be prepared at compositions of $M_{1.0}Mo_{6.2}S_8$, but alternate stoichiometries were also

prepared. A series of lead–lutetium Chevrel phases were synthesized: $Lu_{1-2x}PbMo_6S_8$ ($0 < x \leq 0.2$) and $Lu_{1-2x}Pb_{1-x}Mo_6S_8$ ($0.2 < x \leq 1$) [14]. Details of these procedures are provided below.

Lead, tin, cobalt, and holmium Chevrel phases were synthesized from mixtures of: 200 mesh powdered molybdenum metal (Alfa, m3n+, t2n7) reduced with hydrogen (20 ml/min) in a tube furnace (Lindberg, model 54231) at 1000°C for 18 h; the appropriate metal sulfide of the ternary components (made by the direct combination of the elements in evacuated, fused-silica tubes); and $Mo_{2.06}S_3$ (prepared from 200 mesh molybdenum powder and sulfur (Alfa, t5n5) [10]) (preparation method I). The powders were ground together thoroughly, pressed into 13-mm pellets (with 10,000 lbs total force using a Perkin Elmer die, model 186–0025), and placed in pre-baked fused-silica tubes which were evacuated to less than $10^{-5}$ Torr. The synthesis tubes then were back-filled with argon to a pressure that would produce 1 atm at the reaction temperature. The tubes were sealed and heated in a high-temperature box furnace (Lindberg, model 51333) to temperatures between 1000 and 1200°C for 24–48 h. $PbMo_{6.2}S_8$ and $SnMo_{6.2}S_8$ samples were reground in air, pressed into pellets, evacuated in fused-silica tubes, and reheated at temperatures between 1100 and 1200°C for 12 h.

Dysprosium, lanthanum, lutetium, lead, and lead–lutetium Chevrel phases were prepared from mixtures of reduced molybdenum metal, powdered sulfur, and sulfides of the ternary metals (preparation method II). The materials were processed as described previously and then were heated initially in a muffle furnace (Central Scientific, model

Hoskins FD202C) from 450 to 750°C for a period of 48–72 h. The samples were transferred immediately to the high temperature box furnace at 1200°C for 24 h and quenched in air. After regrinding in air, the materials were pressed into pellets and placed in fused-silica tubes which were evacuated, sealed, and heated for 48 h at 1225°C.

All synthesis tubes were opened in a nitrogen dry box where the pellets were lightly crushed. A 40–100 mesh portion was separated for use in the activity measurements; a small portion was reserved for X-ray photoelectron spectroscopy (XPS) analysis. All subsequent manipulations of these materials were performed in the dry box.

Model unpromoted and cobalt-promoted $MoS_2$ catalysts were prepared for comparisons of catalytic activity. Ammonium tetrathiomolybdate was thermally decomposed in the tube furnace at 1000°C in a flow of helium, resulting in a catalyst referred to as 1000°C $MoS_2$ [25]. A cobalt-promoted $MoS_2$ catalyst was synthesized with a cobalt to molybdenum ratio of 1:4 according to the homogeneous precipitation technique of Candia *et al.* [26]. This material, referred to as $Co_{0.25}$–$Mo_1$–S, was pretreated at 450°C in a 2% $H_2S/H_2$ mixture for 4 h.

## Catalyst Characterization

Catalysts were characterized both prior to and after 10 h of continuous $H_2$–thiophene reaction. The bulk purity of the catalysts was examined with X-ray

powder diffraction and laser Raman spectroscopy. X-ray powder diffraction patterns were acquired with a Siemans D500 diffractometer using Cu$K\alpha$ radiation. Laser Raman spectra were obtained with a Spex 1403 double monochromator using the 514.5-nm line of a Spectra Physics argon ion laser operating at 200 mW (measured at the source). All spectra were collected using backscattering geometry from spinning catalyst pellets. Fifty scans were accumulated with a scanning speed of 2 $cm^{-1}/s$ at 5-$cm^{-1}$ resolution.

X-ray photoelectron spectra were acquired with an AEI 200B spectrometer using Al$K\alpha$ radiation to examine the surface composition and surface oxidation state of the molybdenum in the Chevrel phases. All spectra were referenced to a carbon 1*s* binding energy of 284.6 eV. Spectra of the unused catalysts were obtained from a freshly ground sample; spectra of the used catalysts were obtained from the reactor charge with no further grinding.

The surface areas of the catalysts were determined by the BET method using a Micromeritics 2100E AccuSorb instrument. Krypton was used as the adsorbing gas at liquid nitrogen temperature.

## Activity Measurements

Thiophene HDS activities were measured at 400°C and atmospheric pressure using both pulse and continuous-flow reactor techniques, as described previously [7–11,14]. Thiophene (Alfa, 99%) was fed with a syringe pump (Sage, model 341), and all gases were metered through mass flow controllers (Tylan RC–260). The catalyst

loadings in the 0.25-in stainless-steel reactor were adjusted to give approximately 3% conversion of thiophene after 20 min of continuous reaction (ranging from 0.0074 g for $Co_{0.25}$–$Mo_1$–S to 1.7327 g for $Co_{1.9}Mo_6S_8$). The reactor was filled with fresh catalyst and heated from room temperature to 400°C in a stream of helium at 19 ml/min (STP). After a 1-h helium purge at 400°C, between ten and twenty-five 0.25-ml pulses of 2 mol% thiophene in hydrogen were injected into the reactor at 30 min intervals. The flow was then replaced with a continuous flow of 2 mol% thiophene in hydrogen at 22 ml/min (STP). After 10 h of continuous thiophene reaction, the reactor was purged and cooled in a stream of helium.

Benzothiophene HDS activity analyses were performed using the thiophene reactor apparatus with some slight modifications [15]. Benzothiophene is a solid at room temperature (m.p. 29–32°C), and it was necessary to heat a small chamber surrounding the syringe pump to 40°C. The heated benzothiophene (Aldrich, 97%) was pumped into a saturator (maintained at 230°C) where it was vaporized and mixed with hydrogen. The reactor was loaded with between 0.3120 and 0.5404 g of Chevrel phase ($PbMo_{6.2}S_8$) or 0.1640 g of model catalyst ($Co_{0.25}$–$Mo_1$–S). The reactor was heated from room temperature to the reaction temperature in a flow of helium at 19 ml/min (STP). After a 1-h helium purge at the reaction temperature, the flow was switched to a continuous flow of 2 mol% benzothiophene in hydrogen at 20 ml/min (STP). After 12-h continuous reaction, the reactor was purged and cooled using flowing helium. Reaction temperatures ranged from 250 to 500°C.

Activity measurements for HYD of 1-butene to *n*-butane were also performed as described previously [7–10]. The reactor was loaded with the same amount of fresh catalyst as for the thiophene HDS activity evaluations. The reactor was heated from room temperature to 400°C while using a stream of helium at 19 ml/min (STP). After about 1 h at 400°C (''fresh catalyst''), two 0.1-ml pulses of 2 mol% 1-butene (Matheson, 99.0%) in hydrogen were injected into the reactor at 15-min intervals. Twenty-five 0.1-ml pulses of 2 mol% thiophene in hydrogen were then introduced to the reactor, and the 1-butene pulses were repeated. The catalyst next underwent 2 h of continuous thiophene reaction (2 mol% thiophene in hydrogen at 22 ml/min). The reactor was purged with helium, and the 1-butene pulses were repeated.

Product separation and analysis were performed with an Antek 310/40 ALP gas chromatograph equipped with a flame ionization detector. Peak areas were measured by a Hewlett–Packard 3390A integrator. A 12-ft *n*-octane/Porasil C column was used for the thiophene HDS and 1-butene HYD studies. Identical retention times were found for *trans*-2-butene and 1,3-butadiene, requiring these materials to be combined in the data analysis. An 11-ft 3% SP–2100 on 100–120 mesh Supelcoport column was used for the benzothiophene HDS experiments.

# RESULTS

## Catalyst Characterization

The purity of the bulk Chevrel phase structures was determined primarily by X-ray powder diffraction. For all Chevrel phases studied, there were no apparent changes in the X-ray patterns after thiophene reaction times of up to 10 h, indicating no loss of crystallinity and no formation of other phases.

Laser Raman spectroscopy is a sensitive technique for the detection of both crystalline and poorly-crystalline $MoS_2$ (bands at 383 and 409 $cm^{-1}$) [27]. A slight amount of $MoS_2$ impurity was detected for the cobalt Chevrel phases [7–10]. After reaction, the amount of $MoS_2$ in these materials increased. The presence of a small amount of $MoS_2$ was also detected in $SnMo_6S_8$; this amount remained approximately constant after 10-h thiophene reaction [10]. No $MoS_2$ was detected in any other fresh or used Chevrel phase catalysts.

XPS binding energies of typical Chevrel phases are summarized in Table 2. Table 3 summarizes the binding energies for the compounds prepared at other stoichiometries. The molybdenum $3d_{5/2}$ binding energies for the fresh catalysts listed in

Table 2. XPS binding energies and intensity ratios

| Catalyst | | Binding energies (eV) | | | | | Calculated ratios | |
|---|---|---|---|---|---|---|---|---|
| | | Mo | | *M* | | S | $M^a$/Mo | $S^b$/Mo |
| | | $3d_{3/2}$ | $3d_{5/2}$ | – | – | 2*p* | | |
| Large cation compounds | | | | | | | | |
| $Ho_{1.2}Mo_6S_8$ | A | 230.7 | 227.5 | –[c] | –[c] | 161.6 | –[c] | 0.29 |
| | B | 230.8 | 227.5 | –[c] | –[c] | 161.5 | –[c] | –[d] |
| $Dy_{1.2}Mo_6S_8$ | A | 231.3 | 228.0 | –[c] | –[c] | 162.3 | –[c] | –[d] |
| | B | 231.3 | 228.0 | –[c] | –[c] | 162.6 | –[c] | –[d] |
| $La_{1.2}Mo_6S_8$ | A | 231.1 | 227.9 | 851.4[e1] | 834.6[e2] | 162.2 | –[d] | –[d] |
| | B | 230.9 | 227.7 | 851.0[e1] | 834.1[e2] | 162.2 | –[d] | –[d] |
| $Lu_{1.2}Mo_6S_8$ | A | 231.1 | 227.7 | 207.0[f1] | 197.2[f2] | 161.8 | 0.17[g] | 0.33 |
| | B | 230.8 | 227.6 | 206.5[f1] | 196.8[f2] | 161.8 | 0.19[g] | 0.31 |
| $PbMo_{6.2}S_8$ | A | 230.9 | 227.5 | 142.3[h1] | 137.5[h2] | 161.6 | 0.56[i] | 0.27 |
| (prep. I) | B | 230.8 | 227.5 | 142.5[h1] | 137.5[h2] | 161.8 | 0.56[i] | 0.28 |
| $PbMo_{6.2}S_8$ | A | 231.1 | 227.7 | 143.3[h1] | 138.6[h2] | 162.3 | 0.50[i] | 0.33 |
| (prep. II) | B | 231.0 | 227.9 | 143.0[h1] | 138.3[h2] | 162.4 | 0.50[i] | 0.42 |
| $SnMo_{6.2}S_8$ | A | 231.4 | 228.1 | 494.5[e1] | 486.0[e2] | 161.7 | 0.48[j] | 0.27 |
| | B | 231.2 | 227.9 | 494.5[e1] | 485.9[e2] | 161.8 | 0.45[j] | 0.27 |
| Small cation compounds | | | | | | | | |
| $Co_{1.6}Mo_6S_8$ | A | 231.2 | 227.8 | 796.2[k1] | 780.4[k2] | 161.9 | –[d] | –[d] |
| | B | 231.8 | 228.8 | 796.2[k1] | 780.4[k2] | 161.9 | –[d] | –[d] |
| $Co_{1.7}Mo_6S_8$ | A | 230.6 | 227.3 | 795.1[k1] | 779.4[k2] | 161.8 | 0.29[l] | 0.24 |
| | B | 231.9 | 228.7 | 796.6[k1] | 780.8[k2] | 162.2 | 0.23[l] | 0.31 |

A = fresh catalyst; B = after 10-h continuous $H_2$–thiophene reaction

[a]Raw area ratio of ternary component *M* electrons to Mo 3*d* electrons.
[b]Raw area ratio of S 2*p* electrons to Mo 3*d* electrons.
[c]Ternary metal spectrum too diffuse.
[d]Information not available.
[e]*M* $3d_{3/2}$ (*e1*) and *M* $3d_{5/2}$ (*e2*).
[f]*M* $4d_{3/2}$ (*f1*) and *M* $4d_{5/2}$ (*f2*).
[g]Raw area ratio of *M* 4*d* to Mo 3*d*.
[h]*M* $4f_{5/2}$ (*h1*) and *M* $4f_{7/2}$ (*h2*).
[i]Raw area ratio of *M* 4*f* to Mo 3*d*.
[j]Raw area ratio of *M* 3*d* to Mo 3*d*.
[k]*M* $2p_{1/2}$ (*i1*) and *M* $2p_{3/2}$ (*i2*).
[l]Raw area ratio of *M* $2p_{3/2}$ to Mo 3*d*.

Table 3. XPS binding energies: other stoichiometries

| Catalyst | | Binding energies (eV) | | | | | | |
|---|---|---|---|---|---|---|---|---|
| | | Mo | | Pb | | Lu | | S |
| | | $3d_{3/2}$ | $3d_{5/2}$ | $4f_{5/2}$ | $4f_{7/2}$ | $4d_{3/2}$ | $4d_{5/2}$ | $2p$ |
| $Pb_{0.92}Mo_6S_8$ | A | 231.8 | 228.5 | 143.1 | 138.3 | —[a] | —[a] | 162.0 |
| | B | 231.0 | 227.8 | 142.5 | 137.6 | —[a] | —[a] | 161.9 |
| $Lu_{0.8}Pb_{0.33}Mo_6S_8$ | A | 230.9 | 227.6 | 142.8 | 137.8 | 207.2 | 197.4 | 162.0 |
| | B | 230.8 | 227.6 | 142.6 | 137.9 | 207.0 | 197.4 | 162.2 |
| $Lu_{0.4}Pb_{0.67}Mo_6S_8$ | A | 231.4 | 228.1 | 142.5 | 137.6 | 207.3 | 197.6 | 161.9 |
| | B | 231.0 | 227.6 | 142.6 | 137.7 | 207.0 | 197.2 | 161.8 |
| $Lu_{0.1}PbMo_6S_8$ | A | 231.5 | 228.1 | 143.3 | 138.6 | —[b] | —[b] | 162.1 |
| | B | 231.1 | 227.8 | 142.8 | 138.0 | —[b] | —[b] | 162.1 |

A = fresh catalyst; B = after 10 h of continuous $H_2$–thiophene reaction

[a]Not applicable.
[b]Lu concentration too low to evaluate.

Table 2 are grouped around 227.7 eV, ranging from 227.3 eV ($Co_{1.7}Mo_6S_8$) to 228.1 eV ($SnMo_{6.2}S_8$). These data clearly demonstrate the low molybdenum oxidation states present in these materials. For comparison, the $3d_{5/2}$ binding energy for $MoS_2$ ($Mo^{4+}$) is 228.9 eV, and that for $MoO_3$ ($Mo^{6+}$) is about 232.5 eV [28].

These tables also summarize the changes in the molybdenum $3d$ spectra which occur after 10 h of thiophene reaction. For the large cation compounds, there are no significant shifts in the band positions. However, for the representative small cation compounds, $Co_{1.6}Mo_6S_8$ and $Co_{1.7}Mo_6S_8$, the molybdenum $3d_{5/2}$ bands shift from 227.8 to 228.8 eV and from 227.3 to 228.7 eV, respectively. These small cation

materials show some oxidation of the surface molybdenum species. The molybdenum $3d_{5/2}$ binding energy of fresh $Pb_{0.92}Mo_6S_8$ is the highest of any of the Chevrel phases examined (228.5 eV), however, the binding energy drops to 227.8 eV after 10 h of thiophene reaction. This value is in good agreement with the other Chevrel phases. $Lu_{0.4}Pb_{0.67}Mo_6S_8$ also showed a slight reduction in the molybdenum $3d_{5/2}$ binding energy after reaction (228.1 eV to 227.6 eV). The other lead–lutetium compounds remain stable with respect to molybdenum reduction after reaction.

With the exception of $Lu_{1.2}Mo_6S_8$, $Co_{1.7}Mo_6S_8$, $Pb_{0.92}Mo_6S_8$, and $Lu_{0.1}PbMo_6S_8$, the binding energies of the ternary metal components do not change appreciably. Similarly, the sulfur $2p$ binding energy remains approximately constant (near 162.0 eV) for all catalysts.

Table 2 and Table 4 show ratios of raw peak areas of a core electron orbital for the ternary metals compared to the molybdenum $3d$ electrons. These ratios are not corrected for instrumental or atomic sensitivity factors and are not intended to quantitatively reflect the compositions at the surface. Rather, they are provided to demonstrate changes which occur after thiophene reaction. For the lead and tin Chevrel phases, the ratios *M*/Mo and S/Mo remain approximately the same after reaction. For the small cation materials, the ratio *M*/Mo is smaller after thiophene reaction, indicating the loss of the ternary component from the catalyst surface. Conversely, for the lutetium-containing Chevrel phases, there is an enrichment of the ternary metal at the surface after reaction (an increase in the *M*/Mo ratios).

Table 4. XPS intensity ratios: other stoichiometries

| Catalyst | | Calculated ratios | | |
|---|---|---|---|---|
| | | Pb/Mo[a] | Lu/Mo[b] | S/Mo[c] |
| $Pb_{0.92}Mo_6S_8$ | A | 0.45 | –[d] | 0.28 |
| | B | 0.48 | –[d] | 0.29 |
| $Lu_{0.8}Pb_{0.33}Mo_6S_8$ | A | 0.23 | 0.11 | 0.32 |
| | B | 0.20 | 0.19 | 0.32 |
| $Lu_{0.4}Pb_{0.67}Mo_6S_8$ | A | 0.31 | 0.06 | 0.33 |
| | B | 0.30 | 0.18 | 0.37 |
| $Lu_{0.1}PbMo_6S_8$ | A | 0.48 | –[e] | 0.33 |
| | B | 0.48 | –[e] | 0.37 |

A = fresh catalyst; B = after 10-h continuous $H_2$–thiophene reaction

[a]Raw area ratio of Pb 4*f* electrons to Mo 3*d* electrons.
[b]Raw area ratio of Lu 4*d* electrons to Mo 3*d* electrons.
[c]Raw area ratio of S 2*p* electrons to Mo 3*d* electrons.
[d]Not applicable.
[e]Lu concentration too low to evaluate.

As shown in Table 5, the surface areas of the Chevrel phases prepared by method I generally remained within 10% of their initial values (fresh catalysts) after 10 h of thiophene HDS. However, the surface areas of the compounds prepared by method II increased significantly under thiophene reaction conditions. A comparison of $PbMo_{6.2}S_8$ samples prepared by the different methods indicates that preparation method II leads to slightly higher surface area materials.

Table 5. Thiophene hydrodesulfurization (HDS) activities (400°C)

| Catalyst (preparation method) | | Surface area ($m^2/g$) | Reaction time | Thiophene conversion (%) | HDS rate ($mol/s \cdot m^2$) $\times 10^8$ |
|---|---|---|---|---|---|
| Large cation compounds | | | | | |
| $Ho_{1.2}Mo_6S_8$ | (I) | 0.579 | 20 min | 2.48 | 12.65 |
| | | –[a] | 10 h | 2.20 | 11.23 |
| $Dy_{1.2}Mo_6S_8$ | (II) | 0.785 | 20 min | 2.87 | 8.51 |
| | | 0.984 | 10 h | 2.56 | 7.57 |
| $La_{1.2}Mo_6S_8$ | (II) | 0.766 | 20 min | 1.25 | 1.99 |
| | | 0.990 | 10 h | 0.95 | 1.18 |
| $Lu_{1.2}Mo_6S_8$ | (II) | 0.693 | 20 min | 2.06 | 1.80 |
| | | 1.093 | 10 h | 3.48 | 1.93 |
| $Lu_{0.8}Pb_{0.33}Mo_6S_8$ | (II) | 0.689 | 20 min | 1.64 | 1.55 |
| | | 1.033 | 10 h | 3.17 | 2.00 |
| $Lu_{0.4}Pb_{0.67}Mo_6S_8$ | (II) | 0.563 | 20 min | 1.59 | 4.43 |
| | | 0.644 | 10 h | 1.36 | 3.30 |
| $Lu_{0.1}PbMo_6S_8$ | (II) | 0.649 | 20 min | 2.60 | 8.43 |
| | | 0.952 | 10 h | 2.84 | 6.27 |
| $PbMo_{6.2}S_8$ | (I) | 0.400 | 20 min | 1.92 | 10.03 |
| | | –[a] | 10 h | 1.28 | 6.68 |
| $PbMo_{6.2}S_8$ | (II) | 1.318 | 20 min | 1.59 | 4.53 |
| | | 1.664 | 10 h | 1.16 | 2.61 |
| $Pb_{0.92}Mo_6S_8$ | (I) | 1.23 | 20 min | 2.38 | 9.73 |
| | | –[a] | 10 h | 2.11 | 8.62 |
| $SnMo_{6.2}S_8$ | (I) | 0.388 | 20 min | 1.90 | 3.57 |
| | | –[a] | 10 h | 1.72 | 3.24 |
| $SnMo_6S_8$ | (I) | 0.357 | 20 min | 1.83 | 9.64 |
| | | 0.304 | 10 h | 1.62 | 10.03 |
| $Sn_{1.2}Mo_6S_8$ | (I) | 0.314 | 20 min | 1.24 | 1.61 |
| | | –[a] | 10 h | 0.41 | 0.53 |

[a]No appreciable change in surface area (< 10%).

Table 5. (*continued*)

| Catalyst (preparation method) | Surface area ($m^2/g$) | Reaction time | Thiophene conversion (%) | HDS rate ($mol/s \cdot m^2$) $\times 10^8$ |
|---|---|---|---|---|
| Small cation compounds | | | | |
| $Co_{1.5}Mo_6S_8$ (I) | 0.150 | 20 min | 2.06 | 3.16 |
| | –[a] | 10 h | 0.54 | 0.82 |
| $Co_{1.6}Mo_6S_8$ (I) | 0.099 | 20 min | 1.88 | 4.12 |
| | –[a] | 10 h | 0.47 | 1.02 |
| $Co_{1.7}Mo_6S_8$ (I) | 0.110 | 20 min | 2.05 | 3.65 |
| | –[a] | 10 h | 0.59 | 1.05 |
| $Co_{1.8}Mo_6S_8$ (I) | 0.080 | 20 min | 2.49 | 5.77 |
| | –[a] | 10 h | 0.52 | 1.20 |
| $Co_{1.9}Mo_6S_8$ (I) | 0.079 | 20 min | 2.11 | 4.70 |
| | –[a] | 10 h | 0.51 | 1.13 |
| Model $MoS_2$ compounds | | | | |
| $Co_{0.25}$–$Mo_1$–S | 10.83 | 20 min | 1.94 | 7.37 |
| | –[a] | 10 h | 0.77 | 2.92 |
| 1000°C $MoS_2$ | 3.40 | 20 min | 2.22 | 2.67 |
| | –[a] | 10 h | 0.76 | 0.92 |

## Activity Measurements

The continuous-flow thiophene HDS reaction results for the Chevrel phase catalysts and for the model $MoS_2$-based materials are summarized in Table 5 and Table 6. The thiophene conversion rates have been normalized on the basis of the surface area of the catalysts. The initial surface areas were used for materials that exhibited no

Table 6. $C_4$ distributions resulting from thiophene hydrodesulfurization (400°C)

| Catalyst | Reaction time | $C_4$ product distribution (%) | | | |
|---|---|---|---|---|---|
| | | *n*-butane | 1-butene | *trans*-2-butene | *cis*-2-butene |
| Large cation compounds | | | | | |
| $Ho_{1.2}Mo_6S_8$ | 20 min | 0.9 | 32.2 | 41.2 | 25.7 |
| | 10 h | 0.4 | 40.5 | 34.6 | 24.5 |
| $Dy_{1.2}Mo_6S_8$ | 20 min | 1.0 | 34.3 | 40.1 | 24.6 |
| | 10 h | 0.7 | 38.8 | 36.0 | 24.5 |
| $La_{1.2}Mo_6S_8$ | 20 min | –[a] | 46.6 | 35.2 | 18.2 |
| | 10 h | –[a] | 49.4 | 33.9 | 16.7 |
| $Lu_{1.2}Mo_6S_8$ | 20 min | 3.6 | 37.3 | 34.7 | 24.4 |
| | 10 h | 3.0 | 28.6 | 40.0 | 28.4 |
| $Lu_{0.8}Pb_{0.33}Mo_6S_8$ | 20 min | 2.3 | 44.1 | 32.4 | 21.2 |
| | 10 h | 0.7 | 34.7 | 38.8 | 25.8 |
| $Lu_{0.4}Pb_{0.67}Mo_6S_8$ | 20 min | 1.3 | 48.4 | 31.9 | 18.4 |
| | 10 h | –[a] | 47.9 | 34.3 | 17.8 |
| $Lu_{0.1}PbMo_6S_8$ | 20 min | 0.8 | 53.5 | 26.7 | 19.0 |
| | 10 h | 0.6 | 55.0 | 25.5 | 18.9 |
| $PbMo_{6.2}S_8$ (prep. I) | 20 min | 1.0 | 54.4 | 26.0 | 18.5 |
| | 10 h | 1.0 | 62.0 | 23.8 | 13.2 |
| $PbMo_{6.2}S_8$ (prep. II) | 20 min | –[a] | 65.5 | 20.2 | 14.3 |
| | 10 h | –[a] | 65.6 | 21.8 | 12.6 |
| $Pb_{0.92}Mo_6S_8$ | 20 min | –[a] | 52.5 | 27.2 | 20.3 |
| | 10 h | 0.9 | 56.5 | 24.5 | 18.1 |
| $SnMo_{6.2}S_8$ | 20 min | 0.6 | 60.7 | 22.6 | 16.1 |
| | 10 h | 0.5 | 63.1 | 21.3 | 15.1 |
| $SnMo_6S_8$ | 20 min | 0.6 | 55.3 | 27.0 | 17.1 |
| | 10 h | 0.5 | 59.4 | 25.9 | 14.2 |
| $Sn_{1.2}Mo_6S_8$ | 20 min | –[a] | 65.0 | 22.9 | 12.1 |
| | 10 h | –[a] | 64.7 | 26.0 | 9.3 |

[a]Below detection limit.

Table 6. (*continued*)

| Catalyst | Reaction time | $C_4$ product distribution (%) | | | |
|---|---|---|---|---|---|
| | | *n*-butane | 1-butene | *trans*-2-butene | *cis*-2-butene |
| Small cation compounds | | | | | |
| $Co_{1.5}Mo_6S_8$ | 20 min | 0.4 | 46.4 | 34.2 | 19.0 |
| | 10 h | –[a] | 42.2 | 45.6 | 12.2 |
| $Co_{1.6}Mo_6S_8$ | 20 min | –[a] | 48.0 | 33.2 | 18.8 |
| | 10 h | –[a] | 44.8 | 44.6 | 10.6 |
| $Co_{1.7}Mo_6S_8$ | 20 min | –[a] | 46.1 | 35.5 | 18.4 |
| | 10 h | –[a] | 42.5 | 45.3 | 12.2 |
| $Co_{1.8}Mo_6S_8$ | 20 min | –[a] | 44.4 | 37.2 | 18.4 |
| | 10 h | –[a] | 40.1 | 48.5 | 11.4 |
| $Co_{1.9}Mo_6S_8$ | 20 min | 0.4 | 47.6 | 35.3 | 16.7 |
| | 10 h | –[a] | 42.9 | 46.5 | 10.6 |
| Model $MoS_2$ compounds | | | | | |
| $Co_{0.25}$–$Mo_1$–S | 20 min | 1.3 | 35.9 | 38.0 | 24.8 |
| | 10 h | 1.5 | 36.4 | 41.1 | 21.0 |
| 1000°C $MoS_2$ | 20 min | 2.4 | 41.2 | 32.7 | 23.7 |
| | 10 h | 1.8 | 46.0 | 34.9 | 17.3 |

appreciable surface area changes (< 10%). For catalysts displaying a change in surface area, the initial surface area was used to normalize the HDS activity after 20 min of thiophene reaction, while the activity after 10 h of reaction was normalized using the final surface area.

All Chevrel phase materials exhibit thiophene HDS activities comparable to—or greater than—the model $MoS_2$-based catalysts. The activities of the Chevrel phases can

be grouped according to their structural classification [9–10]. The large cation compounds are the most active, the intermediate cation compounds are less active, and the small cation compounds are the least active. The large cation Chevrel phases also show less deactivation over the 10-h period than do the model $MoS_2$-based catalysts. For example, the ratio of the activity after 10 h of thiophene reaction to that after 20 min is 0.91 for $SnMo_{6.2}S_8$, 0.89 for $Dy_{1.2}Mo_6S_8$, and 0.88 for $Ho_{1.2}Mo_6S_8$, compared to 0.40 for $Co_{0.25}$–$Mo_1$–S, and 0.35 for 1000°C $MoS_2$. The deactivation of small cation compounds is approximately equal to, or greater than, the model $MoS_2$-based materials. For example, the ratio of the activity after 10 h to that after 20 min is 0.25 for $Co_{1.6}Mo_6S_8$ and 0.21 for $Co_{1.8}Mo_6S_8$.

$PbMo_{6.2}S_8$ (method I) and $Pb_{0.92}Mo_6S_8$ have similar thiophene HDS activities (Figure 4) [10]. However, changes in the stoichiometries of the tin Chevrel phases have a more dramatic effect on the catalytic properties [10]. As depicted in Figure 5, after 10 h of thiophene reaction, $SnMo_6S_8$ is 3 times more active than $SnMo_{6.2}S_8$, which in turn is 6 times more active than $Sn_{1.2}Mo_6S_8$. Variations in the stoichiometries of the lead–lutetium Chevrel phases also have a pronounced effect on the catalytic activity (Figure 6). $Lu_{0.1}PbMo_6S_8$ is the most active catalyst of this series, with activity generally decreasing with increasing lutetium concentration. Figure 7 shows the continuous thiophene reaction results for the $Co_xMo_6S_8$ series with $1.5 \leq x \leq 1.9$. After 20 min of reaction, the activity increases in roughly a linear manner with increasing

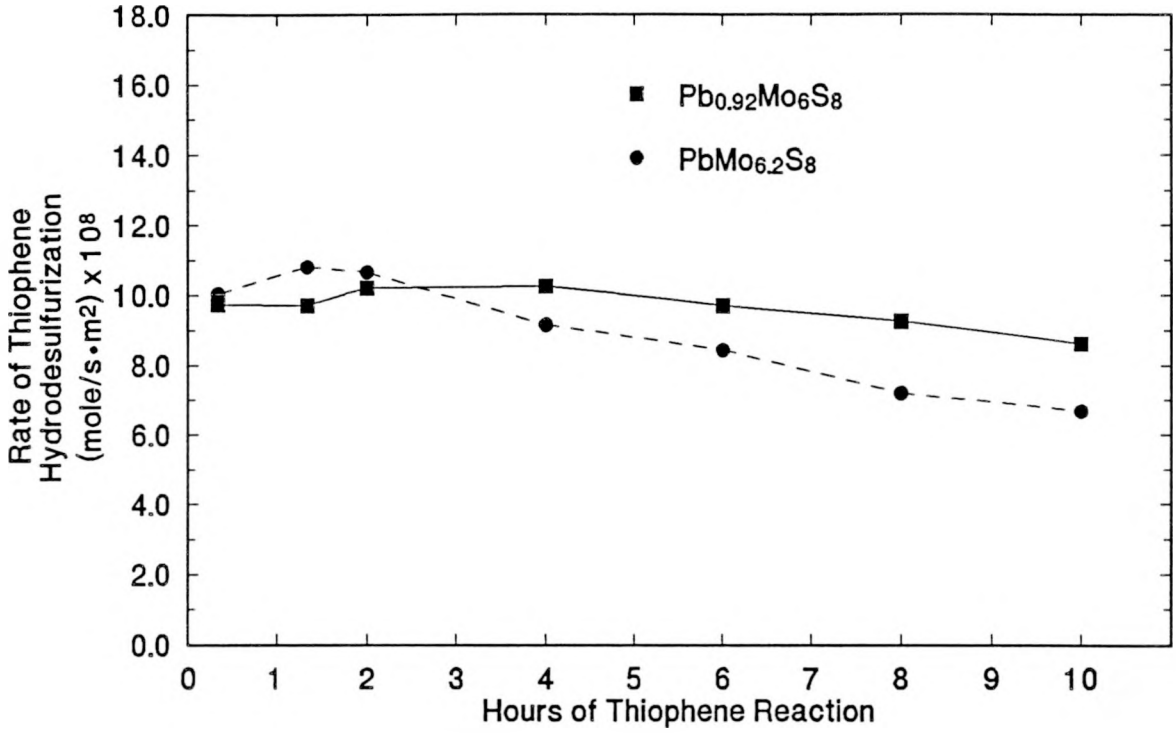


Figure 4. HDS activities of lead Chevrel phases of various stoichiometries [10]

cobalt concentration. The activity differences decreased with reaction time and were approximately equal after 10 h of thiophene reaction [8,10].

The $C_4$ hydrocarbon product distributions resulting from thiophene HDS vary markedly for the Chevrel phase catalysts which have been examined (Table 6). For example, the ratio of the 2-butenes to 1-butene after 10-h thiophene reaction was 2.4 for $Lu_{1.2}Mo_6S_8$, 1.5 for $Ho_{1.2}Mo_6S_8$, 0.58 for $SnMo_{6.2}S_8$, 1.5 for $Co_{1.8}Mo_6S_8$, 1.1 for 1000°C $MoS_2$, and 1.7 for $Co_{0.25}$–$Mo_1$–S. These values differ from the thermodynamic equilibrium value at 400°C for which the ratio of 2-butenes to 1-butene is 2.8 [29].

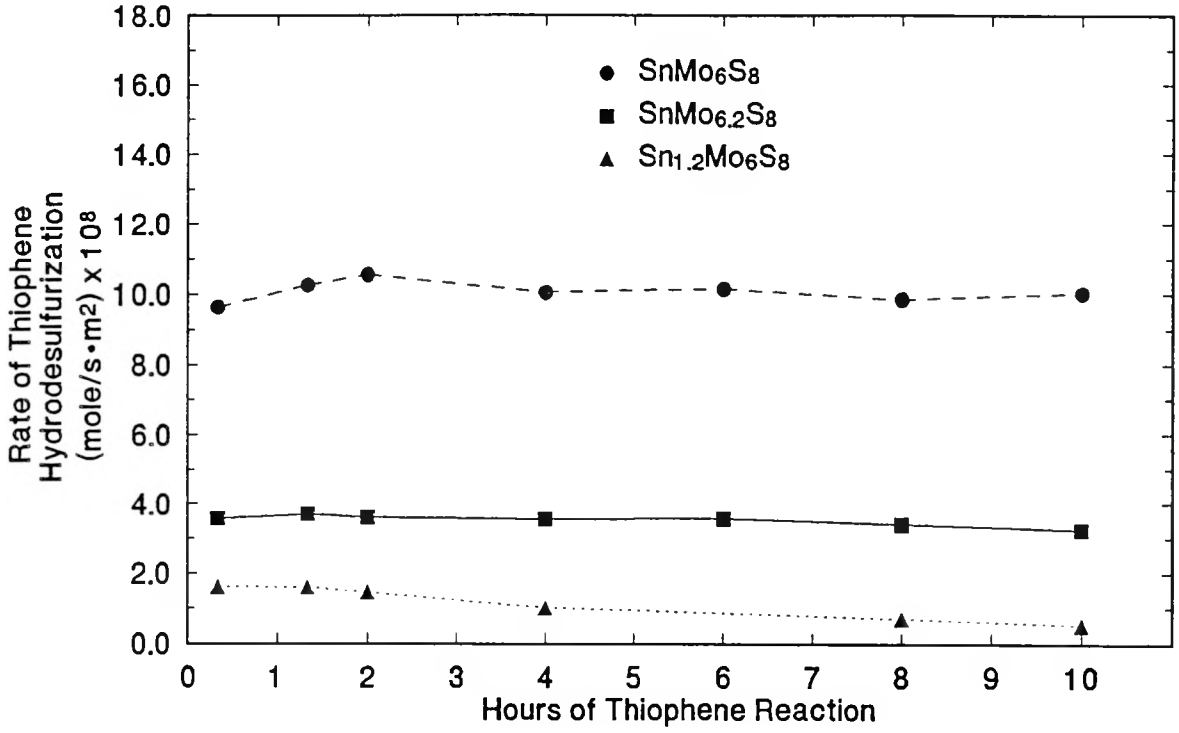


Figure 5. HDS activities of tin Chevrel phases of various stoichiometries [10]

Catalyst activity measurements using benzothiophene are summarized for $PbMo_{6.2}S_8$ (method II) and $Co_{0.25}$–$Mo_1$–S in Table 7. The benzothiophene conversion activities were calculated as the rate of production of ethylbenzene and were normalized on the basis of the catalyst surface area. HDS rates were determined at each reaction temperature after 12 h of continuous benzothiophene reaction. Comparisons between the catalytic activity of $PbMo_{6.2}S_8$ (method II) and $Co_{0.25}$–$Mo_1$–S cannot be readily made from the data. However, it should be noted that the lead Chevrel phase has a lower activity at 400°C for benzothiophene HDS ($1.45 \times 10^{-8}$ mol/s•m$^2$) than for thiophene HDS ($2.61 \times 10^{-8}$ mol/s•m$^2$).

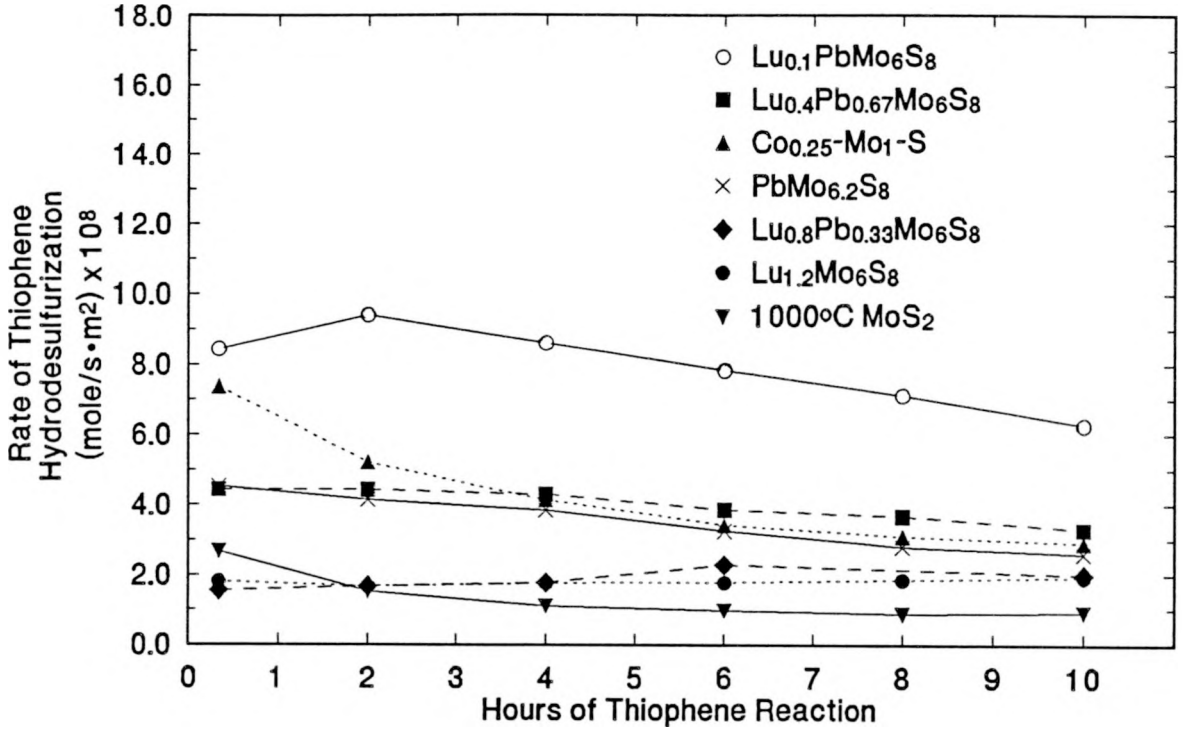


Figure 6. HDS activities of lead–lutetium Chevrel phases

Table 7. Benzothiophene hydrodesulfurization (HDS) activities (12-h reaction)

| Catalyst | Surface area ($m^2/g$) | Reaction temperature (°C) | Benzothiophene conversion (%) | HDS rate ($mol/s \cdot m^2$) $\times 10^8$ |
|---|---|---|---|---|
| $PbMo_{6.2}S_8$ (prep. II) | 1.664[a] | 325 | 0.7 | 0.34 |
| | | 400 | 3.2 | 1.45 |
| | | 450 | 6.0 | 2.72 |
| | | 500 | 14.0 | 3.95 |
| $Co_{0.25}$–$Mo_1$–S | 10.83 | 250 | 8.1 | 0.91 |
| | | 300 | 26.9 | 3.05 |
| | | 350 | 85.6 | 9.70 |

[a]Surface area after 10-h continuous $H_2$–thiophene reaction.

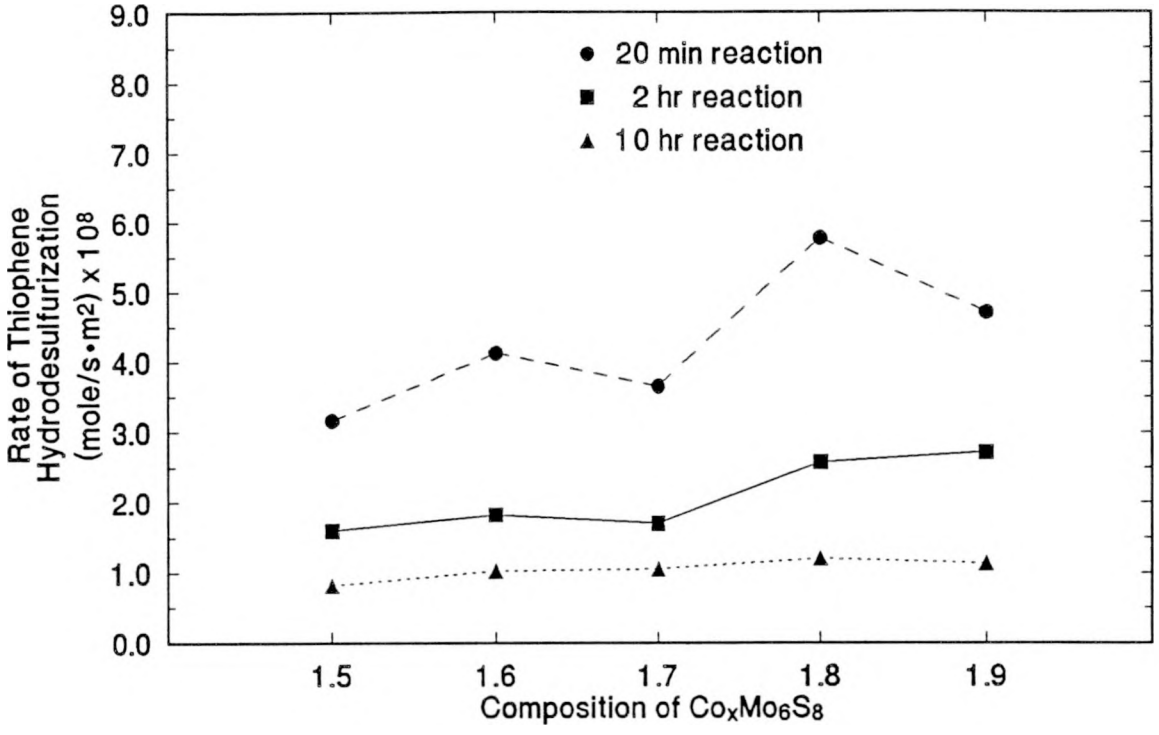


Figure 7. HDS activities of cobalt Chevrel phases [10]

Table 8 summarizes the results of the 1-butene HYD measurements for the Chevrel phases and for the model $MoS_2$-based materials. The activities were calculated as the rate of production of *n*-butane normalized to the surface area of the fresh catalysts. HYD activities are reported for three different times: (A) fresh catalyst, (B) after 25 $H_2$–thiophene pulses, and (C) after 2-h continuous-flow thiophene reaction. All Chevrel phases have HYD activities much lower than the unpromoted and cobalt-promoted $MoS_2$ catalysts (from about 7 to 30 times lower for the fresh catalysts and to between 2 and 10 times lower after 2 h of thiophene reaction). The ratio of HDS to

Table 8. 1-Butene hydrogenation (HYD) activities (400°C)

| Catalyst | | HYD rate ($mol/s \cdot m^2$) $\times 10^9$ | $C_4$ product distribution (%) | | | |
|---|---|---|---|---|---|---|
| | | | *n*-butane | 1-butene | *trans*-2-butene | *cis*-2-butene |
| Large cation compounds | | | | | | |
| $Ho_{1.2}Mo_6S_8$ | A | 3.00 | 0.06 | 90.5 | 4.6 | 4.8 |
| | B | 2.00 | 0.05 | 93.3 | 3.2 | 3.4 |
| | C | 3.00 | 0.06 | 31.2 | 38.6 | 30.1 |
| $Dy_{1.2}Mo_6S_8$ | A | 0.00 | 0.00 | 84.8 | 7.3 | 7.9 |
| | B | 0.69 | 0.02 | 75.1 | 12.2 | 12.6 |
| | C | 1.03 | 0.03 | 29.1 | 39.8 | 31.0 |
| $La_{1.2}Mo_6S_8$ | A | 0.53 | 0.02 | 69.3 | 16.0 | 14.6 |
| | B | 1.06 | 0.04 | 50.7 | 26.5 | 22.6 |
| | C | 0.79 | 0.03 | 53.8 | 24.5 | 21.6 |
| $Lu_{1.2}Mo_6S_8$ | A | 0.23 | 0.03 | 91.7 | 3.5 | 4.7 |
| | B | 0.38 | 0.05 | 92.8 | 3.1 | 4.0 |
| | C | 0.91 | 0.12 | 62.3 | 20.4 | 17.1 |
| $Lu_{0.8}Pb_{0.33}Mo_6S_8$ | A | 0.28 | 0.03 | 89.2 | 5.1 | 5.7 |
| | B | 0.09 | 0.01 | 88.6 | 5.5 | 5.8 |
| | C | 0.83 | 0.09 | 59.6 | 21.5 | 18.8 |
| $Lu_{0.4}Pb_{0.67}Mo_6S_8$ | A | 0.22 | 0.01 | 74.8 | 12.6 | 12.6 |
| | B | 0.66 | 0.03 | 61.6 | 19.9 | 18.5 |
| | C | 0.88 | 0.04 | 54.3 | 24.1 | 21.5 |
| $Lu_{0.1}PbMo_6S_8$ | A | 0.00 | 0.00 | 93.7 | 3.4 | 2.9 |
| | B | 0.00 | 0.00 | 86.9 | 6.9 | 6.2 |
| | C | 0.00 | 0.00 | 88.3 | 5.3 | 6.4 |
| $PbMo_{6.2}S_8$ (prep. I) | A | 2.00 | 0.03 | 90.5 | 4.6 | 4.8 |
| | B | 2.00 | 0.03 | 93.3 | 3.2 | 3.4 |
| | C | 2.00 | 0.03 | 31.2 | 38.6 | 30.1 |
| $PbMo_{6.2}S_8$ (prep. II) | A | 0.24 | 0.01 | 89.1 | 5.6 | 5.3 |
| | B | 0.24 | 0.01 | 59.5 | 21.8 | 18.6 |
| | C | 1.20 | 0.05 | 46.2 | 28.6 | 25.2 |

Table 8. (*continued*)

| Catalyst | | HYD rate (mol/s • $m^2$) × $10^9$ | $C_4$ product distribution (%) | | | |
|---|---|---|---|---|---|---|
| | | | *n*-butane | 1-butene | *trans*-2-butene | *cis*-2-butene |
| $Pb_{0.92}Mo_6S_8$ | A | 3.00 | 0.08 | 69.3 | 16.2 | 14.4 |
| | B | 7.00 | 0.19 | 39.3 | 33.9 | 26.6 |
| | C | 2.00 | 0.06 | 41.4 | 32.1 | 26.4 |
| $SnMo_{6.2}S_8$ | A | 1.00 | 0.05 | 47.0 | 27.9 | 25.0 |
| | B | 1.00 | 0.04 | 39.3 | 32.5 | 28.1 |
| | C | 1.00 | 0.06 | 46.6 | 27.8 | 25.5 |
| Small cation compounds | | | | | | |
| $Co_{1.7}Mo_6S_8$ | A | 1.00 | 0.06 | 47.4 | 26.4 | 26.1 |
| | B | 2.00 | 0.09 | 40.9 | 29.5 | 29.5 |
| | C | 1.00 | 0.06 | 46.1 | 29.7 | 24.1 |
| Model $MoS_2$ compounds | | | | | | |
| $Co_{0.25}$–$Mo_1$–S | A | 26.0 | 0.76 | 32.7 | 38.0 | 28.5 |
| | B | 11.0 | 0.33 | 39.2 | 33.9 | 26.5 |
| | C | 7.1 | 0.21 | 45.6 | 30.0 | 24.2 |
| 1000°C $MoS_2$ | A | 23.0 | 2.05 | 23.6 | 42.9 | 31.4 |
| | B | 24.0 | 2.08 | 23.9 | 42.6 | 31.4 |
| | C | 7.5 | 0.66 | 44.0 | 30.0 | 25.3 |
| Calculated butene equilibrium at 400°C[a] | | | | 26.5 | 43.5 | 30.0 |

A = fresh catalyst; B = after 25 $H_2$–thiophene pulses; C = after 2-h continuous $H_2$–thiophene reaction

[a]See reference 29.

HYD activities after 2 h of continuous thiophene reaction is 39.5 for $Ho_{1.2}Mo_6S_8$, 12.8 for $Co_{1.7}Mo_6S_8$, 7.6 for $Co_{0.25}$–$Mo_1$–S, and 2.3 for 1000°C $MoS_2$.

The catalysts also show large variations in their ability to isomerize the 1-butene pulses to a mixture of 1-butene, *trans*-2-butene, and *cis*-2-butene. For example, after 2 h of continuous thiophene reaction, 46.1% of the 1-butene is not isomerized by $Co_{1.7}Mo_6S_8$, compared to 29.1% for $Dy_{1.2}Mo_6S_8$. At thermodynamic equilibrium for the $C_4$–mono-olefins (400°C), 26.5% 1-butene should be observed [29]. $Lu_{0.1}PbMo_6S_8$ demonstrated no ability to convert 1-butene to *n*-butane under the reaction conditions.

# DISCUSSION OF RESULTS

Thiophene HDS activities of the Chevrel phases are comparable to—or greater than—those of the model unpromoted and cobalt-promoted $MoS_2$-based catalysts. Comparisons between all catalysts are regarded as being approximate only, even though activities have been normalized to the surface areas. Correlations between total surface area and HDS activity have been shown to be inadequate for some catalysts [30]. More definite comparisons can perhaps be made within the isostructural groups of Chevrel phases because of the similarity in surface areas.

The activities of the Chevrel phases for thiophene HDS can be grouped according to their structural classification, as reported previously [9–10]. Large cation compounds are generally more active than intermediate cation compounds. Small cation compounds are generally the least active Chevrel phases. Also, the cobalt (and nickel [9]) Chevrel phases are among the least active materials, even though cobalt and nickel are widely used as promoters in conventional HDS catalysts. The most active thiophene HDS catalysts incorporate unusual "promoters," such as holmium, dysprosium, lead, and tin. Figure 8 illustrates the rate of thiophene HDS for several rare earth "promoted"

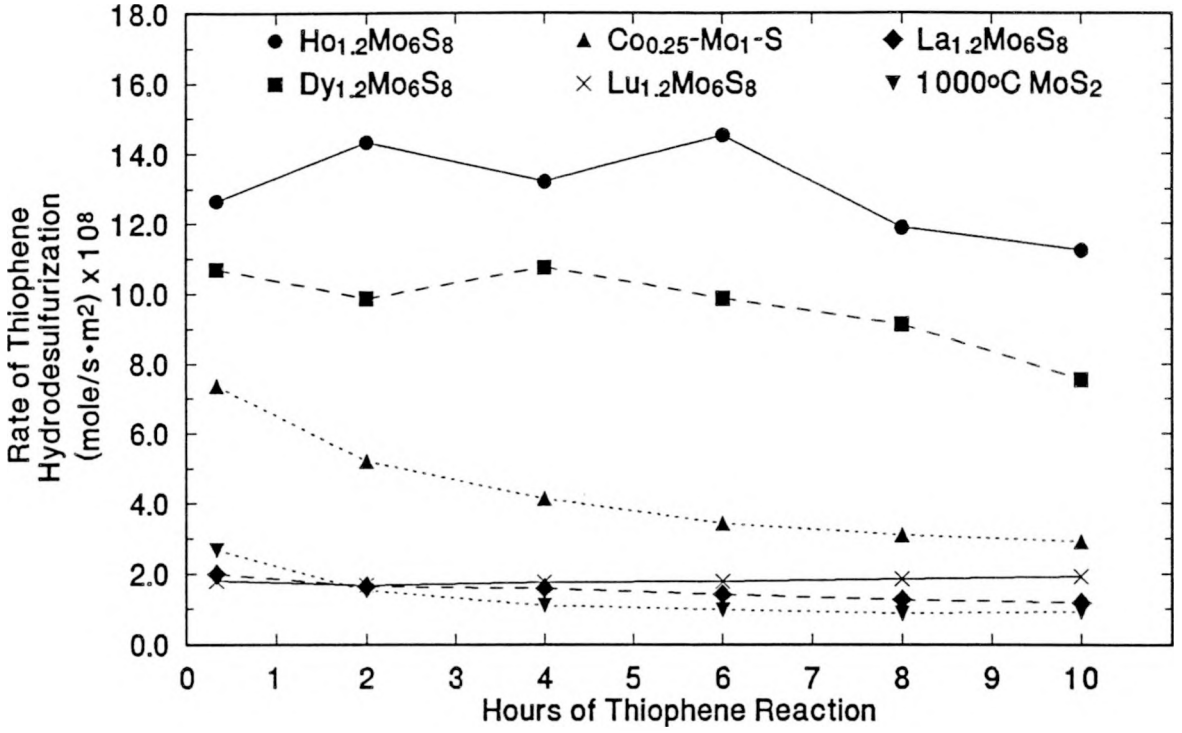


Figure 8. HDS activities of rare earth Chevrel phases

Chevrel phases, as well as data for the model $MoS_2$-based catalysts. After 10 h of thiophene reaction, the rare earth containing materials exhibit thiophene HDS activities comparable to, or much greater than, the model $MoS_2$-based catalysts.

The bulk structure of the Chevrel phases has been demonstrated to be stable using X-ray diffraction and laser Raman spectroscopy analysis. No loss of crystallinity or formation of other phases was detected with X-ray diffraction. X-ray diffraction detected crystalline $MoS_2$ in $SnMo_6S_8$, but none was detected in other fresh or used Chevrel phase catalysts. With the exception of the $Co_xMo_6S_8$ materials, no poorly-crystalline $MoS_2$ was detected by laser Raman spectroscopy.

Utilization of the Chevrel phases as catalysts permits reduced molybdenum oxidation states to be examined directly. For the large cation compounds, the XPS data indicated that molybdenum underwent no apparent oxidation under reaction conditions. $Pb_{0.92}Mo_6S_8$ and $Lu_{0.4}Pb_{0.67}Mo_6S_8$ underwent slight reduction following thiophene reaction. For the $Co_xMo_6S_8$ materials, surface oxidation of molybdenum after 10 h of thiophene HDS was accompanied by the formation of $MoS_2$ (as detected by laser Raman spectroscopy). From studies of other small cation materials in addition to those reported here, it has been established that the large cation materials generally are more stable with respect to surface oxidation of molybdenum than the small cation materials [9–10].

For the $Co_xMo_6S_8$ series, oxidation of the surface molybdenum was accompanied by a loss of the ternary component from the surface (Table 2). $Lu_{1.2}Mo_6S_8$ (Table 2) and the lead–lutetium series materials (Table 4) demonstrate a surface enrichment by lutetium after thiophene reaction. However, lead and tin Chevrel phases exhibit no change in the concentration of the ternary component at the surface.

The movement of the ternary metal is related to the ''delocalization'' of ternary atoms from their crystallographic positions in the Chevrel phase structures. The degree of delocalization is small for the large cation compounds and large for the small cation materials [17]. Thus, under HDS conditions, the ternary component of the small cation materials can ''retreat'' into the bulk structure [9–10]. The low mobility of the ternary component of the large cation materials inhibits possible movement under HDS conditions.

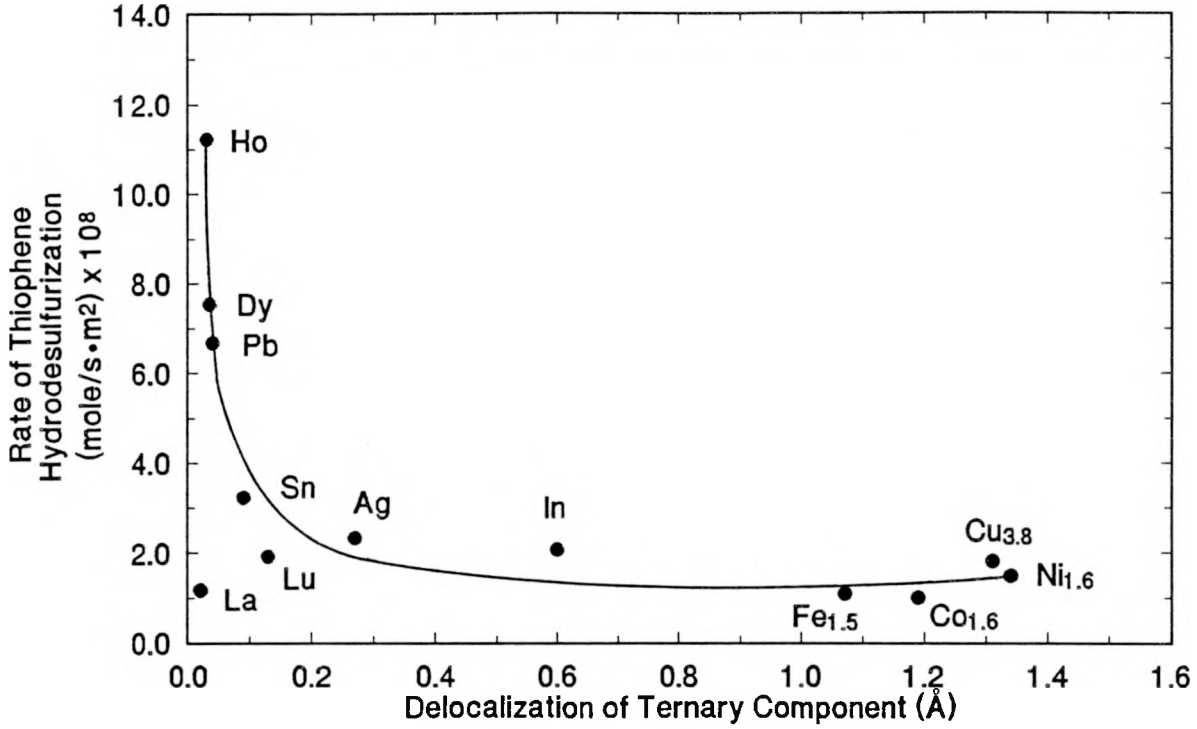


Figure 9. HDS activities (10-h thiophene reaction) versus delocalization of ternary component (adapted from [10])

Figure 9 illustrates the relationship between the amount of ternary metal delocalization and thiophene HDS after 10-h thiophene reaction: the more immobile the ternary component is in the Chevrel phase structure, the greater the long-term catalytic activity [10]. This relationship may provide a method for predicting the activities of other Chevrel phase materials. This relationship is not valid, however, for $La_{1.2}Mo_6S_8$. The low HDS activity of $La_{1.2}Mo_6S_8$ is unexpected and not completely understood.

These generalized observations may be explained by considering the stabilization effects of the ternary metals in the Chevrel phase structures. For example, the binary

compound $Mo_6S_8$ cannot be prepared directly from the elements but must be formed by leaching the ternary component from a small cation compound. Ternary Chevrel phases are stable at high temperatures (with melting points of about 1700°C) [23]. $Mo_6S_8$ decomposes at about 400°C [31] and forms large amounts of $MoS_2$ after thiophene reaction at temperatures as low as 300°C [9]. Ternary metals involved in little delocalization from their positions in the Chevrel phase structures may be capable of stabilizing the catalytically active sites.

The investigation of various stoichiometries for lead, tin and lead–lutetium Chevrel phases displayed some interesting features. A small change in the stoichiometry of the lead Chevrel phase changed the activity little [10]. As shown in Figure 4, similar continuous-flow thiophene HDS activities were found for $Pb_{0.92}Mo_6S_8$ (Pb/Mo = 0.153) and $PbMo_{6.2}S_8$ (Pb/Mo = 0.161). However, as illustrated in Figure 5, changes in the nominal composition of the tin Chevrel phases had a more dramatic effect on the catalytic activity [10]. $SnMo_6S_8$ (Sn/Mo =0.167) (contaminated with $MoS_2$), had a higher activity than $SnMo_{6.2}S_8$ (Sn/Mo = 0.161). Both of these materials were significantly more active than $Sn_{1.2}Mo_6S_8$ (Sn/Mo = 0.200).

The lead–lutetium Chevrel phases also demonstrate large differences in thiophene HDS activity with variations in composition (Figure 6). It is thought that these differences in catalytic activity due to variations in stoichiometry are the result of changes in bulk and surface properties, such as migration of the ternary components with their subsequent electronic effects. Changes in structural properties of the Chevrel

phases may also be important. For example, decreasing the lutetium concentration (increasing the lead concentration) has the effect of increasing the unit cell volume. For this series of compounds, the highest thiophene HDS activity is observed for the material with the largest unit cell volume.

A comparison of the effects of the preparation method on catalyst stability and activity is also of interest. Lead Chevrel phases were synthesized by preparation method I and method II to allow a direct comparison. For Chevrel phases prepared by only one method, comparisons are only indirect. The preparation method used for each catalyst is listed in Table 5.

The most readily apparent difference between the lead Chevrel phases is their surface area. $PbMo_{6.2}S_8$ (method I) has significantly lower surface area (0.400 $m^2/g$) than $PbMo_{6.2}S_8$ (method II) (1.318 $m^2/g$ fresh catalyst and 1.664 $m^2/g$ after 10-h reaction). The surface areas of all Chevrel phases prepared by method II increase after 10 h of thiophene HDS. The surface areas of all Chevrel phases prepared by method I (with the exception of $SnMo_6S_8$) change less than 10% after 10 h of thiophene reaction. The reasons for these effects are unexplained at this time. For example, $PbMo_{6.2}S_8$ (method I) and $PbMo_{6.2}S_8$ (method II) have essentially identical molybdenum 3*d* XPS binding energies (Table 2) indicating the same low oxidation state of molybdenum is present in each sample. Furthermore, the molybdenum 3*d* binding energies do not shift after 10 h of continuous thiophene reaction for either compound.

The benzothiophene studies indicate that at 400°C, $PbMo_{6.2}S_8$ (method II) has a

lower activity for benzothiophene HDS than for thiophene HDS (Table 7). This is not an unexpected result since benzothiophene is, in general, more difficult to desulfurize than thiophene [32]. Even so, it has been suggested that benzothiophene is actually a better model for the study of HDS processes, since it and its derivatives are usually the most predominant type of thiophenic compounds found in crude oils and coal liquids [33].

Although possessing high thiophene HDS activities, Chevrel phase compounds exhibit 1-butene HYD activities which are much lower than the model unpromoted and cobalt-promoted $MoS_2$ catalysts. This result has been reported previously for other Chevrel phases [7–10,14]. The 1-butene HYD activity experiments also provide a measure of the isomerization activity of the Chevrel phases. The ability of the Chevrel phases to isomerize 1-butene is usually reflected in the butene distributions which result from thiophene HDS. For example, $Ho_{1.2}Mo_6S_8$ produces 32% 1-butene after 2 h of thiophene reaction, while 31% of the 1-butene feed is not isomerized during the 1-butene HYD activity measurements. Similarly, $La_{1.2}Mo_6S_8$ produces 46% 1-butene from thiophene and 54% 1-butene from the 1-butene–hydrogen feed. Kolboe and Amberg [34] showed that for HDS of thiophene over $MoS_2$ catalysts, the relative concentrations of the butenes departs from equilibrium. If 1-butene were the initial product of thiophene HDS, then 1-butene should be more readily observed for low conversions. Catalysts with little isomerization activity could also produce larger amounts of 1-butene.

The selectively of the Chevrel phases is also of interest regarding cracking products. Chevrel phases produce no detectable concentrations of cracking products from 1-butene [7–8,10]. This is in sharp contrast to the model unpromoted and promoted $MoS_2$-based catalysts.

# CONCLUSIONS

Chevrel phases possess a rich solid state chemistry which permits the relationship between catalysis and structure, composition, and oxidation state to be examined. The vast majority of Chevrel phases which have been examined have significant catalytic activity for thiophene HDS. The broad range of "promoter" metals which may be used is remarkable. However, there are substantial differences in relative activities of the Chevrel phases. An important factor affecting catalytic activity appears to be structurally dependent. This is evidenced by the large cation Chevrel phases which permit little cation movement. This appears to also result in extended catalyst stability. Loss of ternary components from the surface of the catalysts leads to surface oxidation resulting in a decrease in the "metallic" nature of the catalysts or destabilization to form $MoS_2$ (or both). A unique and apparently advantageous aspect of these Chevrel phases is the "reduced" oxidation state of molybdenum. The ability to systematically vary this oxidation state is an important property of Chevrel phase catalysts and has been the subject of other work [14].

# ACKNOWLEDGMENTS

This work was conducted through the Ames Laboratory which is operated for the U. S. Department of Energy by Iowa State University under Contract W–7405–Eng–82. This research was supported by the Office of Basic Energy Sciences, Chemical Sciences Division. XPS spectra were obtained by J. W. Anderegg of the Ames Laboratory.

# REFERENCES


1. Weisser, O., and Landa, S., "Sulphide Catalysts, Their Properties and Applications." Permagon, Oxford, 1973.

2. Gates, B. C., Katzer, J. R., and Schuit, G. C. A., "Chemistry of Catalytic Processes." McGraw–Hill, New York, 1979.

3. Delmon, B., *in* "Proceedings of the Climax Third International Conference on Chemistry and Uses of Molybdenum" (H. F. Barry and P. C. H. Mitchell, Eds.), p. 73. Climax Molybdenum Co., Ann Arbor, MI, 1979.

4. Ratnasamy, P., and Sivasanker, S., *Catal. Rev.–Sci. Eng.* **22**, 401 (1980).

5. Topsøe, H., and Clausen, B. S., *Catal. Rev.–Sci. Eng.* **26**, 395 (1984).

6. Topsøe, H., Clausen, B. S., Topsøe, N.-Y., and Pedersen, E., *Ind. Eng. Chem. Fund.* **25**, 25 (1986).

7. McCarty, K. F., and Schrader, G. L., *in* "Proceedings, 8th International Congress on Catalysis, Berlin, 1984" (E. Ertl, Ed.), Vol. IV, p. 427. Dechema, Frankfurt-am-Main, 1984.

8. McCarty, K. F., and Schrader, G. L., *Ind. Eng. Chem. Prod. Res. Dev.* **23**, 519 (1984).

9. McCarty, K. F., Anderegg, J. W., and Schrader, G. L., *J. Catal.* **93**, 375 (1985).

10. McCarty, K. F., Ph.D. Dissertation, Iowa State University, Ames, Iowa, 1985.

11. McCarty, K. F., and Schrader, G. L., *J. Catal.* **103**, 261 (1987).

12. Konings, A. J. A., Valster, A., de Beer, V. H. J., and Prins, R., *J. Catal.* **76**, 466 (1982).

13. Valyon, J., and Hall, W. K., *J. Catal.* **84**, 216 (1983).

14. Ekman, M. E., Anderegg, J. W., and Schrader, G. L., *J. Catal.* **117**, 246 (1989).

15. Huckett, S. C., Angelici, R. J., Ekman, M. E., and Schrader, G. L., *J. Catal.* **113**, 36 (1988).

16. Chevrel, R., Sergent, M., and Prigent, J., *J. Solid State Chem.* **3**, 515 (1971).

17. Yvon, K., *in* "Current Topics in Materials Science" (E. Kaldis, Ed.), Vol. 3, p. 53. North-Holland, Amsterdam, 1979.

18. Chevrel, R., and Sergent, M., *in* "Topics in Current Physics" (Ø. Fischer and M. B. Maple, Eds.), Vol. 34, p. 25. Springer-Verlag, Berlin, 1982.

19. Chevrel, R., Hirrien, M., and Sergent, M., *Polyhedron* **5**, 87 (1986).

20. Peña, O., and Sergent, M., *Prog. Solid St. Chem.* **19**, 165 (1989).

21. Tarascon, J. M., DiSalvo, F. J., Murphy, D. W., Hull, G. H., Rietman, E. A., and Waszczak, J. V., *J. Solid State Chem.* **54**, 204 (1984).

22. Fischer, Ø., Treyvaud, A., Chevrel, R., and Sergent, M., *Solid State Comm.* **17**, 721 (1975).

23. Flükiger, R., and Baillif, R., *in* "Topics in Current Physics" (Ø. Fischer and M. B. Maple, Eds.), Vol. 34, p. 113. Springer-Verlag, Berlin, 1982.

24. Lynn, J. W., Shirane, G., Thomlinson, W., Shelton, R., and Moncton, D. E., *Phys. Rev. B* **24**, 3817 (1981).

25. Wildervanck, J. C., and Jellinek, F. Z., *Anorg. Chem.* **328**, 309 (1964).

26. Candia, R., Clausen, B. S., and Topsøe, H., *Bull. Soc. Chim. Belg.* **90**, 1225 (1981).

27. Wieting, T. J., and Verble, J. L., *Phys. Rev. B* **3**, 4286 (1971).

28. Li, C. P., and Hercules, D. M., *J. Phys. Chem.* **88**, 456 (1984).

29. Benson, S. W., and Bose, A. W., *J. Amer. Chem. Soc.* **85**, 1385 (1963).

30. Tauster, S. J., Pecoraro, T. A., and Chianelli, R. R., *J. Catal.* **63**, 515 (1980).

31. Cheung, K. Y., and Steele, B. C. H., *Solid State Ionics* **1**, 337 (1980).

32. Kilanowski, D. R., and Gates, B. C., *J. Catal.* **62**, 70 (1980).

33. Singhal, G. H., Espino, R. L., and Sobel, J. E., *J. Catal.* **67**, 446 (1981).

34. Kolboe, S., and Amberg, C. H., *Can. J. Chem.* **44**, 2623 (1966).

# SECTION II.

# REDUCED MOLYBDENUM FORMAL OXIDATION STATES IN HYDRODESULFURIZATION CATALYSIS BY CHEVREL PHASES

# ABSTRACT

The effect of the oxidation state of molybdenum on the catalytic hydrodesulfurization (HDS) of thiophene was investigated using a series of lead–lutetium Chevrel phases. Polycrystalline catalysts were prepared with compositions of $PbMo_{6.2}S_8$, $Lu_{1.2x}PbMo_6S_8$ for $0 < x \leq 0.2$, and $Lu_{1.2x}Pb_{1-x}Mo_6S_8$ for $0.2 < x \leq 1$. Fresh and used (10-hour thiophene reaction) catalysts were characterized by X-ray powder diffraction, laser Raman spectroscopy, and X-ray photoelectron spectroscopy. Bulk structures and molybdenum oxidation states were found to be stable. HDS activity could be related to the molybdenum formal oxidation state: the maximum rate of thiophene HDS was observed for catalysts having "reduced" oxidation states (compared to $MoS_2$). All Chevrel phase catalysts demonstrated low activity for 1-butene hydrogenation.

# INTRODUCTION

Typical industrial catalysts used in hydrodesulfurization (HDS) processes are prepared from alumina-supported ($\gamma$–$Al_2O_3$) molybdenum ($Mo^{6+}$) oxides which are promoted with cobalt or nickel to improve catalytic activity [1–3]. The oxides become sulfided and reduced under catalytic reaction conditions. The presence of a $MoS_2$ ($Mo^{4+}$) phase has been demonstrated by various researchers using techniques such as X-ray photoelectron spectroscopy (XPS) [4–6], EXAFS [7], X-ray diffraction [8], and laser Raman spectroscopy [9]. Numerous studies of unsupported HDS catalysts have also been performed in an attempt to model supported materials. XPS has revealed that $MoS_2$ is formed from cobalt–molybdenum–oxygen catalysts after treatment at 400°C with $H_2$/thiophene or $H_2/H_2S$ [10]. $MoS_2$ is an active HDS catalyst with properties similar to those of supported catalysts [11]. Topsøe *et al.* [12] have reported the existence of a cobalt–molybdenum–sulfide (Co–Mo–S) phase in both supported and unsupported molybdenum HDS catalysts, determined from Mössbauer emission spectroscopy. This phase is proposed to be the active material involved in industrial HDS catalysts, based on the existence of a linear relationship between the amount of

cobalt in the Co–Mo–S phase and catalytic activity [2]. The phase is considered to be a $MoS_2$-like material in which promoter atoms occupy crystallite edge positions [13].

The role of "reduced" molybdenum oxidation states (lower than the +4 state of $MoS_2$) in HDS has not been clearly established. Several techniques have been used to investigate the nature of the active molybdenum species. For example, XPS measurements for unsupported sulfided cobalt–molybdenum catalysts have demonstrated a decrease in the molybdenum 3*d* binding energies for cobalt concentrations corresponding to the greatest promotional effect for thiophene HDS [14]. From this information, it was postulated that reduced molybdenum species with a charge between +3 and +4 are associated with the active sites. Alstrup *et al.* [15] have also used XPS to study supported and unsupported cobalt–molybdenum catalysts. They found a close similarity between the cobalt 2*p* spectra of Co–Mo–S and $CoMo_2S_4$. This suggests that the electronic state of cobalt in Co–Mo–S is similar to that in $CoMo_2S_4$ (which has a formal molybdenum oxidation state of +3). The two phases are structurally different, however.

Other investigators have deduced the presence of $Mo^{3+}$ and $W^{3+}$ species on supported and unsupported cobalt–molybdenum–, nickel–molybdenum–, and nickel–tungsten–sulfide catalysts using electron paramagnetic resonance (EPR) techniques. Voorhoeve [16] used EPR in the investigation of the hydrogenation of benzene using $WS_2$ catalysts. He concluded that the active centers were $W^{3+}$ ions. Konings *et al.* [17] have observed a correlation between the intensity of an EPR signal

attributed to $Mo^{3+}$ and the rate of thiophene HDS for supported cobalt-promoted molybdenum catalysts. Similarly, Thakur and Delmon [18] investigated unsupported promoted molybdenum and tungsten catalysts and detected the presence of $Mo^{3+}$and $W^{3+}$ species: catalysts having the highest EPR signal also had the greatest HDS activity.

Adsorption studies have also been performed to characterize reduced molybdenum oxidation states on HDS catalysts. Bachelier *et al.* [19] and others (for example [20–22]) have demonstrated a relationship between the chemisorption of $O_2$, CO, or NO and HDS activity. A study of the chemisorption of $O_2$ and NO on a reduced and sulfided supported molybdenum catalyst was interpreted as chemisorption on $Mo^{2+}$ centers [23]. Site-selective adsorption of CO has been proposed to occur on highly reduced molybdenum sites for both $Mo/\gamma-Al_2O_3$ [24] and $Co-Mo/\gamma-Al_2O_3$ catalysts [25]; these reduced sites were associated with HDS activity. Peri [26] reported CO and NO adsorption studies for supported molybdenum catalysts and interpreted the results as indicating the presence of exposed $Mo^{3+}$ or $Mo^{2+}$ sites. Laine *et al.* [27] explained their observations for NO adsorption on supported molybdenum catalysts promoted with both cobalt and nickel in terms of a minor reduction of molybdenum below the +4 oxidation state.

The complexity of the typical industrial catalysts—and even the uncertainties associated with unsupported catalysts—has made identification of reduced molybdenum oxidation states difficult. Due to the presence of a large amount of $MoS_2$ (or other

related phases with predominantly $Mo^{4+}$ oxidation states) in these catalysts, the role of reduced molybdenum states has been difficult to study.

Theoretical investigations, however, have indicated that reduced molybdenum oxidation states are involved as the active sites in HDS. Duben [28] has provided support for the existence of an active $Mo^{3+}$ species using simple Hückel theory. According to his calculations, this oxidation state would be the most effective for carbon–sulfur bond breaking and would allow for easy removal of the surface bound sulfur atom to regenerate the active site. Harris [29–30] and Harris and Chianelli [31–32] have discussed molecular-orbital calculations for the electronic structures of $MS_6^{n-}$clusters ($M$ = first- and second-row transition metals) and promoted molybdenum clusters, $M'MoS_9^{m-}$($M'$ = first-row transition-metal promoters, V–Zn). Calculated trends in electronic factors and bonding were related to dibenzothiophene HDS activity to establish an electronic explanation for catalytic activity. Promoters such as cobalt or nickel transfer electrons to molybdenum, reducing the molybdenum formal oxidation state relative to $MoS_2$. For a cluster containing copper (a metal which poisons the activity of $MoS_2$-based catalysts), molybdenum is oxidized relative to $MoS_2$.

In recent years, the results of HDS studies with reduced molybdenum sulfides known as Chevrel phases have been reported [33–39]. Chevrel *et al.* [40] reported the initial synthesis and characterization of these ternary molybdenum chalcogenides in 1971. Chevrel phases have a general formula $M_xMo_6Z_8$, with $Z$ being sulfur, selenium, or tellurium and with $M$ being a ternary metal component. The Chevrel phase structure

can be described as a stacking of $Mo_6Z_8$ building blocks or clusters. The ternary metal cations are incorporated in channels or voids created by the chalcogen atom network. When *M* is a large cation, such as Pb or Sn, a second component, such as a rare earth (*RE*), may be incorporated to produce a series of compounds with nominal formulas $RE_xM_{1-x}Mo_6Z_8$. Extensive reviews concerning Chevrel phases have been provided [41–44]. Chevrel phases have been shown to have high activity for thiophene HDS [33–36,39]. The solid state chemistry of Chevrel phases offers an opportunity to investigate the effect of the oxidation state of molybdenum on HDS activity. Direct preparation of catalysts with reduced molybdenum oxidation states (compared to $MoS_2$) is possible. The formal oxidation state of molybdenum can be varied by using Chevrel phases with different compositions or ternary elements or both. The results reported in this section evaluate a series of lead–lutetium Chevrel phase catalysts.

# EXPERIMENTAL METHODS

## Catalyst Preparation

The Chevrel phases were prepared by solid state synthesis from mixtures of: 200 mesh powdered molybdenum metal (Alfa, m3n+, t2n7) reduced with hydrogen (20 ml/min) in a tube furnace (Lindberg, model 54231) at 1000°C for 18 h; sulfides of lead (Alfa, m5n+) and lutetium (Ames Lab rare earth group) (PbS and $Lu_2S_3$, respectively) which were made by direct combination of the elements in evacuated, fused-silica tubes; and sulfur (Alfa, t5n5). The mixtures were ground together thoroughly, pressed into 13-mm pellets with 10,000 lbs total force (Perkin Elmer die, model 186–0025), and sealed in pre-baked evacuated fused-silica tubes back-filled with argon to 20-in Hg vacuum. The tubes were heated slowly in a muffle furnace (Central Scientific, model Hoskins FD202C) from 450 to 750°C over a period of 48–72 h, transferred immediately to a high-temperature box furnace (Lindberg, model 51333) at 1200°C for 24 h, and quenched in air. The materials were reground in air, pressed into pellets, and reheated for 48 h at 1225°C. After the final heating, the tubes were opened in a nitrogen dry box where the pellets were lightly crushed. The 40–100 mesh portion was separated for

use in the activity measurements, and a small amount was reserved for XPS analysis. All subsequent manipulations of the catalysts were performed in the dry box.

Some differences concerning the exact stoichiometries necessary to obtain pure single phases of these materials exist in the literature. The content of the ternary element *M* is reported to be variable (*e.g.*, $M_{1.0}Mo_6S_8$ and $M_{1.2}Mo_6S_8$ for the rare earth materials); the stoichiometric ratio of molybdenum to sulfur can also deviate from the "ideal" value of 6/8. Chevrel phases prepared at a nominal composition of $M_{1.2}Mo_6S_8$ may be multiphasic, having a predominance of $MMo_6S_8$ with very small amounts of $MoS_2$, $Mo_2S_3$, and *M*-sulfides which cannot be detected by X-ray diffraction [45].

Homogeneous polycrystalline samples were obtained for compositions prepared at $Lu_{1.2x}PbMo_6S_8$ for $0 < x \leq 0.2$ and at $Lu_{1.2x}Pb_{1-x}Mo_6S_8$ for $0.2 < x \leq 1$. A loss of lead is observed when $x$ is greater than 0.2, demonstrating that there is a limit of rare earth insertion [46]. It is necessary to prepare the lead compound with a composition of $PbMo_{6.2}S_8$ to obtain the purest single-phase material [47], containing about 1 wt% $MoO_2$ and less than 1 wt% of other impurities ($MoS_2$, $Mo_2S_3$) [48].

## Catalyst Characterization

The catalysts were characterized before and after 10 h of continuous thiophene reaction.

The surface areas of the catalysts were determined by the BET method using a Micromeritics 2100E AccuSorb instrument. Krypton was used as the adsorbate at liquid

nitrogen temperature. A krypton atomic adsorption area of 21.0 $Å^2$ per krypton atom was assumed.

X-ray powder diffraction patterns were acquired with a Siemans D500 diffractometer using Cu$K\alpha$ radiation. The diffractometer was interfaced to a DEC PDP 11/23 computer. Samples were mounted on double-sided adhesive tape and scanned in the 2$\Theta$ range from 10 to 50 with a count of 1.0 s and step size of 0.04 2$\Theta$.

Laser Raman spectra were collected using a Spex 1403 double monochromator and a Spectra Physics argon ion laser operating at 514.5 nm and 200 mW measured at the source. A Nicolet 1180E data acquisition system was used to accumulate 50 scans at a scanning speed of 2 $cm^{-1}$/s with 5-$cm^{-1}$ resolution. The middle slits of the spectrometer were closed to 1000 microns to reduce the intensity of the Rayleigh line. Data were collected using backscattering geometry with 13-mm spinning catalyst pellets.

X-ray photoelectron spectra were obtained with an AEI 200B spectrometer using Al$K\alpha$ radiation. Signal averaging was performed using a Nicolet 1180 computer system. All spectra are referenced to a carbon 1*s* binding energy of 284.6 eV. Air contamination of the samples was avoided by opening all synthesis tubes and the reactor in a nitrogen dry box. Samples for XPS analysis were sealed inside Pyrex tubes, which were opened in a helium dry box attached directly to the spectrometer. Fresh catalyst samples were reserved immediately after the synthesis tubes were opened. Samples of used catalysts were obtained from a 40–100 mesh portion removed from the reactor with no further grinding.

## Activity Measurements

Hydrodesulfurization activities were measured at atmospheric pressure using a microreactor system, described in detail elsewhere [33–36]. The composition and flow rate of the gases fed to the 0.25-in stainless-steel reactor were controlled by mass flow controllers (Tylan, model FC–260). Thiophene (Alfa, 99%) was fed with a syringe pump (Sage, model 341). Catalyst loadings were adjusted to achieve less than 3% conversion of thiophene after 20 min of continuous reaction (ranging from 0.0795 g for $PbMo_{6.2}S_8$ to 0.4906 g for $Lu_{1.2}Mo_6S_8$). The reactor was heated from room temperature to 400°C in a flow of helium (Air Products Zero grade) at 19 ml/min (STP). After 1 h at 400°C with flowing helium, ten 0.25-ml pulses of 2 mol% thiophene in hydrogen (Air Products Zero grade) were injected into the reactor at 30-min intervals. A continuous flow of 2 mol% thiophene in hydrogen at 22 ml/min (STP) was used to determine steady-state activity. After 10 h of continuous reaction, the reactor was purged and cooled in a stream of helium.

Activity measurements for the hydrogenation (HYD) of 1-butene to *n*-butane were performed as described previously [33–36]. The reactor was filled with the same amount of fresh catalyst as in the HDS activity measurements and was heated from room temperature to 400°C in a flow of helium at 19 ml/min (STP). After it was held at 400°C in the stream of helium for about 1 h (fresh catalyst), two 0.10-ml pulses of 2 mol% 1-butene (Matheson, 99.0%) in hydrogen were injected into the reactor at 15-min intervals. Twenty-five 0.10-ml pulses of 2 mol% thiophene in hydrogen were then

injected into the reactor, and the 1-butene pulses were repeated. A continuous flow of thiophene in hydrogen for 2 h at 22 ml/min (STP) followed. The reactor was purged with helium, and the 1-butene pulses were repeated.

Product separation and analysis were performed using a 12-ft *n*-octane/Porasil C column and an Antek Model 310/40 ALP gas chromatograph equipped with a flame ionization detector. Peak areas were measured by a Hewlett–Packard 3390A integrator. Since *trans*-2-butene and 1,3-butadiene have the same retention times, these materials were combined in the data analysis.

# RESULTS

## Catalyst Characterization

A representative X-ray powder diffraction pattern of the catalysts used in this work is shown in Figure 1. The powder diffraction peaks were indexed on the basis of a rhombohedral unit cell. The data show $Lu_{0.1}PbMo_6S_8$ before and after 10 h of thiophene reaction with no apparent change in the X-ray pattern. This result was typical for all of the Chevrel phases studied, and indicates no loss in crystallinity and no formation of other phases or impurities.

Raman spectra could not be obtained for the Chevrel phases, but $MoS_2$ impurities can be detected using this technique. Raman spectroscopy is a sensitive probe for both crystalline and poorly crystalline $MoS_2$ (bands at 383 and 409 $cm^{-1}$) [49–50]. The Raman spectra for all of the Chevrel phases used in this study are devoid of any $MoS_2$ features, for fresh catalysts and for catalysts after 10 h of thiophene reaction.

Representative X-ray photoelectron spectra for the catalysts are shown in Figure 2 ($Lu_{1.2}Mo_6S_8$ before and after 10-h continuous-flow $H_2$–thiophene reaction). A nonlinear least-squares fitting program was used to analyze the spectra [51]. The

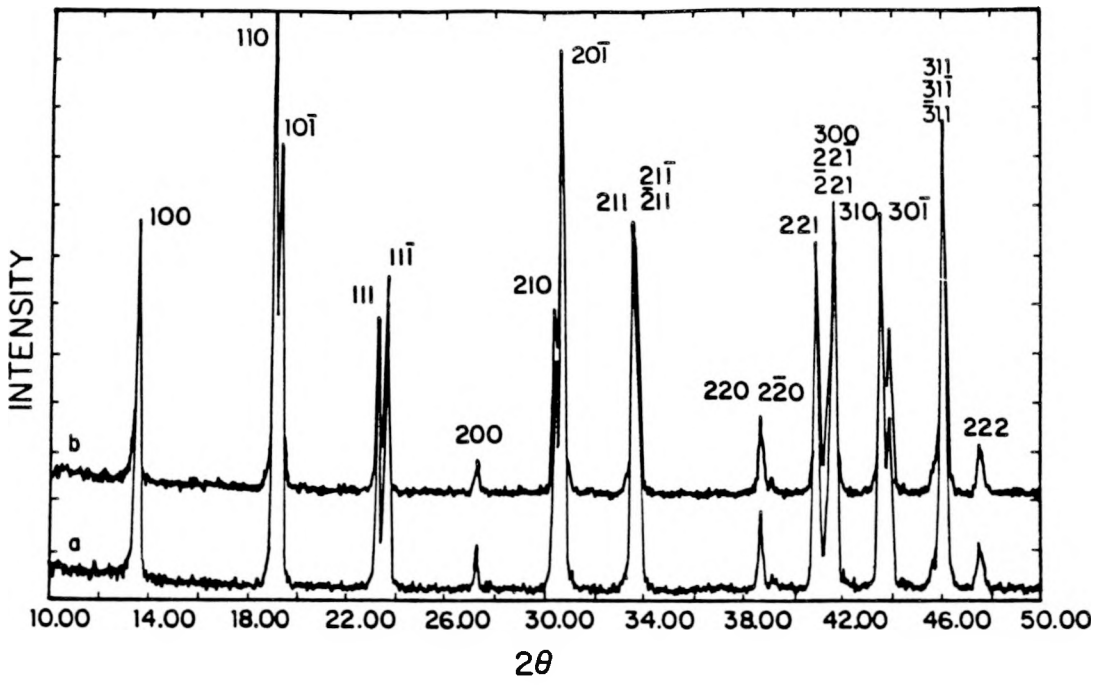


Figure 1. X-ray powder diffraction pattern of (a) fresh and (b) used (10-h thiophene reaction) $Lu_{0.1}PbMo_6S_8$ with rhombohedral *hkl* indexes

contribution of the sulfur 2*s* signal at lower binding energies (225.5 eV) was eliminated using this program. Two components with a peak separation between the molybdenum $3d_{3/2}$ and $3d_{5/2}$ lines of 3.2 eV were required to fit the molybdenum data region. The curve-fitting procedure revealed the presence of a small amount of a molybdenum-containing impurity with $3d_{3/2}$ and $3d_{5/2}$ binding energies of 234.6 and 231.4 eV, respectively. These binding energies are indicative of $MoO_2$ [52–53], which presumably was formed by the high-temperature reaction of the Chevrel phases with the fused-silica tubes [48]. Similarly, Swartz and Hercules have reported that the surface

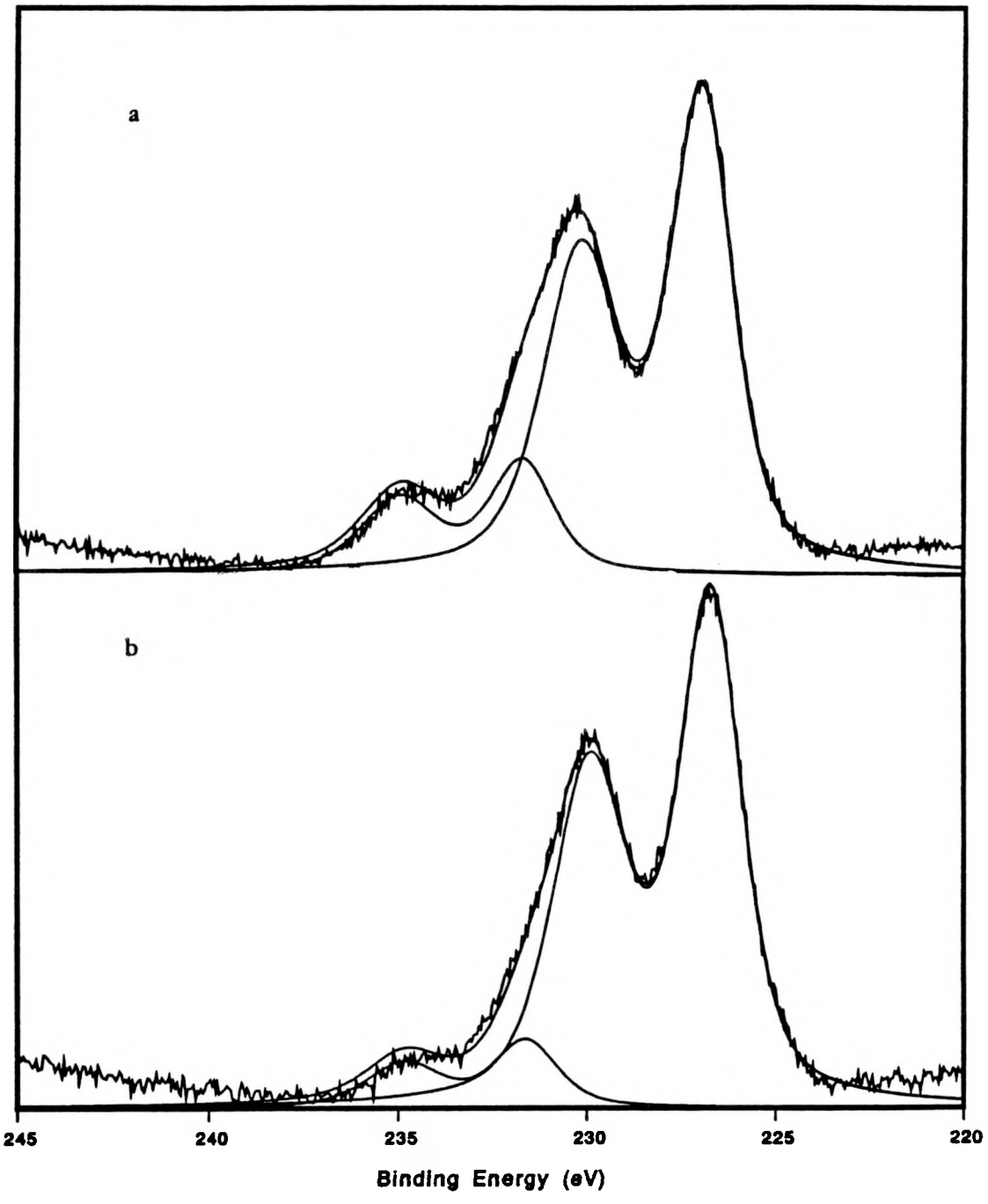


Figure 2. Molybdenum 3*d* XPS spectra of (a) fresh and (b) used (10-h thiophene reaction) $Lu_{1.2}Mo_6S_8$

oxidation of molybdenum powder results in the formation of $MoO_2$ rather than $MoO_3$ [52]. A comparison of the $MoO_2$ peaks for the fresh (Figure 2a) and used (Figure 2b) catalysts demonstrates that a decrease in signal intensity by a factor of 2 occurs. This trend was observed for all Chevrel phases examined in this study.

The XPS data for all catalysts are summarized in Table 1 and Table 2. The binding energies were calculated from the actual XPS data without the use of the curve-fitting procedure. For comparison, the $3d_{5/2}$ binding energy for $Mo^{4+}$ in $MoS_2$ is about 228.9 eV, and that for $Mo^{6+}$ is about 232.5 eV [4]. There were no significant shifts in the molybdenum 3*d* binding energies after 10-h continuous-flow $H_2$–thiophene reaction. Small shifts to lower binding energies (observed for only some of the catalysts) were due to the reduction of $MoO_2$. The molybdenum $3d_{5/2}$ binding energies for the fresh catalysts are grouped around 227.8 eV, ranging from 228.1 for $Lu_{0.4}Pb_{0.67}Mo_6S_8$ and $Lu_{0.1}PbMo_6S_8$ to 227.6 eV for $Lu_{0.8}Pb_{0.33}Mo_6S_8$. These results confirm the anticipated low oxidation states for molybdenum. Due to the presence of varying amounts of $MoO_2$ incorporated in the catalysts and the resultant peak broadening, the molybdenum $3d_{3/2}$–$3d_{5/2}$ peak separations varied slightly.

Table 2 shows the ratios of the raw peak areas for the lead 4*f* and lutetium 4*d* electrons compared to the molybdenum 3*d* electrons. These ratios are not intended to quantitatively reflect the surface compositions since they are not corrected for instrumental or atomic sensitivity factors. Rather, they are intended to indicate changes in the surface compositions which occur after thiophene reaction. The ratio of surface

Table 1. XPS binding energies

| Catalyst | | Binding energies (eV) | | | | | | |
|---|---|---|---|---|---|---|---|---|
| | | Mo | | Pb | | Lu | | S |
| | | $3d_{3/2}$ | $3d_{5/2}$ | $4f_{5/2}$ | $4f_{7/2}$ | $4d_{3/2}$ | $4d_{5/2}$ | $2p$ |
| $Lu_{1.2}Mo_6S_8$ | A | 231.1 | 227.7 | –[a] | –[a] | 207.0 | 197.2 | 161.8 |
| | B | 230.8 | 227.6 | –[a] | –[a] | 206.5 | 196.8 | 161.8 |
| $Lu_{0.8}Pb_{0.33}Mo_6S_8$ | A | 230.9 | 227.6 | 142.8 | 137.8 | 207.2 | 197.4 | 162.0 |
| | B | 230.8 | 227.6 | 142.6 | 137.9 | 207.0 | 197.4 | 162.2 |
| $Lu_{0.4}Pb_{0.67}Mo_6S_8$ | A | 231.4 | 228.1 | 142.5 | 137.6 | 207.3 | 197.6 | 161.9 |
| | B | 231.0 | 227.6 | 142.6 | 137.7 | 207.0 | 197.2 | 161.9 |
| $PbMo_{6.2}S_8$ | A | 231.1 | 227.7 | 143.3 | 138.6 | –[a] | –[a] | 162.3 |
| | B | 231.0 | 227.9 | 143.0 | 138.3 | –[a] | –[a] | 162.4 |
| $Lu_{0.1}PbMo_6S_8$ | A | 231.5 | 228.1 | 143.3 | 138.6 | –[b] | –[b] | 162.1 |
| | B | 231.1 | 227.8 | 142.8 | 138.0 | –[b] | –[b] | 162.1 |

A = fresh catalyst; B = after 10 h of continuous $H_2$–thiophene reaction

[a]Not applicable.
[b]Lu concentration too low to evaluate.

lead atoms to surface molybdenum atoms remained approximately the same under the reaction conditions. However, the ratio of surface lutetium atoms to surface molybdenum atoms increased significantly relative to the fresh catalysts after 10 h of thiophene reaction. The delocalization of the ternary atoms from their crystallographic positions in the Chevrel phase structure is related to the movement of the ternary metal. This delocalization is strong for small cations, resulting in high mobilities; in contrast large cations have low mobilities in the crystal lattice [43]. Lutetium atoms apparently migrate from the bulk to the surface of the catalyst under reaction conditions. Because

Table 2. XPS intensity ratios

| Catalyst | | Calculated ratios | | |
|---|---|---|---|---|
| | | Pb/Mo[a] | Lu/Mo[b] | S/Mo[c] |
| $Lu_{1.2}Mo_6S_8$ | A | –[d] | 0.17 | 0.33 |
| | B | –[d] | 0.19 | 0.31 |
| $Lu_{0.8}Pb_{0.33}Mo_6S_8$ | A | 0.23 | 0.11 | 0.32 |
| | B | 0.20 | 0.19 | 0.32 |
| $Lu_{0.4}Pb_{0.67}Mo_6S_8$ | A | 0.31 | 0.06 | 0.33 |
| | B | 0.30 | 0.18 | 0.37 |
| $PbMo_{6.2}S_8$ | A | 0.50 | –[d] | 0.33 |
| | B | 0.50 | –[d] | 0.42 |
| $Lu_{0.1}PbMo_6S_8$ | A | 0.48 | –[e] | 0.33 |
| | B | 0.48 | –[e] | 0.37 |

A = fresh catalyst; B = after 10 h of continuous $H_2$–thiophene reaction

[a]Raw area ratio of Pb 4*f* electrons to Mo 3*d* electrons.
[b]Raw area ratio of Lu 4*d* electrons to Mo 3*d* electrons.
[c]Raw area ratio of S 2*p* electrons to Mo 3*d* electrons.
[d]Not applicable.
[e]Lu concentration too low to evaluate.

of the difficulty in quantifying the surface concentrations, it was unrealistic to calculate molybdenum formal oxidation states based on an estimate of the stoichiometry at the surface.

## Activity Measurements

The continuous-flow thiophene reaction results for the Chevrel phases after 20 min and 10 h of reaction are summarized in Table 3 and Table 4. The empty reactor

Table 3. Thiophene hydrodesulfurization (HDS) activities (400°C)

| Catalyst (formal Mo oxidation state) | | Surface area ($m^2/g$) | Reaction time | Thiophene conversion (%) | HDS rate ($mol/s \cdot m^2$) $\times 10^8$ |
|---|---|---|---|---|---|
| $Lu_{1.2}Mo_6S_8$ | (2.07) | 0.693 | 20 min | 2.06 | 1.80 |
| | | 1.093 | 10 h | 3.48 | 1.93 |
| $Lu_{0.8}Pb_{0.33}Mo_6S_8$ | (2.16) | 0.689 | 20 min | 1.64 | 1.55 |
| | | 1.033 | 10 h | 3.17 | 2.00 |
| $Lu_{0.4}Pb_{0.67}Mo_6S_8$ | (2.24) | 0.563 | 20 min | 1.59 | 4.43 |
| | | 0.644 | 10 h | 1.36 | 3.30 |
| $PbMo_{6.2}S_8$ | (2.26) | 1.318 | 20 min | 1.59 | 4.53 |
| | | 1.664 | 10 h | 1.16 | 2.61 |
| $Lu_{0.1}PbMo_6S_8$ | (2.28) | 0.649 | 20 min | 2.60 | 8.43 |
| | | 0.952 | 10 h | 2.84 | 6.27 |

Table 4. $C_4$ distributions resulting from thiophene hydrodesulfurization (400°C)

| Catalyst | Reaction time | $C_4$ product distribution (%) | | | |
|---|---|---|---|---|---|
| | | *n*-butane | 1-butene | *trans*-2-butene | *cis*-2-butene |
| $Lu_{1.2}Mo_6S_8$ | 20 min | 3.6 | 37.3 | 34.7 | 24.4 |
| | 10 h | 3.0 | 28.6 | 40.0 | 28.4 |
| $Lu_{0.8}Pb_{0.33}Mo_6S_8$ | 20 min | 2.3 | 44.1 | 32.4 | 21.2 |
| | 10 h | 0.7 | 34.7 | 38.8 | 25.8 |
| $Lu_{0.4}Pb_{0.67}Mo_6S_8$ | 20 min | 1.3 | 48.4 | 31.9 | 18.4 |
| | 10 h | –[a] | 47.9 | 34.3 | 17.8 |
| $PbMo_{6.2}S_8$ | 20 min | –[a] | 65.5 | 20.2 | 14.3 |
| | 10 h | –[a] | 65.6 | 21.8 | 12.6 |
| $Lu_{0.1}PbMo_6S_8$ | 20 min | 0.8 | 53.5 | 26.7 | 19.0 |
| | 10 h | 0.6 | 55.0 | 25.5 | 18.9 |

[a]Below detection limit.

converted 0.3% of the thiophene to $C_4$ products. This value was subtracted from the $C_4$ yields before the HDS activities were calculated. All catalysts had an increase in surface area after 10 h of reaction. Therefore, the initial surface areas were used to normalize the HDS activities after 20 min of thiophene reaction, while the activities after 10 h of reaction were normalized using the final surface areas. After 10 h of thiophene HDS, most materials showed a decrease in activity [35–36], except $Lu_{1.2}Mo_6S_8$ and $Lu_{0.8}Pb_{0.33}Mo_6S_8$ which showed a slight increase. The $C_4$ hydrocarbon product distributions resulting from thiophene HDS varied with the catalysts. The ratio of 2-butenes to 1-butene after 10 h of reaction was 2.4 for $Lu_{1.2}Mo_6S_8$, 1.9 for $Lu_{0.8}Pb_{0.33}Mo_6S_8$, 1.0 for $Lu_{0.4}Pb_{0.67}Mo_6S_8$, 0.81 for $Lu_{0.1}PbMo_6S_8$, and 0.52 for $PbMo_{6.2}S_8$. These values differed from the thermodynamic equilibrium value at 400°C for which the ratio of 2-butenes to 1-butene is about 2.8 [54].

The 1-butene HYD activities were normalized on the basis of the initial surface areas and calculated as the rate of production of *n*-butane. The results are presented in Table 5. The empty reactor produced 0.06% *n*-butane, and this value was subtracted from the *n*-butane yields before the activities were calculated. The activities are reported for three different times: (A) fresh catalyst, (B) after 25 $H_2$–thiophene pulses, and (C) after 2 h of continuous-flow thiophene reaction. $Lu_{0.1}PbMo_6S_8$ showed no ability to hydrogenate 1-butene. All other catalysts showed an increase in HYD activity after 2 h of continuous-flow thiophene reaction. This may indicate a necessary period of activation for these materials toward the hydrogenation of 1-butene. No detectable

Table 5. 1-Butene hydrogenation (HYD) activities (400°C)

| Catalyst | | HYD rate ($mol/s \cdot m^2$) $\times 10^9$ | $C_4$ product distribution (%) | | | |
|---|---|---|---|---|---|---|
| | | | *n*-butane | 1-butene | *trans*-2-butene | *cis*-2-butene |
| $Lu_{1.2}Mo_6S_8$ | A | 0.23 | 0.03 | 91.7 | 3.5 | 4.7 |
| | B | 0.38 | 0.05 | 92.8 | 3.1 | 4.0 |
| | C | 0.91 | 0.12 | 62.3 | 20.4 | 17.1 |
| $Lu_{0.8}Pb_{0.33}Mo_6S_8$ | A | 0.28 | 0.03 | 89.2 | 5.1 | 5.7 |
| | B | 0.09 | 0.01 | 88.6 | 5.5 | 5.8 |
| | C | 0.83 | 0.09 | 59.6 | 21.5 | 18.8 |
| $Lu_{0.4}Pb_{0.67}Mo_6S_8$ | A | 0.22 | 0.01 | 74.8 | 12.6 | 12.6 |
| | B | 0.66 | 0.03 | 61.6 | 19.9 | 18.5 |
| | C | 0.88 | 0.04 | 54.3 | 24.1 | 21.5 |
| $PbMo_{6.2}S_8$ | A | 0.24 | 0.01 | 89.1 | 5.6 | 5.3 |
| | B | 0.24 | 0.01 | 59.5 | 21.8 | 18.6 |
| | C | 1.20 | 0.05 | 46.2 | 28.6 | 25.2 |
| $Lu_{0.1}PbMo_6S_8$ | A | 0.00 | 0.00 | 93.7 | 3.4 | 2.9 |
| | B | 0.00 | 0.00 | 86.9 | 6.9 | 6.2 |
| | C | 0.00 | 0.00 | 88.3 | 5.3 | 6.4 |
| Calculated butene equilibrium at 400°C[a] | | | | 26.5 | 43.5 | 30.0 |

A = fresh catalyst; B = after 25 $H_2$–thiophene pulses; C = after 2 h of continuous $H_2$–thiophene reaction

[a]See reference [54].

cracking products were observed. The HYD activity experiments also indicate the ability of the catalysts to isomerize 1-butene to *trans*-2-butene and *cis*-2-butene. A considerable departure from the thermodynamic equilibrium value at 400°C was noted for all catalysts. After 2 h of thiophene reaction, 62% of the 1-butene was unconverted

for $Lu_{1.2}Mo_6S_8$ compared to 46% for $PbMo_{6.2}S_8$. For thermodynamic equilibrium at 400°C, about 26.5% 1-butene would be observed [54].

# DISCUSSION OF RESULTS

Previous investigations with Chevrel phases have demonstrated that these materials have thiophene HDS activities comparable to—or greater than—model unpromoted and cobalt-promoted $MoS_2$-based catalysts [33–36,39]. In this study, the effect of a systematic variation in molybdenum oxidation state on catalytic activity for thiophene HDS was examined using a series of lead–lutetium Chevrel phases. By using this substitutional series of compounds, the formal oxidation state of molybdenum could be directly controlled either by inserting $Lu^{3+}$ into $PbMo_6S_8$ or by substituting $Lu^{3+}$ for $Pb^{2+}$ in the Chevrel phase structure. The Chevrel phases can be referred to as reduced molybdenum sulfides (compared to $MoS_2$) and are known to possess a metallic nature; ternary components such as lead and lutetium transfer valence electrons to the $Mo_6$ octahedral (cluster) units [43–44]. The extent of the charge transfer can be altered by varying the concentration of the ternary component or by using ternary components with different valences. This results in a change in the formal oxidation state of the molybdenum.

Figure 3 illustrates the trends for the rate of thiophene HDS versus the formal

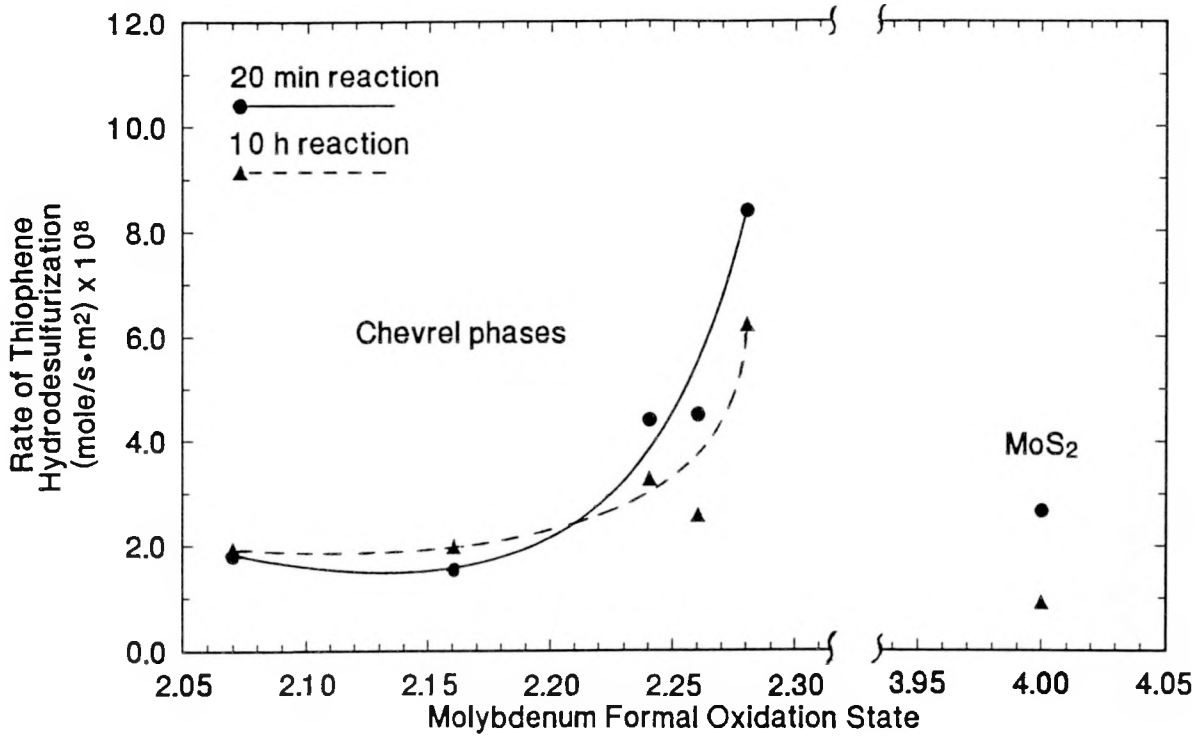


Figure 3. Thiophene hydrodesulfurization activities (400°C) as a function of the formal oxidation state of molybdenum for 20 min and 10 h of thiophene reaction

oxidation state of molybdenum for 20-min and 10-h reaction times. The formal oxidation state of molybdenum was calculated from the nominal stoichiometries by assuming valences of $Lu^{3+}$, $Pb^{2+}$, and $S^{2-}$. Previous work with an unpromoted $MoS_2$ catalyst ($Mo^{4+}$) has determined thiophene HDS rates of $2.67 \times 10^{-8}$ mol/s•m$^2$ and $0.92 \times 10^{-8}$ mol/s•m$^2$ for 20-min and 10-h reaction times, respectively [35–36]. Considering all of these data, it is possible to propose a general correlation of thiophene HDS activity and molybdenum formal oxidation state. Specifically, the rate of thiophene HDS apparently approaches a maximum between the highest molybdenum

oxidation state (+2.28) for the Chevrel phase catalyst and the molybdenum oxidation state (+4) for $MoS_2$. Of course, it is not possible to eliminate all structural and compositional effects on HDS activity in comparing these compounds. These factors have been shown to exist for Chevrel phases [39] and $MoS_2$-based catalysts. It is not possible to prepare a Chevrel phase with a molybdenum formal oxidation state near +3. The highest molybdenum oxidation state attainable for Chevrel phases is +2.67, corresponding to the binary compound $Mo_6S_8$. This material, however, decomposes at 400°C [55] and forms large amounts of $MoS_2$ during thiophene HDS at 300°C for as little as 2 h [35–36].

XPS analysis indicated that the molybdenum oxidation states at the surface of the Chevrel phase catalysts were indeed reduced compared to $MoS_2$. Oxidation of molybdenum in the surface regions could not be appreciably observed after 10 h of thiophene reaction. The XPS data did, however, reveal some degree of ternary metal delocalization due to the reaction conditions. Lead, a large cation, demonstrated the expected low mobility, but lutetium appeared to migrate to some small degree from the bulk to the surface. The oxidation state of surface molybdenum apparently either is unaffected by this limited migration or perhaps becomes very slightly reduced.

Experimental and theoretical evidence for an electronic theory of HDS catalysis has been offered by several research groups. Harris [29–30] and Harris and Chianelli [31–32] have provided an SCF–SW–X$\alpha$ method for modeling the energy levels and charge distributions for $MS_6^{n-}$ clusters (first-row transition metals $M$ = Ti–Ni and

second-row transition metals $M$ = Zr–Pd) and $M'MoS_9^{m-}$ clusters (first-row transition-metal "promoters" $M'$ = V–Zn). These calculations are consistent with the XPS spectra of the sulfides and indicate that bonding in the 4*d* transition-metal sulfides is considerably more covalent than in the 3*d* sulfides. The activity of the unpromoted transition-metal clusters (sulfides) for dibenzothiophene HDS activity was correlated with the orbital occupation of the highest occupied molecular orbital (HOMO) and the metal–sulfur covalent-bond strength [31]. The role of the promoters for molybdenum clusters was to affect the number of electrons in the HOMO, that is, the number of *d* electrons on molybdenum. For cobalt–molybdenum and nickel–molybdenum clusters, the number of electrons is increased by the presence of the promoter; copper has the opposite effect. These calculations also correlate with the activity for dibenzothiophene HDS activity [32]: cobalt and nickel are excellent promoters while copper acts as a poison. Vissers *et al.* [56] also report a correlation between thiophene HDS activity for second- and third-row transition metals and the shift in XPS binding energies between metal and metal sulfide phases. The most active transition-metal sulfides were observed to preserve their metallic character in the sulfide phase under reaction conditions. Specifically, these materials were proposed to be sulfur-deficient, highly reduced sulfides having valence electrons in the metal–sulfur molecular orbitals which maintain their metallic nature.

Chevrel phases are part of a group of "metal-rich" compounds including halides, oxides, and other ligands. For Chevrel phases the fundamental cubic structure is

defined by the presence of $Mo_6S_8$ units consisting of a molybdenum cluster or octahedron. The Mo–Mo bond distances within a cluster are relatively short, typically in the range of 2.65–2.80 Å, compared to 2.72 Å for metallic Mo [41]. The $Mo_6$ cluster is capable of playing an electron (*e*) donor–acceptor role [44]. The $Mo_6S_8$ compound (no ternary metal) is the most electron-poor compound (20*e* per $Mo_6$ cluster) with electron-deficient Mo–Mo bonds; it is a metastable compound. The addition of ternary metals adds electrons to the cluster and stabilizes the cluster unit. The Mo–Mo bond distance becomes shorter, and the octahedron becomes regular for 24*e* per $Mo_6$ cluster. The high catalytic activity of the Chevrel phases correlates with the metallic or "reduced" nature of these sulfides: indeed, by comparing the activity to conventional $MoS_2$-based catalysts, higher activity is obtained when the molybdenum formal oxidation state is reduced below $Mo^{4+}$. The results of this work indicate that a maximum in activity may exist between $Mo^{2+}$ and $Mo^{4+}$.

The observation of a maximum in the rate of thiophene HDS is not unexpected. Recent kinetic measurements have indicated that thiophene adsorption and reaction with surface nucleophiles (to produce dihydrothiophene intermediates) are likely the rate-limiting steps in HDS [57–58]. Although the adsorption state of thiophene is still unclear, $\eta^5$-binding apparently would give rise to carbon–sulfur bond weakening [59]. Thiophene is more likely to bond to metals in the lower oxidation state based on an analysis of model organometallic compounds [60]. However, nucleophilic attack to produce hydrogenated intermediates (2,3-dihydrothiophene and 2,5-dihydrothiophene),

which are highly reactive toward HDS, would be promoted by sulfides in higher molybdenum oxidation states. This may explain why a maximum is observed in considering Figure 3 and the data for typical $MoS_2$-based catalysts.

Consistent with this observation is the low activity of the lead–lutetium Chevrel phases for 1-butene hydrogenation. This is not unexpected since similar results have been reported for other Chevrel phases [33–36,39]. For comparison, model unpromoted and cobalt-promoted $MoS_2$-based catalysts have 1-butene HYD activities of $7.5 \times 10^{-9}$ and $7.1 \times 10^{-9}$ mol/s•m$^2$ after 2 h of thiophene HDS, respectively [35–36]. The Chevrel phases do exhibit an increase in 1-butene HYD following 2 h of continuous thiophene HDS; however, this activity is still approximately eight times lower than the model $MoS^2$-based materials. Undoubtedly some of this effect is due to the migration of Lu atoms to the surface. The XPS data, however, indicated little effect on the molybdenum oxidation state.

# CONCLUSIONS

The thiophene HDS activities of the lead–lutetium series Chevrel phase catalysts investigated were found to be comparable to those of previously examined Chevrel phases and to those of model unpromoted and cobalt-promoted $MoS_2$ catalysts, indicating that they are potentially useful HDS catalysts. These materials also demonstrated low 1-butene HYD activities, making them rather selective catalysts. The bulk structures and the reduced surface molybdenum oxidation states have been determined to be stable under reaction conditions. It was possible to relate catalyst activity to the formal oxidation state of molybdenum for these compounds: thiophene HDS activity is associated with ''reduced'' molybdenum oxidation states, apparently reaching a maximum between $Mo^{2+}$ and $Mo^{4+}$.

# ACKNOWLEDGMENTS

This work was conducted through the Ames Laboratory which is operated for the U. S. Department of Energy by Iowa State University under Contract W–7405–Eng–82. This research was supported by the Office of Basic Energy Sciences, Chemical Sciences Division. XPS spectra were obtained by J. W. Anderegg of the Ames Laboratory.

# REFERENCES


1. Grange, P., *Catal. Rev.—Sci. Eng.* **21**, 135 (1980).

2. Wivel, C., Candia, R., Clausen, B. S., Mørup, S., and Topsøe, H., *J. Catal.* **68**, 453 (1981).

3. Bachelier, J., Duchet, J. C., and Cornet, D., *J. Catal.* **87**, 283 (1984).

4. Li, C. P., and Hercules, D. M., *J. Phys. Chem.* **88**, 456 (1984).

5. Zingg, D. S., Makovsky, L. E., Tisher, R. E., Brown, F. R., and Hercules, D. M., *J. Phys. Chem.* **84**, 2898 (1980).

6. Patterson, T. A., Carver, J. C., Leyden, D. E., and Hercules, D. M., *J. Phys. Chem.* **80**, 1700 (1976).

7. Parham, T. G., and Merrill, R. P., *J. Catal.* **85**, 295 (1984).

8. Pollack, S. S., Makovsky, L. E., and Brown, F. R., *J. Catal.* **59**, 452 (1979).

9. Schrader, G. L., and Cheng, C. P., *J. Catal.* **80**, 369 (1983).

10. Okamoto, Y., Shimokawa, T., Imanaka, T., and Teranishi, S., *J. Catal.* **57**, 153 (1979).

11. Furimsky, E., *Catal. Rev.—Sci. Eng.* **22**, 371 (1980).

12. Topsøe, H., Clausen, B. S., Wivel, C., and Mørup, S., *J. Catal.* **68**, 433 (1981).

13. Topsøe, H., Candia, R., Topsøe, N.-Y., and Clausen, B. S., *Bull. Soc. Chim. Belg.* **93**, 783 (1984).

14. Delvaux, G., Grange, P., and Delmon, B., *J. Catal.* **56**, 99 (1979).

15. Alstrup, I., Chorkendorff, I., Candia, R., Clausen, B. S., and Topsøe, H., *J. Catal.* **77**, 397 (1982).

16. Voorhoeve, R. J. H., *J. Catal.* **23**, 236 (1971).

17. Konings, A. J. A., Valster, A., de Beer, V. H. J., and Prins, R., *J. Catal.* **76**, 466 (1982).

18. Thakur, D. S., and Delmon, B., *J. Catal.* **91**, 308 (1985).

19. Bachelier, J., Duchet, J. C., and Cornet, D., *Bull. Soc. Chim. Belg.* **90**, 1301 (1981).

20. Tauster, S. J., Pecoraro, T. A., and Chianelli, R. R., *J. Catal.* **63**, 515 (1980).

21. Jung, H. J., Schmitt, J. L., and Ando, H., *in* "Proceedings of the Climax Fourth International Conference on Chemistry and Uses of Molybdenum" (H. F. Barry and P. C. H. Mitchell, Eds.), p. 246. Climax Molybdenum Co., Ann Arbor, MI, 1982.

22. Segawa, K.-I., and Hall, W. K., *J. Catal.* **77**, 221 (1983).

23. Valyon, J., and Hall, W. K., *J. Catal.* **84**, 216 (1983).

24. Delgado, E., Fuentes, G. A., Hermann, C., Kunzmann, G., and Knözinger, H., *Bull. Soc. Chim. Belg.* **93**, 735 (1984).

25. Bachelier, J., Tilliette, M. J., Cornac, M., Duchet, J. C., Lavalley, J. C., and Cornet, D., *Bull. Soc. Chim. Belg.* **93**, 743 (1984).

26. Peri, J. B., *J. Phys. Chem.* **86**, 1615 (1982).

27. Laine, J., Severino, F., Cáceres, C. V., Fierro, J. L. G., and López Agudo, A., *J. Catal.* **103**, 228 (1987).

28. Duben, A. J., *J. Phys. Chem.* **82**, 348 (1978).

29. Harris, S., *Chem. Phys.* **67**, 229 (1982).

30. Harris, S., *Polyhedron* **5**, 151 (1986).

31. Harris, S., and Chianelli, R. R., *J. Catal.* **86**, 400 (1984).

32. Harris, S., and Chianelli, R. R., *J. Catal.* **98**, 17 (1986).

33. McCarty, K. F., and Schrader, G. L., *in* "Proceedings, 8th International Congress on Catalysis, Berlin, 1984" (E. Ertl, Ed.), Vol. IV, p. 427. Dechema, Frankfurt-am-Main, 1984.

34. McCarty, K. F., and Schrader, G. L., *Ind. Eng. Chem. Prod. Res. Dev.* **23**, 519 (1984).

35. McCarty, K. F., Anderegg, J. W., and Schrader, G. L., *J. Catal.* **93**, 375 (1985).

36. McCarty, K. F., Ph.D. Dissertation, Iowa State University, Ames, Iowa, 1985.

37. McCarty, K. F., and Schrader, G. L., *J. Catal.* **103**, 261 (1987).

38. Huckett, S. C., Angelici, R. J., Ekman, M. E., and Schrader, G. L., *J. Catal.* **113**, 36 (1988).

39. Schrader, G. L., and Ekman, M. E., *in* "Advances in Hydrotreating Catalysts" (M. L. Occelli and R. G. Anthony, Eds.), Vol. 50, p. 41. Elsevier, Amsterdam, 1989.

40. Chevrel, R., Sergent, M., and Prigent, J., *J. Solid State Chem.* 3, 515 (1971).

41. Chevrel, R., and Sergent, M., *in* "Topics in Current Physics" (Ø. Fischer and M. B. Maple, Eds.), Vol. 34, p. 25. Springer-Verlag, Berlin, 1982.

42. Yvon, K., *in* "Topics in Current Physics" (Ø. Fischer and M. B. Maple, Eds.), Vol. 34, p. 87. Springer-Verlag, Berlin, 1982.

43. Yvon, K., *in* "Current Topics in Materials Science" (E. Kaldis, Ed.), Vol. 3, p. 53. North-Holland, Amsterdam, 1979.

44. Chevrel, R., Hirrien, M., and Sergent, M., *Polyhedron* 5, 87 (1986).

45. Tarascon, J. M., DiSalvo, F. J., Murphy, D. W., Hull, G. W., Rietman, E. A., and Waszczak, J. V., *J. Solid State Chem.* **54**, 204 (1984).

46. Sergent, M., Chevrel, R., Rossel, C., and Fischer, Ø., *J. Less-Common Met.* **58**, 179 (1978).

47. Flükiger, R., and Baillif, R., *in* "Topics in Current Physics" (Ø. Fischer and M. B. Maple, Eds.), Vol. 34, p. 113. Springer-Verlag, Berlin, 1982.

48. Miller, W. M., and Ginsberg, D. M., *Phys. Rev. B* **28**, 3765 (1983).

49. Chang, C. H., and Chan, S. S., *J. Catal.* **72**, 139 (1981).

50. Wieting, T. J., and Verble, J. L., *Phys. Rev. B* **3**, 4286 (1971).

51. Luly, M. H., "APES – A FORTRAN Program to Analyze Photoelectron Spectra." Ames Laboratory, DOE, Iowa State University, Ames, 1979.

52. Swartz, W. E., and Hercules, D. M., *Anal. Chem.* **43**, 1774 (1971).

53. Brox, B., and Olefjord, I., *Surf. Interface Anal.* **13**, 3 (1988).

54. Benson, S. W., and Bose, A. W., *J. Amer. Chem. Soc.* **85**, 1385 (1963).

55. Cheung, K. Y., and Steele, B. C. H., *Solid State Ionics* **1**, 337 (1980).

56. Vissers, J. P. R., Groot, C. K., van Oers, E. M., de Beer, V. H. J., and Prins, R., *Bull. Soc. Chim. Belg.* **93**, 813 (1984).

57. Markel, E. J., Schrader, G. L., Sauer, N. N., and Angelici, R. J., *J. Catal.* **116**, 11 (1989).

58. Sauer, N. N., Markel, E. J., Schrader, G. L., and Angelici, R. J., *J. Catal.* **117**, 295 (1989).

59. Zonnevylle, M. C., Hoffmann, R., and Harris, S., *Surf. Sci.* **199**, 320 (1988).

60. Angelici, R. J., *Acc. Chem. Res.* **21**, 387 (1988).

# SECTION III.

# $O_2$ AND NO CHEMISORPTION AS PROBES OF REDUCED MOLYBDENUM OXIDATION STATES IN HYDRODESULFURIZATION CATALYSIS BY CHEVREL PHASES

# ABSTRACT

The chemisorption of $O_2$ and NO as probe molecules of the active sites for hydrodesulfurization (HDS) catalysts was evaluated using a lead–lutetium series of Chevrel phases. Polycrystalline catalysts were prepared with compositions of $PbMo_{6.2}S_8$, $Lu_{1.2x}PbMo_6S_8$ for $0 < x \leq 0.2$, and $Lu_{1.2x}Pb_{1-x}Mo_6S_8$ for $0.2 < x \leq 1$. A model unsupported $MoS_2$ catalyst was prepared for comparisons of continuous-flow thiophene HDS at 400°C and of dynamic (pulsed) $O_2$ and NO adsorption at ambient temperature. Catalysts were characterized by X-ray powder diffraction, laser Raman spectroscopy, and X-ray photoelectron spectroscopy. Bulk structures and molybdenum oxidation states were found to be stable. The chemisorption of $O_2$ and NO could be related to HDS activity and the formal oxidation state of molybdenum: the same reduced molybdenum species which exhibited the greatest activity for thiophene HDS also have the greatest uptake of $O_2$ and NO.

# INTRODUCTION

The removal of sulfur from oil by catalytic hydrodesulfurization (HDS) is one of the largest processes practiced by the petroleum industry. A better understanding of how current HDS catalysts function is required to develop more active and efficient HDS catalysts, desired for several important reasons: tighter environmental standards require reductions in sulfur oxide emissions; most catalysts which are used for further processing of oil products (*e.g.*, precious metals for catalytic reforming) are poisoned by sulfur; and shorter supplies of "clean" petroleum feed-stocks have created the need to more efficiently process sulfur-rich crude oil residua.

Typical industrial HDS catalysts are prepared from molybdenum ($Mo^{6+}$) oxides supported on alumina ($\gamma-Al_2O_3$). The addition of cobalt (Co) or nickel (Ni) promoters increases their catalytic activity. The oxidic precursor is transformed into the working HDS catalyst through sulfiding, to form a $MoS_2$ ($Mo^{4+}$) phase. The presence of this $MoS_2$ phase has been demonstrated by various techniques such as X-ray photoelectron spectroscopy (XPS) [1–3], extended X-ray absorption fine structure techniques (EXAFS) [4–5], X-ray diffraction [6], and laser Raman spectroscopy [7]. Unsupported reduced

(with $H_2$) or sulfided (with $H_2/H_2S$) $MoS_2$ is also an active HDS catalyst with properties similar to those of supported catalysts [8]. For this reason, unsupported $MoS_2$-based materials have been used extensively to model the more complex supported HDS catalysts.

Information concerning the structure of the catalytically active phase incorporating the promoter has been more difficult to obtain. Using *in-situ* Mössbauer emission spectroscopy, Topsøe *et al.* [9] reported the presence of a cobalt–molybdenum–sulfide (Co–Mo–S) phase in both unsupported and supported cobalt-promoted HDS catalysts. This phase is considered to be the most catalytically significant phase present, based on a linear correlation between the amount of cobalt in the Co–Mo–S phase and thiophene HDS [10]. It is believed to be a $MoS_2$-like phase in which promoter atoms occupy crystallite edge positions.

The precise nature of the catalytically active sites is not known. However, it is generally believed that coordinatively unsaturated sites (CUS), formed by the introduction of anion (sulfur) vacancies on molybdenum ions during reduction and sulfidation are the active sites for HDS [11–14]; and that these sites may be titrated by the use of suitable probe molecules. The first suggestion of a site-specific adsorbate for HDS catalysts came from the work of Bahl *et al.* [15]. They investigated single crystals of $MoS_2$ and found that the edge plane oxidized much more readily than the basal plane. This work pointed to the possible use of oxygen ($O_2$) as a suitable probe for HDS catalysts.

Parekh and Weller [16–17] devised a method to determine the specific surface area of supported molybdenum catalysts in their reduced state, based on the static adsorption of $O_2$ at liquid nitrogen temperatures. Similarly, Millman and Hall [18] investigated $O_2$ chemisorption on reduced Mo/$\gamma$–$Al_2O_3$ catalysts. They reported linear correlations between the amount of $O_2$ adsorbed and the anion vacancies (CUS), as well as the rate of propylene HYD. Vyskočil and Tomanová [19] described the application of a dynamic (pulsed) $O_2$ adsorption method for reduced Co–Mo/$\gamma$–$Al_2O_3$ catalysts, and correlated $O_2$ chemisorption with cyclohexene hydrogenation (HYD).

The application of $O_2$ chemisorption to sulfided HDS catalysts was first described by Tauster *et al.* [20], in which they observed a linear correlation between the amount of $O_2$ adsorbed on unsupported $MoS_2$ catalysts and HDS activity. In light of the work of Bahl *et al.* [15], they proposed that the edge planes of $MoS_2$ were where the catalytically active sites were located, and that $O_2$ selectively titrated these sites. Since then, the use of $O_2$ as a selective probe of catalytically active sites on several types of unsupported and supported molybdenum-based catalysts has been investigated extensively [12,21–65]. Correlations have been established between the amount of $O_2$ chemisorbed and HDS for both unpromoted [20,23,26,29,31–32,35,40,45,49,58–59] and promoted [27–28,34,42,46,58,61–62] catalysts, hydrodenitrogenation (HDN) [46,63], HYD of olefins [18–19,33,50,59,64] and CO [39], dehydrogenation [26], and the concentration of molybdenum CUS [18,22,25,41,54,58–59].

Other investigations have revealed that the validity of such relationships may be

restricted to narrow families of similar materials. Suitable correlations for many promoted catalysts have not been found, resulting in reservations concerning the use of $O_2$ as a site-specific probe of the catalytically active centers [12,19,22,33,36,39–41, 47,50–51,57,60]. It was concluded that $O_2$ may not be selective, and may indiscriminately count different types of active sites on the catalyst surface; thereby titrating not only molybdenum edge sites, but also more active sites associated with promoters [22,33,39,51]. The specific interaction of $O_2$ with the catalyst surface remains unknown since the adsorbed $O_2$ cannot be examined by spectroscopic techniques.

In contrast, nitric oxide (NO) adsorption can be followed by infrared (IR) spectroscopy, and its use as a selective probe of catalytically active sites has been examined by many investigators [12,25,37,41,47,56–57,65–93]. It has been proposed that NO and $O_2$ adsorb on the same sites [18,25,41,65]: single crystal studies have demonstrated that NO adsorbs on the edge sites of $MoS_2$ [71]. NO has also been shown to act as a poison for catalytic activity, leading to the conclusion that adsorption sites and HDS sites are identical [25,66–67,76]. Linear correlations have been reported between the amount of NO adsorbed and HDS [49,65,89,92], HYD [25,65,93], and the concentration of molybdenum CUS [25,67,70,73]. The absence of suitable correlations has also been reported [47,90,92–93].

NO adsorption can occur on the promoter atoms in cobalt- or nickel-promoted molybdenum catalysts. However, it is possible to selectively analyze the adsorption of

NO on either the molybdenum or promoter ions using IR spectroscopy. Good correlations have been found to exist between the intensity of the IR band associated with NO adsorbed on promoter atoms and HDS [12,37,47,57,74,77,80,83,88] and HYD [86,88] reactions.

Carbon monoxide (CO), although a preferred surface probe for many catalyst systems, has received much less attention for molybdenum-based catalysts [25,29,42,51, 64,69,75,94–99]. It has been proposed that CO adsorbs on the same sites as $O_2$ or NO, indicating its specificity for the catalytically active sites [25,51,96]. In addition, linear correlations have been reported between the chemisorption of CO and HDS [29,42,64,97–99], HDN [64], and the concentration of the molybdenum CUS [25]. As with $O_2$ and NO, some reservations concerning the use of CO as a probe of the catalytically active sites have been expressed [42,51,95].

Other probes such as $H_2S$ [36,51], $CO_2$ [73,78,85,91,100], $H_2$ [30], and various hydrocarbons [40,78,101] have received some attention, but have not been developed further.

The literature does not provide a universal relationship between chemisorption data and catalytic activity; nor does it specify the nature of the adsorption or catalytically active sites. However, it has been established that various probe molecules (*e.g.*, $O_2$, NO, and CO) titrate only a small fraction (approximately 5–10%) of the total available molybdenum CUS [12,26,33,37,39–41,47,49,51,54,69–70,72,76,84]. This supports a concept of selective adsorption on edge or corner sites on $MoS_2$ or $MoS_2$-like

structures on HDS catalysts [20,27,40]. The observation that similar correlations between HDS activity and chemisorption are obtained for unsupported $MoS_2$, $Mo/\gamma-Al_2O_3$, $Co-Mo/\gamma-Al_2O_3$, and $Ni-Mo/\gamma-Al_2O_3$ catalysts suggests the same kind of specific catalytic sites are involved in all four types of catalysts. Based on the low degree of catalyst surface coverage by probe molecules, it has been submitted that only a select group of surface molybdenum CUS with some special properties are able to chemisorb suitable probe molecules. These properties are envisioned to include, among others, the chemical state (oxidation state) of molybdenum [54].

The valence state of the molybdenum centers on which the chemisorbed species are bound must be lower than $Mo^{6+}$ (found in $MoO_3$) since chemisorption is observed only after a specific minimum amount of reduction of the HDS catalyst [41]. The presence of $MoS_2$ or $MoS_2$-like phases in active HDS catalysts leads to a predominance of $Mo^{4+}$ species; however, several investigations have shown the possible presence of catalytically active sites with molybdenum oxidation states lower than $Mo^{4+}$. Studies of the chemisorption of $O_2$ and NO on reduced and sulfided supported molybdenum catalysts were interpreted by Hall *et al.* [41,53,67,79,85] as adsorption on $Mo^{2+}$ centers. They noted that for their particular catalysts, molybdenum ions with oxidation states less than $Mo^{4+}$ were invariably present, and that these species were responsible for higher catalytic activity. Laine *et al.* [87] explained their observations for NO adsorption on supported molybdenum catalysts promoted with both nickel and cobalt in terms of a minor reduction of molybdenum below the +4 oxidation state. Cáceres *et*

*al.* [56] reported that NO may adsorb on $Mo^{3+}$ or $Mo^{2+}$ sites. Peri [75] examined NO and CO adsorption on supported molybdenum catalysts and concluded that lower oxidation states than $Mo^{4+}$ exist in the sulfided materials. Bachelier *et al.* [97] and Duchet *et al.* [64] reported that highly reduced molybdenum and tungsten sites were responsible for the adsorption of CO on Co–Mo/$\gamma$–$Al_2O_3$ and Ni–W/$\gamma$–$Al_2O_3$ catalysts, respectively: these reduced sites were associated with HDS and HDN activity. Similarly, Delgado *et al.* [96] suggested that $Mo^{2+}$–CO adsorption complexes are formed on sulfided Mo/$\gamma$–$Al_2O_3$ catalysts.

Other analytical techniques have detected the presence of catalytically important reduced molybdenum oxidation states (relative to $Mo^{4+}$) as well. For example, XPS measurements of unsupported sulfided cobalt–molybdenum catalysts have demonstrated a decrease in the molybdenum 3*d* binding energies for cobalt concentrations corresponding to the greatest promotional effect for thiophene HDS [102]. These results led to the postulation that molybdenum species with a charge between +3 and +4 were associated with the active sites. Alstrup *et al.* [103] reported a close similarity between the cobalt 2*p* spectra of Co–Mo–S and $CoMo_2S_4$, based on XPS studies of unsupported and supported cobalt–molybdenum catalysts. This suggests that the electronic state of cobalt in Co–Mo–S is similar to that in $CoMo_2S_4$ (which has a formal molybdenum oxidation state of +3). However, the two phases are structurally different. McIntyre *et al.* [104] have also used XPS to investigate supported sulfided cobalt–molybdenum thin film catalysts. They found a molybdenum $3d_{5/2}$ peak which they labelled as $MoS_{2-x}$, with a

greater electron density on molybdenum than found in $MoS_2$. This component exhibited detectable HDS activity.

Electron paramagnetic resonance (EPR) techniques have been used to associate more highly reduced molybdenum species with the catalytically active sites. Voorhoeve [14b] used EPR in the investigation of the hydrogenation of benzene using $WS_2$ (analogous to $MoS_2$) catalysts and concluded that the active centers were $W^{3+}$ (or $Mo^{3+}$) ions. Konings *et al.* [105] have observed a correlation between the intensity of an EPR signal assigned to $Mo^{3+}$ and the rate of thiophene HDS for supported cobalt–molybdenum catalysts. Similarly, Thakur and Delmon [106] detected the presence of $Mo^{3+}$ and $W^{3+}$ species on unsupported promoted molybdenum and tungsten catalysts: catalysts having the highest EPR signal also had the greatest HDS activity.

The complexity of typical industrial catalysts—and even the uncertainties associated with unsupported catalysts—has made identification of reduced molybdenum species difficult. Due to the presence of a large amount of $MoS_2$ (or other related phases with predominately $Mo^{4+}$ oxidation states) in these catalysts, the role of more deeply reduced molybdenum species has been difficult to verify.

Theoretical investigations, however, have indicated that reduced molybdenum oxidation states are involved as the active sites in HDS catalysts. Using simple Hückel theory, Duben [107] concluded that $Mo^{3+}$ would be the most effective molybdenum species for carbon–sulfur bond breaking and for easy removal of the surface bound

sulfur atom required to regenerate the active site. Harris [108–109] and Harris and Chianelli [110–111] have proposed an "electronic" model for HDS catalysts based on SCF–Xα scattered wave method molecular-orbital calculations for $MS_6^{n-}$ ($M$ = first- and second-row transition metals) and $M'MoS_9^{m-}$ ($M'$ = first-row transition-metal promoters, V–Zn) clusters. In their model, several electronic factors are related to catalytic activity, such as the number of electrons in the highest occupied molecular orbital (HOMO), the degree of covalency of the metal–sulfur bond, and the metal–sulfur bond strength. These factors were incorporated into an activity parameter, $A_2$, shown to correlate with dibenzothiophene HDS. Their calculations indicate that promoters, such as cobalt and nickel, donate electrons to molybdenum, reducing the molybdenum formal oxidation state relative to $MoS_2$. Copper, a metal which poisons the activity of $MoS_2$-based catalysts, formally oxidizes molybdenum relative to $MoS_2$. Ternan [112] extended their results to demonstrate correlations between the activity parameter $A_2$ and heavy gas oil HDS, HDN, and HYD. Bouwens *et al.* [113] also suggest that HDS activity differences should be explained in terms of electron donation to the molybdenum atoms, based on EXAFS studies of cobalt-promoted molybdenum catalysts supported on carbon. Vissers *et al.* [114] reported a correlation between thiophene HDS and the shift in XPS binding energies between metal and metal sulfide phases (for second- and third-row transition metals). The most active transition-metal sulfides were observed to better preserve their metallic character under reaction conditions. These active HDS materials were proposed to be sulfur-deficient, highly reduced sulfides having valence electrons in

the metal–sulfur molecular orbitals which maintain their metallic nature, with a correspondingly low positive charge on the metal atom.

A new class of HDS catalysts—"reduced" molybdenum sulfides known as Chevrel phases—has been reported previously [115–123]. Direct preparation of catalysts with reduced molybdenum oxidation states (relative to $Mo^{4+}$ in $MoS_2$) is possible with these materials. Chevrel phases have been shown to have activities comparable to, or exceeding those of, conventional $MoS_2$ or Co–Mo–S materials for thiophene and benzothiophene HDS.

The initial synthesis and characterization of these ternary molybdenum chalcogenides was first presented by Chevrel *et al.* [124] in 1971. Chevrel phases have the general formula $M_xMo_6Z_8$ (M = ternary metal; $Z$ = sulfur, selenium, or tellurium; $0 \leq x \leq 4$). Extensive reviews of Chevrel phases have been provided [125–132]. The basis for the structure of sulfide Chevrel phases is the $Mo_6S_8$ cluster. The stacking of these fundamental building blocks results in the formation of channels or voids in the chalcogen atom network; these channels contain the ternary metal cations. When $M$ is a large cation, such as Pb or Sn, a second component, such as a rare earth ($RE$), may be incorporated to produce a series of compounds with nominal formulas $RE_xM_{1-x}Mo_6S_8$.

The oxidation state of molybdenum in the metal-rich Chevrel phases is low relative to $MoS_2$. Based on simple calculations of formal oxidation states, the $Mo_6S_8$ binary compound has a valence of +2.67. Introduction of the ternary metal decreases the molybdenum oxidation state by the transfer of electrons from the ternary component

cation to the molybdenum cluster [125,128,130–131,133]. For example, the formal oxidation state of molybdenum in $Cu_4Mo_6S_8$ can be calculated as +2.

The rich solid state chemistry of Chevrel phases offers a unique opportunity to investigate the role of the molybdenum oxidation state in HDS catalysts. This section examines the chemisorption of $O_2$ and NO as probes of catalytically active reduced molybdenum sites using a lead–lutetium series of Chevrel phases.

# EXPERIMENTAL METHODS

## Catalyst Preparation

The Chevrel phases were synthesized by the solid state reaction of 200 mesh powdered molybdenum metal (Alfa, m3n+, t2n7), sulfides of lead (PbS) and lutetium ($Lu_2S_3$), and sulfur (Alfa, t5n5). The ternary metal sulfides were prepared by the direct combination of lead (Alfa, m5n+) or lutetium (Ames Lab rare earth group) with sulfur in evacuated, fused-silica tubes. The molybdenum was reduced with hydrogen (20 ml/min) in a tube furnace (Lindberg, model 54231) at 1000°C for 18 h prior to use. The mixtures were ground together thoroughly, pressed into 13-mm pellets with 10,000 lbs total force (Perkin Elmer die, model 186–0025), and evacuated to less than $10^{-5}$ Torr in baked (heated to "white-hot" while under vacuum) fused-silica tubes. The tubes were back-filled with argon to 20-in Hg vacuum and sealed. The synthesis tubes were heated slowly in a muffle furnace (Central Scientific, model Hoskins FD202C) from 450 to 750°C over a period of 48–72 h, transferred immediately to a high-temperature box furnace (Lindberg, model 51333) at 1200°C for 24 h, and quenched in air. The materials were reground in air, pressed into pellets, and reheated in evacuated

fused-silica tubes for 48 h at 1225°C. After the final heating, the tubes were opened in an argon dry box, where the pellets were lightly crushed. The 40–100 mesh portion was separated for use in the activity and chemisorption studies. All subsequent manipulations of the catalysts were performed in the dry box.

Discrepancies often appear in the literature concerning the exact stoichiometries necessary to obtain pure single phase materials. The content of the rare earth (*RE*) element is reported to be variable (*e.g.*, $RE_{1.0}Mo_6S_8$ and $RE_{1.2}Mo_6S_8$) [134], and the ratio of molybdenum to sulfur can deviate from the "ideal" value of 6/8. Single crystal studies have demonstrated that stoichiometric ratios of $RE_{1.0}Mo_6S_8$ exist [135–136]. The rare earth element can react with the fused-silica tube during synthesis to form oxysulfides, resulting in a rare earth deficient Chevrel phase. To compensate for this deficiency, the starting composition is shifted toward the rare earth rich limit, leading to a non-stoichiometric formula $RE_xMo_6S_8$, with $x$ generally bracketed between 1.0 and 1.2. The resulting rare earth concentration in the Chevrel phases is typically not larger than $x = 1.0$ [132].

In this work, homogeneous polycrystalline samples were obtained for compositions prepared at $Lu_{1.2x}PbMo_6S_8$ for $0 < x \leq 0.2$ and at $Lu_{1.2x}Pb_{1-x}Mo_6S_8$ for $0.2 < x \leq 1$. A loss of lead is observed when $x$ is greater than 0.2, demonstrating a limit of rare earth insertion [137]. The lead compound must be prepared with a composition of $PbMo_{6.2}S_8$ to obtain the purest single-phase material, containing about 1 wt% $MoO_2$ and less than 1 wt% of other impurities ($MoS_2$, $Mo_2S_3$) [138–139].

A model unpromoted $MoS_2$ catalyst was prepared to be used as a "conventional" material for comparisons with the Chevrel phases. The unsupported $MoS_2$ sample was synthesized by the thermal decomposition of ammonium tetrathiomolybdate [118,140]. Ammonium tetrathiomolybdate was prepared by dissolving 40 g of ammonium paramolybdate (Fisher Scientific) in 100 ml of water and 400 ml of concentrated ammonium hydroxide (Fisher Scientific). $H_2S$ (MG Industries, 99.5%) was bubbled through the solution, resulting in the precipitation of ammonium tetrathiomolybdate. The red precipitate was filtered, washed with water and ethanol, and dried at 100°C in a vacuum oven.

Six grams of ammonium tetrathiomolybdate were placed in a fused-silica boat in a fused-silica calcining tube. The tube was heated from room temperature to 600°C for 6 h, with helium flowing over the sample at 100 ml/min (STP). The product was pressed into pellets and placed in a fused-silica tube, evacuated, sealed, and heated to 1000°C for 10 h. The tube was opened in an argon dry box and the final product, crystalline $MoS_2$, was lightly crushed. The 40–100 mesh portion was reserved as above.

## Catalyst Characterization

The surface areas of the catalysts were determined by the BET method using a Micromeritics 2100E instrument. Krypton was used as the adsorbate at liquid nitrogen temperatures. An atomic adsorption area of 21.0 $Å^2$ per krypton atom was assumed.

X-ray powder diffraction patterns were obtained with a Siemans D500 diffractometer interfaced to a DEC PDP 11/23 computer. Samples were mounted on double-sided adhesive tape and scanned in the 2θ range from 10 to 50 using Cu$K\alpha$ radiation. A count time of 1.0 s and step size of 0.04 2θ were employed.

Laser Raman spectra were collected using a Spex 1403 double monochromator. The excitation energy was provided by a Spectra Physics argon ion laser operating at 514.5 nm and 200 mW, measured at the source. A Nicolet 1180E computer was used to accumulate 50 scans at a scanning speed of 2 $cm^{-1}/s$ with 5-$cm^{-1}$ resolution. The intensity of the Rayleigh line was reduced by closing the middle slits of the spectrometer to 1000 microns. Data were collected using backscattering geometry with 13-mm spinning catalyst pellets.

X-ray photoelectron spectra were acquired with an AEI 200B spectrometer using Al$K\alpha$ radiation. All spectra are referenced to a carbon 1$s$ binding energy of 284.6 eV. Signal averaging was performed using a Nicolet 1180 computer system.

## HDS Activity Measurements

Hydrodesulfurization activities were measured using a 0.25-in stainless steel reactor, operated at atmospheric pressure, as described in detail previously [115–122]. The composition and flow rate of the gases fed to the reactor were controlled by mass flow controllers (Tylan, model FC–260). Thiophene (Alfa, 99%) was fed with a syringe pump (Sage, model 341) to a saturator maintained at 110°C, where it was

vaporized and mixed with hydrogen (Air Products Zero grade). Catalyst loadings were adjusted to achieve less than 3% conversion of thiophene after 20 min reaction. The reactor was heated from room temperature to 400°C in a stream of helium (Air Products Zero grade) at 19 ml/min (STP). After 1 h at 400°C with flowing helium, a continuous flow of 2 mol% thiophene in hydrogen at 22 ml/min (STP) was started through the reactor. After 10 h of continuous reaction, the steady-state thiophene HDS activities were determined.

Product separation and analysis were performed using a 12-ft *n*-octane/Porasil C column and an Antek 310/40 ALP gas chromatograph equipped with a flame ionization detector. Peak areas were measured by a Hewlett–Packard 3390A digital integrator.

### $O_2$ and NO Chemisorption Measurements

Fresh catalyst samples were loaded into the reactor to determine their capacities for $O_2$ and NO chemisorption. The reactor was heated from room temperature to 400°C in a flow of helium at 19 ml/min (STP). After being held at 400°C in the stream of helium for about 1 h, a continuous flow of 2 mol% thiophene in hydrogen was started through the reactor at 100 ml/min (STP). Following 2 h of continuous thiophene reaction, the reactor was purged with helium for 1 h at 400°C. The reactor was cooled to room temperature, continuing the helium purge for at least 1 h more. The reactor was isolated and five calibration pulses of $O_2$ or NO were taken, bypassing the reactor.

The reactor was returned on-line, and the $O_2$ or NO adsorption capacities of the catalysts were then determined.

A dynamic (pulsed) technique similar to that first reported by Tauster *et al.* [20] was used for the $O_2$ adsorption measurements. A dynamic technique was employed to prevent oxidation of sulfur or subsurface penetration of $O_2$, reported to lead to the formation of sulfate-type species and $SO_2$ [29,33,40,51]. Evidence has been provided indicating that pulse-flow measurements at 25°C are surface selective and comparable to volumetric (static) adsorption at -78°C [40]. Based on this prior research, $O_2$ chemisorption was determined at ambient temperature by injecting 0.10-ml pulses of 10% $O_2$ (Air Products, 99.5%) in helium (0.41 $\mu$mol $O_2$/pulse), at 2-min intervals, into the helium carrier gas by means of a six-port sampling valve (Valco zero volume) upstream of the catalyst bed. Effluent gas from the reactor was routed through a 6-ft molecular sieve column (13x, 80–100 mesh), maintained at 100°C, to a thermal conductivity cell on an Antek 310/40 ALP gas chromatograph. Helium flowed through the reference side of the detector following a 6-ft Porapak Q column. Non-adsorbed $O_2$ peak areas were measured by a Hewlett–Packard 3390A integrator. In general, the first few $O_2$ pulses were completely adsorbed, and then peaks due to non-adsorbed $O_2$ began to emerge and increase in size. The pulses were terminated when successive peak areas differed by less than 1%. At this point, the catalytically active sites were considered saturated [20,27]. A small residual uptake of $O_2$ continued, possibly due to bulk or

surface oxidation of the sulfide phases [27,33]. This was reduced by minimizing the duration of exposure and the concentration of the $O_2$ pulses.

A pulsed technique was also used to measure NO adsorption (similar to [41,65,89–90,92]). A 0.25-ml pulse of 3% NO in helium (Matheson, Primary Standard grade) (0.31 $\mu$mol NO/pulse) was injected at room temperature through the reactor at 2-min intervals. The effluent gas, containing any non-adsorbed NO, was analyzed in the same manner as in the $O_2$ chemisorption experiments. The first few pulses of NO were completely adsorbed, similar to the $O_2$ studies. When the emerging NO peaks reached a nearly constant area ($<$ 1% change), saturation of the catalyst was assumed and the total NO uptake was calculated.

# RESULTS

## Catalyst Characterization

The bulk purities of the Chevrel phases and the $MoS_2$ sample were determined primarily by X-ray powder diffraction. A representative X-ray diffraction pattern of the Chevrel phases is shown in Figure 1. The powder diffraction peaks are indexed on the basis of a rhombohedral unit cell. The data show $Lu_{0.8}Pb_{0.33}Mo_6S_8$ before and after 10 h of thiophene reaction, with no apparent change in the X-ray pattern, indicating no loss of crystallinity and no formation of other phases under the reaction conditions. This result was typical for all of the Chevrel phases studied.

Figure 2 presents the X-ray diffraction pattern of the unsupported $MoS_2$ catalyst. The peaks are indexed on the basis of a hexagonal unit cell. For this material, the degree of crystallinity is high, as indicated by the generally sharp, intense diffraction peaks. However, some of the peaks are more broad, due to stacking faults in the S–Mo–S layers [140].

Laser Raman spectroscopy is a sensitive technique for the detection of both crystalline and poorly crystalline $MoS_2$. The $MoS_2$ material contained bands about 383

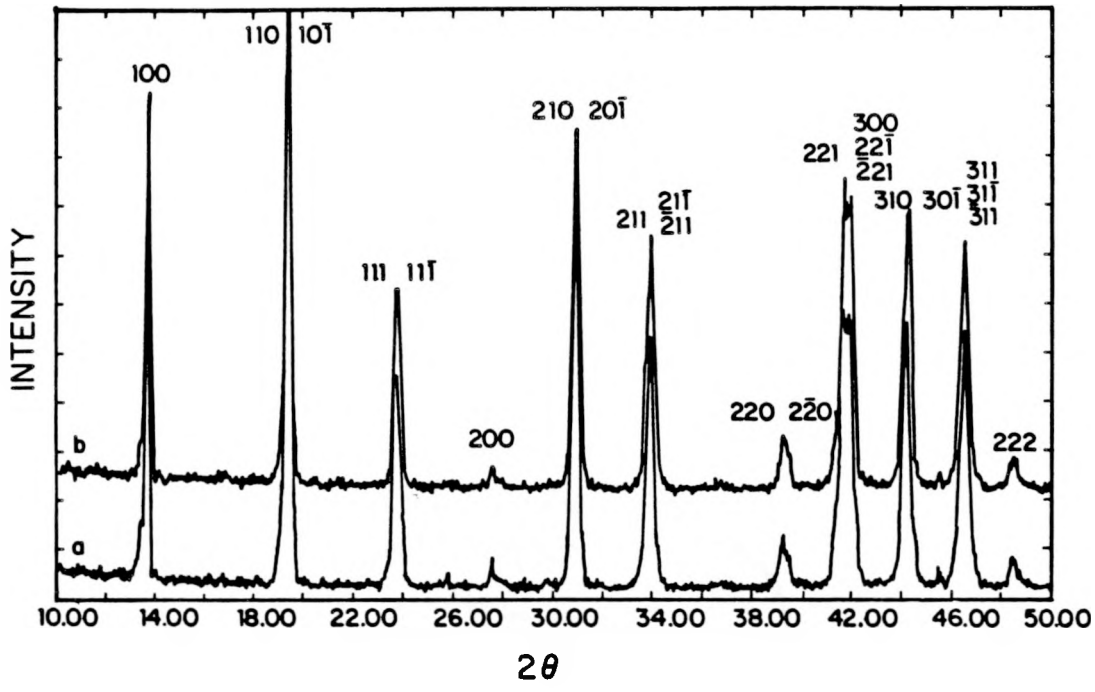


Figure 1. X-ray powder diffraction pattern of (a) fresh and (b) used (10 h of thiophene reaction) $Lu_{0.8}Pb_{0.33}Mo_6S_8$ with rhombohedral *hkl* indexes

and 407 $cm^{-1}$, compared to the 383 and 409 $cm^{-1}$ bands reported for highly crystalline $MoS_2$ [141]. No $MoS_2$ impurities were detected in any fresh or used (10-h thiophene reaction) Chevrel phases.

The XPS data for fresh and used Chevrel phases are presented in Table 1. The molybdenum $3d_{5/2}$ binding energies for the fresh catalysts are grouped around 227.8 eV, ranging from 227.6 eV for $Lu_{0.8}Pb_{0.33}Mo_6S_8$ to 228.1 eV for both $Lu_{0.4}Pb_{0.67}Mo_6S_8$ and $Lu_{0.1}PbMo_6S_8$. For comparison, the $3d_{5/2}$ binding energy for $MoS_2$ ($Mo^{4+}$) is 228.9 eV, and that for $Mo^{6+}$ is about 232.5 eV [1]. These data clearly demonstrate the

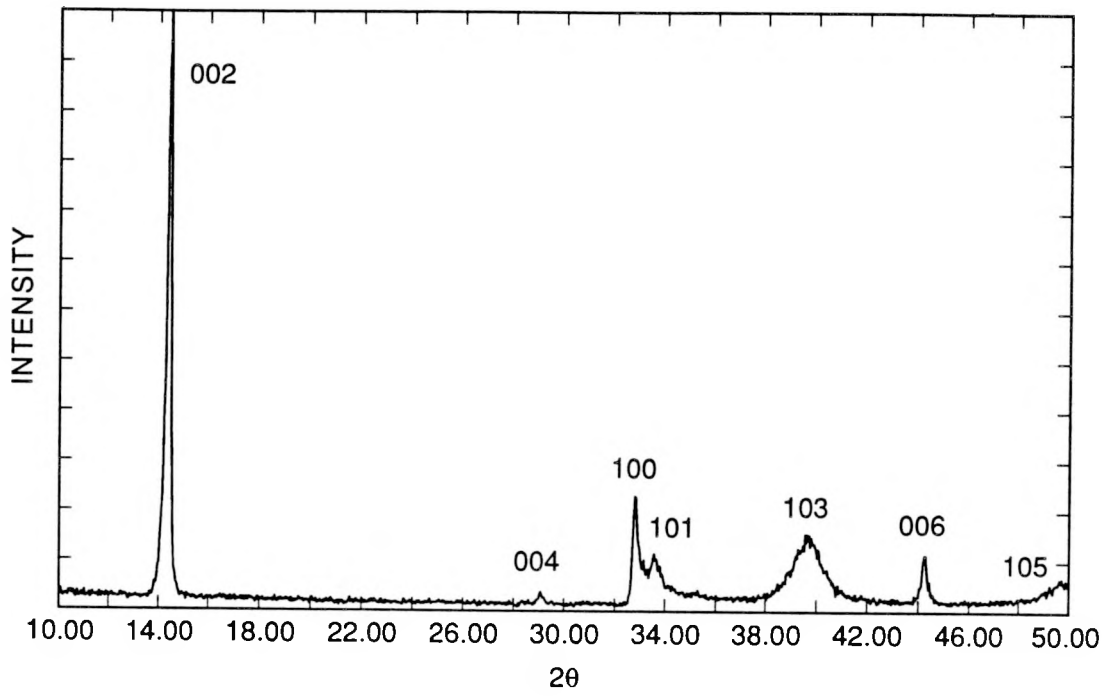


Figure 2. X-ray powder diffraction of fresh $MoS_2$ with hexagonal *hkl* indexes

low molybdenum oxidation states present in the Chevrel phases. No significant shifts in the molybdenum 3*d* binding energies after 10-h continuous flow thiophene reaction were observed. Minor shifts to lower binding energies, as well as slight variations in the molybdenum $3d_{3/2}$–$3d_{5/2}$ peak separations, were observed for some of the catalysts after thiophene HDS. These changes can be accounted for by the reduction, during thiophene HDS, of small amounts of $MoO_2$ impurities, formed by the high temperature reaction of the Chevrel phases with the fused-silica synthesis tubes [121].

Table 1. XPS binding energies

| Catalyst | | Binding energies (eV) | | | | | | |
|---|---|---|---|---|---|---|---|---|
| | | Mo | | Pb | | Lu | | S |
| | | $3d_{3/2}$ | $3d_{5/2}$ | $4f_{5/2}$ | $4f_{7/2}$ | $4d_{3/2}$ | $4d_{5/2}$ | $2p$ |
| $Lu_{1.2}Mo_6S_8$ | A | 231.1 | 227.7 | –[a] | –[a] | 207.0 | 197.2 | 161.8 |
| | B | 230.8 | 227.6 | –[a] | –[a] | 206.5 | 196.8 | 161.8 |
| $Lu_{0.8}Pb_{0.33}Mo_6S_8$ | A | 230.9 | 227.6 | 142.8 | 137.8 | 207.2 | 197.4 | 162.0 |
| | B | 230.8 | 227.6 | 142.6 | 137.9 | 207.0 | 197.4 | 162.2 |
| $Lu_{0.4}Pb_{0.67}Mo_6S_8$ | A | 231.4 | 228.1 | 142.5 | 137.6 | 207.3 | 197.6 | 161.9 |
| | B | 231.0 | 227.6 | 142.6 | 137.7 | 207.0 | 197.2 | 161.9 |
| $PbMo_{6.2}S_8$ | A | 231.1 | 227.7 | 143.3 | 138.6 | –[a] | –[a] | 162.3 |
| | B | 231.0 | 227.9 | 143.0 | 138.3 | –[a] | –[a] | 162.4 |
| $Lu_{0.1}PbMo_6S_8$ | A | 231.5 | 228.1 | 143.3 | 138.6 | –[b] | –[b] | 162.1 |
| | B | 231.1 | 227.8 | 142.8 | 138.0 | –[b] | –[b] | 162.1 |

A = fresh catalyst; B = after 10 h of continuous $H_2$–thiophene reaction

[a]Not applicable.
[b]Lu concentration too low to evaluate.

## Activity Measurements

The 10-h continuous-flow thiophene HDS reaction results are summarized in Table 2. The HDS rates were determined from the production of $C_4$ hydrocarbons, and were normalized on the basis of the surface area of the catalysts. The empty reactor converted 0.3% of the thiophene to $C_4$ products. This value was subtracted from the $C_4$ yields before the HDS activities were calculated. It is evident from the data that the

Table 2. $O_2$ and NO uptake following 2 h of continuous $H_2$–thiophene reaction

| Catalyst (formal Mo oxidation state) | | Surface area ($m^2/g$) | HDS rate[a] ($mol/s \cdot m^2$) $\times 10^8$ | $O_2$ chemisorption ($\mu mol/m^2$) | NO chemisorption ($\mu mol/m^2$) |
|---|---|---|---|---|---|
| $Lu_{1.2}Mo_6S_8$ | (2.07) | 0.584 | 1.93 | 1.96 | 0.87 |
| $Lu_{0.8}Pb_{0.33}Mo_6S_8$ | (2.16) | 0.439 | 2.00 | 2.99 | 1.24 |
| $Lu_{0.4}Pb_{0.67}Mo_6S_8$ | (2.24) | 0.719 | 3.30 | 3.18 | 1.21 |
| $PbMo_{6.2}S_8$ | (2.26) | 0.510 | 2.61 | 3.40 | 1.29 |
| $Lu_{0.1}PbMo_6S_8$ | (2.28) | 0.663 | 6.27 | 3.67 | 1.79 |
| $MoS_2$ | (4.00) | 2.756 | 0.92 | 0.30 | 0.40 |

[a]After 10 h of continuous $H_2$–thiophene reaction (400°C) [120].

Chevrel phases exhibit thiophene HDS activities significantly greater (approximately 2–7 times greater) than the model $MoS_2$ material.

## $O_2$ and NO Chemisorption Measurements

Table 2 also presents the $O_2$ and NO uptake data for the Chevrel phases and the $MoS_2$ catalyst. The amount of $O_2$ and NO adsorbed were easily calculated from the number of pulses and peak areas of the eluting non-adsorbed gas. Empty reactor evaluations resulted in a system uptake of 0.045 $\mu$mole $O_2$ and 0.049 $\mu$mole NO. These values were subtracted from the adsorption data before the chemisorption values were calculated.

The tabulated chemisorption values were determined following 2 h of continuous thiophene HDS. In some cases, $O_2$ and NO uptakes were determined for catalysts

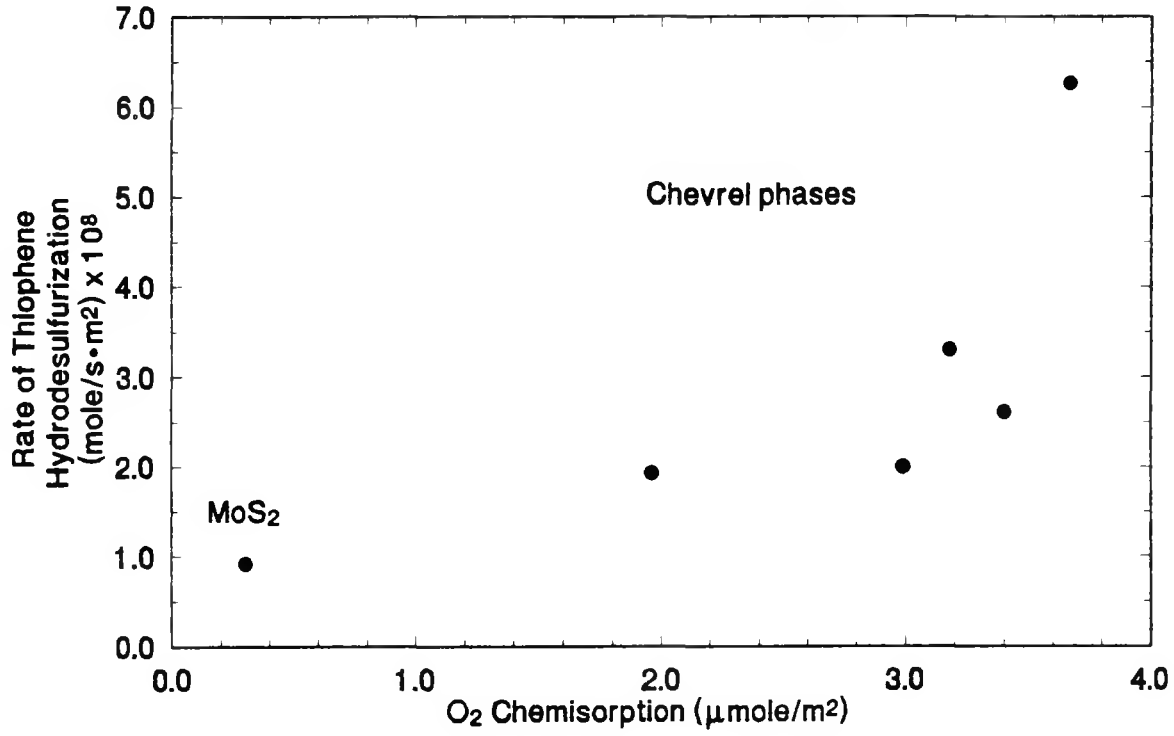


Figure 3. Thiophene hydrodesulfurization activities (400°C) as a function of oxygen chemisorption

without thiophene pretreatment. Compared to these values, those obtained after pretreatment were somewhat higher. The thiophene HDS activity data show an increase in catalytic activity for reaction times of up to 2 h of thiophene reaction before levelling off or slowly decreasing, indicating an initial activation the catalyst [122]. Accordingly, the pretreated samples provide a much better representation of the working catalyst.

Although not quite linear, the amount of $O_2$ adsorbed by the catalysts generally increases with increasing activity for thiophene HDS, as illustrated in Figure 3. Figure 4 demonstrates that a similar correlation is observed for NO. All of the Chevrel phases

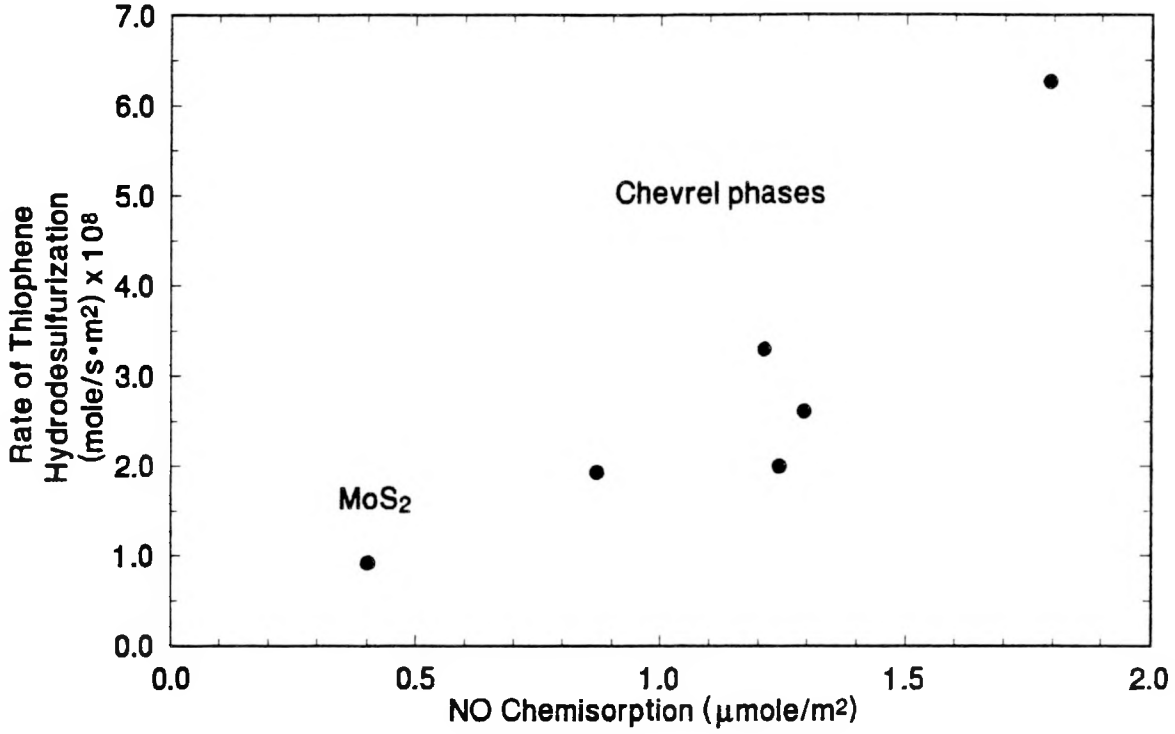


Figure 4. Thiophene hydrodesulfurization activities (400°C) as a function of nitric oxide chemisorption

had significantly greater capacities for $O_2$ and NO chemisorption than the model $MoS_2$material. Larger amounts of $O_2$ were adsorbed by the Chevrel phases than NO; the reverse was true for the $MoS_2$ catalyst.

# DISCUSSION OF RESULTS

Previous investigations have demonstrated that Chevrel phases have thiophene HDS activities comparable to, or greater than, model unpromoted and cobalt-promoted $MoS_2$-based catalysts [115–119,121–122]. These materials have also been found to have very low 1-butene HYD activities, making them rather selective catalysts [115–119,121–122]. Although structural and compositional effects cannot be completely eliminated, their high HDS activities are attributed primarily to the presence of highly reduced molybdenum formal oxidation states (relative to $Mo^{4+}$). Depending upon the identity or concentration (or both) of the ternary metal present, Chevrel phases have molybdenum oxidation states ranging from +2 to +2.67.

The data in Table 2 demonstrate the high HDS activities of the Chevrel phases compared to $MoS_2$. The thiophene HDS activities have been normalized to the surface areas of the various catalysts. Correlations between total surface area and HDS activity have been shown to be inadequate for some catalysts [20]. However, these involved series of catalysts prepared by more than one method. Better relationships have been reported for catalysts prepared by very similar techniques [39]. In this regard, among

the isostructural Chevrel phases, catalytic activity normalized to the surface areas may provide more definite comparisons.

X-ray diffraction and laser Raman spectroscopy have demonstrated the purity and the stability of the bulk structures for the lead–lutetium Chevrel phases under thiophene HDS conditions at 400°C. XPS analysis indicates that the molybdenum oxidations states at the surface are indeed reduced (relative to $Mo^{4+}$); and that these reduced molybdenum oxidation states are stable under the reaction conditions [121].

As reported in Table 2, considerably larger amounts of $O_2$ were adsorbed by the Chevrel phases than NO. This trend also occurs when $O_2$ and CO are compared as probe molecules for conventional HDS catalysts [29]. In contrast, $MoS_2$ was observed to adsorb slightly less $O_2$ than NO. Although other investigators have reported that smaller amounts of $O_2$ than NO are chemisorbed by supported cobalt- or nickel-promoted catalysts (*e.g.*, [12,47]), Cáceres *et al.* [56] reported that the amount of $O_2$ uptake on $Mo/\gamma-Al_2O_3$ catalysts was much higher than the corresponding irreversible NO adsorption. However, total NO adsorption was found to be approximately five times higher than irreversible NO uptake. They suggested that the irreversibly adsorbed NO may be chemisorbed on $Mo^{3+}$ or $Mo^{2+}$ sites.

From the chemisorption and surface area data (Table 2), it is possible to estimate $O_2$ and NO adsorption cross-sectional areas, *i.e.*, the effective surface area occupied by one $O_2$ or NO molecule. These values are presented in Table 3. For the unsupported $MoS_2$ material, a value of 5.54 $nm^2/O_2$ molecule was calculated. Similar $O_2$ adsorption

Table 3. Adsorption cross-sectional areas of $O_2$ and NO[a]

| Catalyst | $O_2$ adsorption cross-sectional area ($nm^2/O_2$ molecule) | NO adsorption cross-sectional area ($nm^2$/NO molecule) |
|---|---|---|
| $Lu_{1.2}Mo_6S_8$ | 0.85 | 1.91 |
| $Lu_{0.8}Pb_{0.33}Mo_6S_8$ | 0.56 | 1.34 |
| $Lu_{0.4}Pb_{0.67}Mo_6S_8$ | 0.52 | 1.37 |
| $PbMo_{6.2}S_8$ | 0.49 | 1.29 |
| $Lu_{0.1}PbMo_6S_8$ | 0.45 | 0.93 |
| $MoS_2$ | 5.54 | 4.15 |

[a]Calculated as the ratio of catalyst surface area to $O_2$ or NO chemisorption (Table 2).

cross-sectional areas for unsupported $MoS_2$ have been reported previously, ranging from 0.61 $nm^2/O_2$ to 9.8 $nm^2/O_2$ molecule [20,39–40,44,48]. It is assumed that differences in pretreatment and preparation contribute to the wide variation in $O_2$ adsorption areas on $MoS_2$ [40,44]. Comparison of the $O_2$ adsorption area of 5.54 $nm^2/O_2$ molecule to the area of 0.146 $nm^2$/molecule for physisorbed oxygen [142] leads to the conclusion that only about 3% of the $MoS_2$ surface is covered by oxygen at saturation. Therefore, $O_2$ measures only a small fraction of the total number of molybdenum atoms present. This supports the concept of selective adsorption on special types of molybdenum sites, most likely located at edge or corner molybdenum CUS on $MoS_2$ catalysts.

The Chevrel phases exhibited much lower $O_2$ adsorption cross-sectional areas than the model $MoS_2$ material, ranging from 0.45 $nm^2/O_2$ for $Lu_{0.1}PbMo_6S_8$ to 0.85

$nm^2/O_2$ for $Lu_{1.2}Mo_6S_8$ (Table 3). Further comparison reveals that the differences in the $O_2$ adsorption areas can be related to differences in thiophene HDS activities for the Chevrel phases: lower $O_2$ adsorption cross-sectional areas (or higher surface coverage by $O_2$) are found for Chevrel phases exhibiting higher catalytic activity for thiophene HDS. Taken as a group, on average, approximately 25% of the Chevrel phase surface is covered by $O_2$ at saturation compared to 3% for the $MoS_2$ catalyst.

The NO adsorption cross-sectional areas provide similar trends (Table 3). The unsupported $MoS_2$ catalyst has a calculated value of 4.15 $nm^2$/NO molecule. Adsorption cross-sectional areas for NO on unsupported $MoS_2$ have not been reported previously in the literature. This value is considerably higher than the values determined for the Chevrel phases, which range from 0.93 to 1.91 $nm^2$/NO molecule. Assuming a cross-sectional area of 0.157 $nm^2$/molecule for physisorbed NO [142] indicates that approximately 12% of the surface is titrated by NO, on average, for the Chevrel phases compared to only 4% for $MoS_2$.

As illustrated in Figure 3 and Figure 4, Chevrel phases provide reasonable correlations between the rate of thiophene HDS and $O_2$ or NO chemisorption. In addition, the $O_2$ and NO adsorption cross-sectional areas indicate that a much larger fraction of the catalyst surface is titrated by these adsorbates for the Chevrel phases than for the model $MoS_2$ material. This leads to the conclusion that $O_2$ and NO may effectively titrate the active sites for thiophene HDS on these catalysts. These sites are proposed to be reduced (relative to $Mo^{4+}$) molybdenum species.

Theoretical studies by Harris [108–109] and Harris and Chianelli [110–111] have related catalytic activity to several electronic factors based on SCF–X$\alpha$ scattered wave method molecular orbital calculations. These factors include the number of *d* electrons in the HOMO, the degree of covalency of the metal–sulfur bond, and the metal–sulfur covalent bond strength, although the dominant factor is proposed to be the number of *d* electrons formally associated with molybdenum. In their model, promotion of HDS catalysts requires interaction between molybdenum 4*d* electrons and promoter (cobalt or nickel) 3*d* electrons, which results in a net charge transfer and an increase in the number of 4*d* electrons in the HOMO of $MoS_2$. Copper, a poison for HDS catalysts, withdraws electron density from the highest occupied 4*d* orbitals of $MoS_2$. Thus, promotion occurs with formal reduction of $Mo^{4+}$ species and poisoning with oxidation of $Mo^{4+}$ ions. It could not be differentiated whether promotion resulted in the formation of new active sites (more active than unpromoted sites), or in the stabilization of active sites already present.

The molybdenum 4*d* electrons are also known to play an important role in some of the physical properties of the Chevrel phases [131]. These electrons are stongly localized at the $Mo_6$ octahedra. The addition of ternary metal cations results in a donation of electrons (*e*) to the $Mo_6$ clusters, increasing the number of valence electrons on the molybdenum atoms (*e*/Mo), and resulting in their stabilization [125,128,130–131,133]. For example, $Mo_6S_8$ is metastable (decomposes at 400–470°C [143–144]), containing only 20 electrons per $Mo_6$ cluster (3.33 *e*/Mo). Addition of

ternary metals results in a charge transfer, or donation of electrons, to the cluster, up to the maximum value of 24 electrons per $Mo_6$ cluster (4 *e*/Mo), and stabilizes the cluster unit.

Hall *et al.* [18,41,53,67,79,85] have investigated the chemisorption of $O_2$ and NO on reduced and sulfided Mo/$\gamma$–$Al_2O_3$ catalysts. The amount of $O_2$ or NO was correlatable with the concentration of molybdenum CUS. They interpreted their results on the basis of the extent of molybdenum reduction, *e*/Mo, defined as the average number of electrons the $Mo^{6+}$ ions have been reduced, and have found that a substantial fraction of the molybdenum ions have *e*/Mo $\geq$ 2 (*i.e.*, valence states lower than $Mo^{4+}$). They proposed that the primary reaction centers were low-valent $Mo^{2+}$ ions, located on the edge or corner sites of $MoS_2$, with multiple coordinative unsaturation (double or triple CUS). The amount of $O_2$ or NO adsorbed by the catalysts was also related to the extent of reduction: for values of *e*/Mo ranging from 0.5 to 2.0, increasing amounts of $O_2$ were adsorbed for higher values of *e*/Mo [18]. Since the formal oxidation state of molybdenum is simply related to the extent of reduction (equal to 6 – *e*/Mo), this suggests possible relationships between molybdenum formal oxidation states and $O_2$ or NO chemisorption.

These relationships are examined using the lead–lutetium series of Chevrel phases in Figure 5 and Figure 6, depicting the amount of $O_2$ and NO chemisorbed as a function of the formal oxidation state of molybdenum, respectively. For the Chevrel phases, increasing amounts of $O_2$ or NO are adsorbed as the molybdenum oxidation

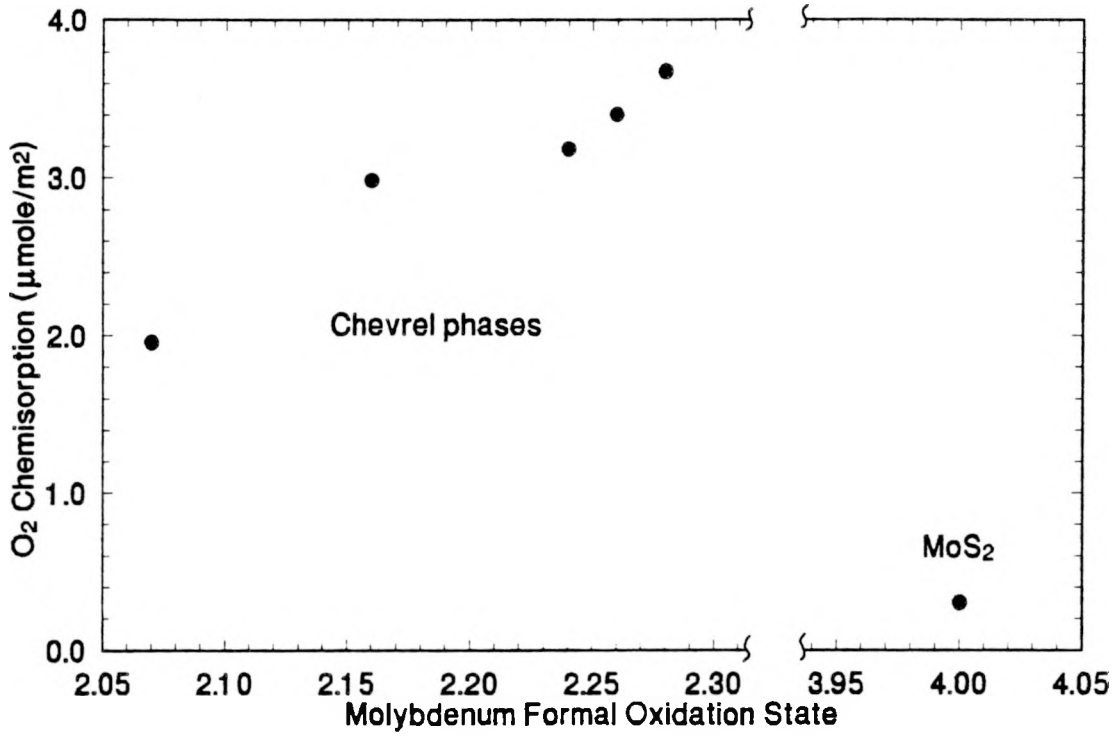


Figure 5. Oxygen chemisorption as a function of the formal oxidation state of molybdenum

state increases from +2.07 to +2.28. $MoS_2$, with a molybdenum formal oxidation state of +4, adsorbs much less $O_2$ or NO than even the lowest amount found for any of the Chevrel phases examined in this study. Considering these data, along with the data of Hall *et al.* [18], a maximum in $O_2$ or NO adsorption may exist between the highest oxidation state for the Chevrel phases (+2.28) and the molybdenum oxidation state (+4) for $MoS_2$.

A similar trend was reported between the rate of thiophene HDS and the formal oxidation state of molybdenum for a lead–lutetium series of Chevrel phases and $MoS_2$

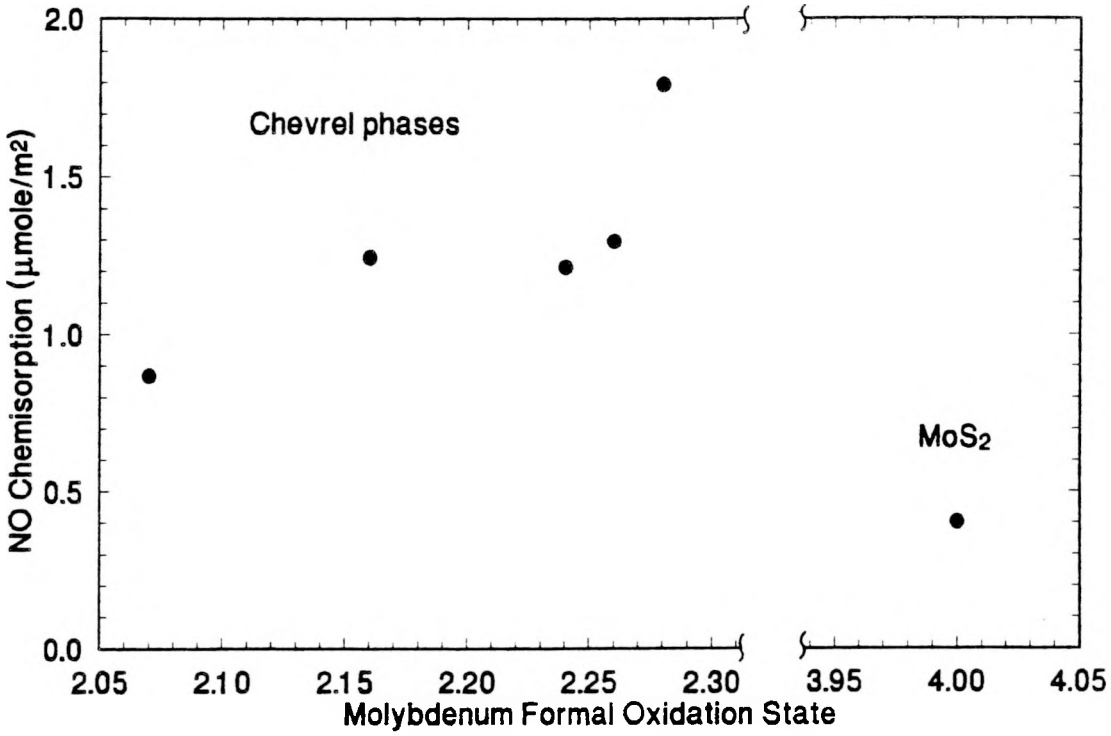


Figure 6. Nitric oxide chemisorption as a function of the formal oxidation state of molybdenum

[121]. Thiophene HDS activity was associated with reduced molybdenum oxidation states (relative to $Mo^{4+}$), apparently reaching a maximum between $Mo^{2+}$ and $Mo^{4+}$. The chemisorption of $O_2$ and NO molecules also apparently reach a maximum between these values. Therefore, the same reduced sites which exhibit the greatest catalytic activity for thiophene HDS also are responsible as the adsorption sites for probe molecules such as $O_2$ and NO for these materials.

The potential of chemisorption techniques as rapid screening tests of HDS catalyts has long been a subject of debate. Both very negative conclusions and

encouraging correlations have been reported in the literature. However, it appears that uptake is more or less sensitive to changes in HDS activity, whether or not linear correlations exist. In addition, no clear consensus exists about the sites on which probe molecules chemisorb; nor for sites on which HDS reactions take place.

In general, it has been shown that the HDS activity of unpromoted molybdenum-based catalysts correlates with both the amount of adsorbed $O_2$ [20,23,26,29,31–32,35, 40,45,49,58–59] and NO [49,65,89,92]. In contrast to unpromoted catalysts, promoted catalysts generally do not show valid linear correlations between catalytic activity and $O_2$ [12,22,33,36,47,51,57] or NO [47,90,93] adsorption. The vast literature concerning promoted molybdenum catalysts indicates that the relative proportions of different catalytic phases may vary with preparation techniques. Lack of suitable correlations for promoted catalysts may be related to the variety of preparations, and hence, proportions of different sulfide phases. This may also be explained by the fact that $O_2$ and NO may adsorb on more than one type of site: on both the less active, unpromoted molybdenum atoms and on the more active promoted molybdenum species (including dual HDS sites or both HDS and HYD sites). For example, Candia *et al.* [12] have reported that $O_2$ and NO adsorb on both unpromoted molybdenum sites and promoted sites associated with cobalt atoms present as a Co–Mo–S phase. Moon and Ihm [65] have proposed that NO adsorbs on both single and double molybdenum CUS. Okamoto *et al.* [93] suggested, on the basis of parabolic relationships between NO uptake and thiophene

HDS activities, that HDS proceeds effectively on dual molybdenum sites, proposed to be double or triple molybdenum CUS.

Chevrel phases posses predominantly one type of catalytic site—reduced molybdenum species responsible primarily for HDS. Chevrel phases posses a high degree of thiophene HDS acitivity; however, they are very selective catalysts in that they exhibit very low activity for 1-butene HYD [115–118,121–122]. In contrast, the model $MoS_2$ material has a much greater (about 2 to 10 times greater) activity for 1-butene HYD [115–118,121–122], indicating the possibility of more than one type of catalytically active site. Even so, the Chevrel phases, with their higher HDS activities, adsorb larger quantities of $O_2$ and NO. Although $O_2$ or NO may titrate more than one type of site on typical industrial catalysts, considering the results of chemisorption on Chevrel phases, it is likely that reduced (relative to $Mo^{4+}$) sites also chemisorb $O_2$ and NO on these catalysts, and that these reduced sites play an important role in HDS mechanisms.

# CONCLUSIONS

Lead–lutetium Chevrel phases were found to chemisorb $O_2$ and NO in larger quantities than those of the model $MoS_2$ catalyst. It was possible to relate the chemisorption data and the catalytic activity: the same reduced oxidation states (relative to $Mo^{4+}$) which display the greatest activity for thiophene HDS are also responsible as the adsorption sites for $O_2$ and NO. These sites have molybdenum formal oxidation states between $Mo^{2+}$ and $Mo^{4+}$. In direct analogy to conventional HDS catalysts, these reduced molybdenum species are believed to play an important role in HDS mechanisms.

# ACKNOWLEDGMENTS

This work was conducted through the Ames Laboratory which is operated for the U. S. Department of Energy by Iowa State University under Contract W–7405–Eng–82. This research was supported by the Office of Basic Energy Sciences, Chemical Sciences Division. XPS spectra were obtained by J. W. Anderegg of the Ames Laboratory.

# REFERENCES


1. Li, C. P., and Hercules, D. M., *J. Phys. Chem.* **88**, 456 (1984).

2. Zingg, D. S., Makovsky, L. E., Tisher, R. E., Brown, F. R., and Hercules, D. M., *J. Phys. Chem.* **84**, 2898 (1980).

3. Patterson, T. A., Carver, J. C., Leyden, D. E., and Hercules, D. M., *J. Phys. Chem.* **80**, 1700 (1976).

4. Parham, T. G., and Merrill, R. P., *J. Catal.* **85**, 295 (1984).

5. Clausen, B. S., Topsøe, H., Candia, R., Villadsen, J., Lengeler, B., Als-Nielsen, J., and Christensen, F., *J. Phys. Chem.* **85**, 3868 (1981).

6. Pollack, S. S., Makovsky, L. E., and Brown, F. R., *J. Catal.* **59**, 452 (1979).

7. Schrader, G. L., and Cheng, C. P., *J. Catal.* **80**, 369 (1983).

8. Furimsky, E., *Catal. Rev.—Sci. Eng.* **22**, 371 (1980).

9. Topsøe, H., Clausen, B. S., Candia, R., Wivel, C., and Mørup, S., *J. Catal.* **68**, 433 (1981).

10. Wivel, C., Candia, R., Clausen, B. S., Mørup, S., and Topsøe, H., *J. Catal.* **68**, 453 (1981).

11. Hall, W. K., and Lo Jacono, M. *in* "Proceedings, 6th International Congress on Catalysis, London, 1976" (G. C. Bond, P. B. Wells, and F. C. Tompkins, Eds.), Vol. I, p. 245. The Chemical Society, London, 1977.

12. Candia, R., Clausen, B. S., Bartholdy, J., Topsøe, N.-Y., Lengeler, B., and Topsøe, H., *in* "Proceedings, 8th International Congress on Catalysis, Berlin, 1984" (E. Ertl, Ed.), Vol. II, p. 375. Dechema, Frankfurt-am-Main, 1984.

13. Massoth, F. E., and Kibby, C. L., *J. Catal.* **47**, 300 (1977).

14. (a) Voorhoeve, R. J. H., and Stuiver, J. C. M., *J. Catal.* **23**, 228, 243 (1971). (b) Voorhoeve, R. J. H., *J. Catal.* **23**, 236 (1971).

15. Bahl, O. P., Evans, E. L., and Thomas, J. M., *Proc. Roy. Soc., London Ser. A* **306**, 53 (1968).

16. Parekh, B. S., and Weller, S. W., *J. Catal.* **47**, 100 (1977).

17. Parekh, B. S., and Weller, S. W., *J. Catal.* **55**, 58 (1978).

18. Millman, W. S., and Hall, W. K., *J. Catal.* **59**, 311 (1979).

19. Vyskočil, V., and Tomanová, D., *React. Kinet. Catal. Lett.* **10**, 37 (1979).

20. Tauster, S. J., Pecoraro, T. A., and Chianelli, R. R., *J. Catal.* **63**, 515 (1980).

21. Srinivasan, R., Liu, H.-C., and Weller, S. W., *J. Catal.* **57**, 87 (1979).

22. Chung, K. S., and Massoth, F. E., *J. Catal.* **64**, 332 (1980).

23. Bachelier, J., Duchet, J. C., and Cornet, D., *J. Phys. Chem.* **84**, 1925 (1980).

24. Liu, H.-C., Yuan, L., and Weller, S. W., *J. Catal.* **61**, 282 (1980).

25. Lombardo, E., Lo Jacono, M., and Hall, W. K., *J. Catal.* **64**, 150 (1980).

26. Liu, H.-C., and Weller, S. W., *J. Catal.* **66**, 65 (1980).

27. Tauster, S. J., and Riley, K. L., *J. Catal.* **67**, 250 (1981).

28. Tauster, S. J., and Riley, K. L., *J. Catal.* **70**, 230 (1981).

29. Bachelier, J., Duchet, J. C., and Cornet, D., *Bull. Soc. Chim. Belg.* **90**, 1301 (1981).

30. Wright, C. J., Fraser, D., Moyes, R. B., and Wells, P. B., *Appl. Catal.* 1, 49 (1981).

31. López Agudo, A., Gil Llambías, F. J., Reyes, P., and Fierro, J. L. G., *Appl. Catal.* 1, 59 (1981).

32. Bachelier, J., Tilliette, M. J., Duchet, J. C., and Cornet, D., *J. Catal.* **76**, 300 (1982).

33. Zmierczak, W., MuraliDhar, G., and Massoth, F. E., *J. Catal.* **77**, 432 (1982).

34. Bodrero, T. A., Bartholomew, C. H., and Pratt, K. C., *J. Catal.* **78**, 253 (1982).

35. Silbernagel, B. G., Pecoraro, T. A., and Chianelli, R. R., *J. Catal.* **78**, 380 (1982).

36. Burch, R., and Collins, A., *in* "Proceedings of the Climax Fourth International Conference on Chemistry and Uses of Molybdenum" (H. F. Barry and P. C. H. Mitchell, Eds.), p. 379. Climax Molybdenum Co., Ann Arbor, MI, 1982.

37. Jung, H. J., Schmitt, J. L., and Ando, H., *in* "Proceedings of the Climax Fourth International Conference on Chemistry and Uses of Molybdenum" (H. F. Barry and P. C. H. Mitchell, Eds.), p. 246. Climax Molybdenum Co., Ann Arbor, MI, 1982.

38. Weller, S. W., *Acc. Chem. Res.* **16**, 101 (1983).

39. Concha, B. E., and Bartholomew, C. H., *J. Catal.* **79**, 327 (1983).

40. Bodrero, T. A., and Bartholomew, C. H., *J. Catal.* **84**, 145 (1983).

41. Valyon, J., and Hall, W. K., *J. Catal.* **84**, 216 (1983).

42. Bachelier, J., Duchet, J. C., and Cornet, D., *J. Catal.* **87**, 283 (1984).

43. Concha, B. E., Bartholomew, G. L., and Bartholomew, C. H., *J. Catal.* **89**, 536 (1984).

44. Fierro, J. L. G., Gonzalez Tejuca, L., López Agudo, A., and Weller, S. W., *J. Catal.* **89**, 111 (1984).

45. Vissers, J. P. R., Bachelier, J., ten Doeschate, H. J. M., Duchet, J. C., de Beer, V. H. J., and Prins, R., *in* "Proceedings, 8th International Congress on Catalysis, Berlin, 1984" (E. Ertl, Ed.), Vol. II, p. 387. Dechema, Frankfurt-am-Main, 1984.

46. Millman, W. S., Bartholomew, C. H., and Richardson, R. L., *J. Catal.* **90**, 10 (1984).

47. López Agudo, A., Gil Llambías, F. J., Tascón, J. M. D., and Fierro, J. L. G., *Bull. Soc. Chim. Belg.* **93**, 719 (1984).

48. Prada Silvy, R., Beuken, J. M., Bertrand, P., Hodnett, B. K., Delannay, F., and Delmon, B., *Bull. Soc. Chim. Belg.* **93**, 775 (1984).

49. Topsøe, H., Candia, R., Topsøe, N.-Y., and Clausen, B. S., *Bull. Soc. Chim. Belg.* **93**, 783 (1984).

50. MuraliDhar, G., Concha, B. E., Bartholomew, G. L., and Bartholomew, C. H., *J. Catal.* **89**, 274 (1984).

51. Burch, R., and Collins, A., *Appl. Catal.* **17**, 273 (1985).

52. Reddy, B. M., Chary, K. V. R., Subrahmanyam, V. S., and Nag, N. K., *J. Chem. Soc., Faraday Trans. I* **81**, 1655 (1985).

53. Valyon, J., and Hall, W. K., *J. Catal.* **92**, 155 (1985).

54. Nag, N. K., *J. Catal.* **92**, 432 (1985).

55. Kalthod, D. G., and Weller, S. W., *J. Catal.* **95**, 455 (1985).

56. Cáceres, C. V., Fierro, J. L. G., López Agudo, A., Blanco, M. N., and Thomas, H. J., *J. Catal.* **95**, 501 (1985).

57. Cáceres, C., Fierro, J. L. G., López Agudo, A., Severino, F., and Laine, J., *J. Catal.* **97**, 219 (1986).

58. Reddy, B. M., and Subrahmanyam, V. S., *Appl. Catal.* **27**, 1 (1986).

59. Reddy, B. M., Chary, K. V. R., Rama Rao, B., Subrahmanyam, V.S., Sunandana, C. S., and Nag, N. K., *Polyhedron* **5**, 191 (1986).

60. Rodrigo, L., Marcinkowska, K., Adnot, A., Roberge, P. C., Kaliaguine, S., Stencel, J. M., Makovsky, L. E., and Diehl, J. R., *J. Phys. Chem.* **90**, 2690 (1986).

61. Gosselink, J. W., Schaper, H., de Jonge, J. P., and Stork, W. H. J., *Appl. Catal.* **32**, 337 (1987).

62. Gosselink, J. W., and Stork, W. H. J., *Bull. Soc. Chim. Belg.* **96**, 901 (1987).

63. Brunet, S., Karmal, S., Duprez, D., and Perot, G., *Catal. Lett.* **1**, 255 (1988).

64. Duchet, J. C., Lavalley, J. C., Housni, S., Ouafi, D., Bachelier, J., Lakhdar, M., Mennour, A., and Cornet, D., *Catal. Today* **4**, 71 (1988).

65. Moon, S.-J., and Ihm, S.-K., *Appl. Catal.* **42**, 307 (1988).

66. Howe, R. F., and Kemball, C., *J. Chem. Soc., Faraday Trans. I* **70**, 1153 (1974).

67. Millman, W. S., and Hall, W. K., *J. Phys. Chem.* **83**, 427 (1979).

68. Kazusaka, A., and Howe, R. F., *J. Catal.* **63**, 447 (1980).

69. Yao, H. C., *J. Catal.* **70**, 440 (1981).

70. Okamoto, Y., Katoh, Y., Mori, Y., Imanaka, T., and Teranishi, S., *J. Catal.* **70**, 445 (1981).

71. Suzuki, K., Soma, M., Onishi, T., and Tamaru, K., *J. Electron. Spectrosc. Relat. Phenom.* **24**, 283 (1981).

72. Topsøe, N.-Y., and Topsøe, H., *J. Catal.* **75**, 354 (1982).

73. Segawa, K.-I., and Hall, W. K., *J. Catal.* **77**, 221 (1982).

74. Topsøe, N.-Y., and Topsøe, H., *J. Catal.* **77**, 293 (1982).

75. Peri, J. B., *J. Phys. Chem.* **86**, 1615 (1982).

76. Hardee, J. R., and Hightower, J. W., *J. Catal.* **83**, 182 (1983).

77. Topsøe, N.-Y., and Topsøe, H., *J. Catal.* **84**, 386 (1983).

78. Valyon, J., Schneider, R. L., and Hall, W. K., *J. Catal.* **85**, 277 (1984).

79. Rosen, R. P., Segawa, K.-I., Millman, W. S., and Hall, W. K., *J. Catal.* **90**, 368 (1984).

80. Topsøe, N.-Y., Topsøe, H., Sørensen, O., Clausen, B. S., and Candia, R., *Bull. Soc. Chim. Belg.* **93**, 727 (1984).

81. Daly, F. P., Schmitt, J. L., and Sturm, E. A., *J. Catal.* **97**, 248 (1986).

82. Segawa, K.-I., and Millman, W. S., *J. Catal.* **101**, 218 (1986).

83. Morales, A., and Ramírez de Agudelo, M. M., *Appl. Catal.* **23**, 23 (1986).

84. Topsøe, H., and Clausen, B. S., *Appl. Catal.* **25**, 273 (1986).

85. Millman, W. S., Segawa, K.-I., Smrz, D., and Hall, W. K., *Polyhedron* **5**, 169 (1986).

86. Obara, T., Yamada, M., and Amano, A., *Chem. Lett.*, 2003 (1986).

87. Laine, J., Severino, F., Cáceres, C. V., Fierro, J. L. G., and López Agudo, A., *J. Catal.* **103**, 228 (1987).

88. Arteaga, A., Prada Silvy, R., and Delmon, B., *Bull. Soc. Chim. Belg.* **96**, 909 (1987).

89. Miciukiewicz, J., Zmierczak, W., and Massoth, F. E., *Bull. Soc. Chim. Belg.* **96**, 915 (1987).

90. Prada Silvy, R., Fierro, J. L. G., Grange, P., and Delmon, B., *Prepr.—Am. Chem. Soc., Div. Pet. Chem.* **32**, 287 (1987).

91. O'Young, C.-L., Yang, C.-H., de Canio, S. J., Patel, M. S., and Storm, D. A., *J. Catal.* **113**, 307 (1988).

92. Saini, A. R., Johnson, B. G., and Massoth, F. E., *Appl. Catal.* **40**, 157 (1988).

93. Okamoto, Y., Maezawa, A., and Imanaka, T., *J. Catal.* **120**, 29 (1989).

94. Millman, W. S., Crespin, M., Cirillo, A. C. Jr., Abdo, S., and Hall, W. K., *J. Catal.* **60**, 404 (1979).

95. Ramakrishnan, N. R., and Weller, S. W., *J. Catal.* **67**, 237 (1981).

96. Delgado, E., Fuentes, G. A., Hermann, C., Kunzmann, G., and Knözinger, H., *Bull. Soc. Chim. Belg.* **93**, 735 (1984).

97. Bachelier, J., Tilliette, M. J., Cornac, M., Duchet, J. C., Lavalley, J. C., and Cornet, D., *Bull. Soc. Chim. Belg.* **93**, 743 (1984).

98. Bouwens, S. M. A. M., Vissers, J. P. R., de Beer, V. H. J., and Prins, R., *J. Catal.* **112**, 401 (1988).

99. Bouwens, S. M. A. M., van der Kraan, A. M., de Beer, V. H. J., and Prins, R., *J. Catal.* **128**, 559 (1991).

100. Zmierczak, W., Qader, Q., and Massoth, F. E., *J. Catal.* **106**, 65 (1987).

101. Zdražil, M., *J. Catal.* **58**, 436 (1979).

102. Delvaux, G., Grange, P., and Delmon, B., *J. Catal.* **56**, 99 (1979).

103. Alstrup, I., Chorkendorff, I., Candia, R., Clausen, B. S., and Topsøe, H., *J. Catal.* **77**, 397 (1982).

104. McIntyre, N. S., Chan, T. C., Spevack, P. A., and Brown, J. R., *Appl. Catal.* **63**, 391 (1990).

105. Konings, A. J. A., Valster, A., de Beer, V. H. J., and Prins, R., *J. Catal.* **76**, 466 (1982).

106. Thakur, D. S., and Delmon, B., *J. Catal.* **91**, 308 (1985).

107. Duben, A. J., *J. Phys. Chem.* **82**, 348 (1978).

108. Harris, S., *Chem. Phys.* **67**, 229 (1982).

109. Harris, S., *Polyhedron* **5**, 151 (1986).

110. Harris, S., and Chianelli, R. R., *J. Catal.* **86**, 400 (1984).

111. Harris, S., and Chianelli, R. R., *J. Catal.* **98**, 17 (1986).

112. Ternan, M., *J. Catal.* **104**, 256 (1987).

113. Bouwens, S. M. A. M., Prins, R., de Beer, V. H. J., and Koningsberger, D. C., *J. Phys. Chem.* **94**, 3711 (1990).

114. Vissers, J. P. R., Groot, C. K., van Oers, E. M., de Beer, V. H. J., and Prins, R., *Bull. Soc. Chim. Belg.* **93**, 813 (1984).

115. McCarty, K. F., and Schrader, G. L., *in* "Proceedings, 8th International Congress on Catalysis, Berlin, 1984" (E. Ertl, Ed.), Vol. IV, p. 427. Dechema, Frankfurt-am-Main, 1984.

116. McCarty, K. F., and Schrader, G. L., *Ind. Eng. Chem. Prod. Res. Dev.* **23**, 519 (1984).

117. McCarty, K. F., Anderegg, J. W., and Schrader, G. L., *J. Catal.* **93**, 375 (1985).

118. McCarty, K. F., Ph.D. Dissertation, Iowa State University, Ames, Iowa, 1985.

119. McCarty, K. F., and Schrader, G. L., *J. Catal.* **103**, 261 (1987).

120. Huckett, S. C., Angelici, R. J., Ekman, M. E., and Schrader, G. L., *J. Catal.* **113**, 36 (1988).

121. Ekman, M. E., Anderegg, J. W., and Schrader, G. L., *J. Catal.* **117**, 246 (1989).

122. Schrader, G. L., and Ekman, M. E., *in* "Advances in Hydrotreating Catalysts" (M. L. Occelli and R. G. Anthony, Eds.), Vol. 50, p. 41. Elsevier, Amsterdam, 1989.

123. Kareem, S. A., and Miranda, R., *J. Molec. Catal.* **53**, 275 (1989).

124. Chevrel, R., Sergent, M., and Prigent, J., *J. Solid State Chem.* **3**, 515 (1971).

125. Yvon, K., *in* "Current Topics in Materials Science" (E. Kaldis, Ed.), Vol. 3, p. 53. North-Holland, Amsterdam, 1979.

126. Fischer, Ø., and Maple, M. B., *in* "Topics in Current Physics" (Ø. Fischer and M. B. Maple, Eds.), Vol. 34, p. 1. Springer-Verlag, Berlin, 1982.

127. Chevrel, R., and Sergent, M., *in* "Topics in Current Physics" (Ø. Fischer and M. B. Maple, Eds.), Vol. 34, p. 25. Springer-Verlag, Berlin, 1982.

128. Yvon, K., *in* "Topics in Current Physics" (Ø. Fischer and M. B. Maple, Eds.), Vol. 34, p. 87. Springer-Verlag, Berlin, 1982.

129. Chevrel, R., Potel, M., Sergent, M., and Prigent, J., *Ann. Chim. Fr.* **7**, 92 (1982).

130. Chevrel, R., Gougeon, P., Potel, M., and Sergent, M., *J. Solid State Chem.* **57**, 25 (1985).

131. Chevrel, R., Hirrien, M., and Sergent, M., *Polyhedron* **5**, 87 (1986).

132. Peña, O., and Sergent, M., *Prog. Solid St. Chem.* **19**, 165 (1989).

133. Yvon, K., and Paoli, A., *Solid State Comm.* **24**, 41 (1977).

134. Fischer, Ø., Treyvaud, A., Chevrel, R., and Sergent, M., *Solid State Comm.* **17**, 721 (1975).

135. Peña, O., Gougeon, P., Sergent, M., and Horyn, R., *J. Less-Common Met.* **99**, 225 (1984).

136. Peña, O., Horyn, R., Potel, M., Padiou, J., and Sergent, M., *J. Less-Common Met.* **105**, 105 (1985).

137. Sergent, M., Chevrel, R., Rossel, C., and Fischer, Ø., *J. Less-Common Met.* **58**, 179 (1978).

138. Flükiger, R., and Baillif, R., *in* "Topics in Current Physics" (Ø. Fischer and M. B. Maple, Eds.), Vol. 34, p. 113. Springer-Verlag, Berlin, 1982.

139. Miller, W. M., and Ginsberg, D. M., *Phys. Rev. B* **28**, 3765 (1983).

140. Wildervanck, J. C., Jellinek, F., *Z. Anorg. Chem.* **328**, 309 (1964).

141. Wieting, T. J., and Verble, J. L., *Phys. Rev. B* **3**, 4286 (1971).

142. McClellan, A. L., and Harnsberger, H. F., *J. Colloid and Interface Sci.* **23**, 577 (1967).

143. Cheung, K. Y., and Steele, B. C. H., *Solid State Ionics* **1**, 337 (1980).

144. Chevrel, R., Sergent, M., and Prigent, J., *Mater. Res. Bull.* **9**, 1487 (1974).

# SECTION IV.

# DESIGN AND OPERATION OF AN ULTRA-HIGH VACUUM INFRARED REFLECTION–ABSORPTION SPECTROSCOPY SYSTEM

# ABSTRACT

An infrared reflection–absorption spectroscopy (IRRAS) cell, capable of obtaining spectra under conditions ranging from atmospheric pressure to ultra-high vacuum conditions, was designed, constructed, and tested. Modifications to the standard infrared beam path were achieved by the incorporation of new optical components. A cosine-emitter gas doser was designed and evaluated by observing the response of a mass spectrometer to pulses of CO, He, and Kr. The detection of CO adsorbed on a thin film of palladium and the analysis of a poly(methyl methacrylate) layer deposited on silicon–copper thin film structures were used to evaluate the operation of the completed system. The gas doser was found to operate in an ''on/off'' manner without affecting the overall system pressure. Comparable results with previous IRRAS studies were obtained for the analysis of the thin film structures, indicating the successful completion of the system.

# INTRODUCTION

The hydrodesulfurization (HDS) process by which sulfur is removed from crude oil feed is dependent upon catalytically active transition-metal sulfides dispersed on high surface area supports. Typical industrial HDS catalysts are prepared from molybdenum oxides supported on alumina ($\gamma-Al_2O_3$). The addition of cobalt or nickel promoters increases their catalytic activity. These materials are transformed into the working catalyst through sulfiding, generally by a mixture of $H_2$ and $H_2S$ or by the organosulfur compound itself. Bulk characterization techniques, such as extended X-ray absorption fine structure techniques (EXAFS) [1–2], X-ray diffraction [3], and laser Raman spectroscopy [4], have established the presence of a catalytically important $MoS_2$ phase in the working catalyst. Surface techniques, such as X-ray photoelectron spectroscopy (XPS) [5–7], have also detected $MoS_2$.

The addition of promoters results in the introduction of other possible phases. For example, cobalt can exist in several forms on a promoted $Mo/\gamma-Al_2O_3$ catalyst. In the sulfidic form, cobalt may be present as $Co_9S_8$ crystallites on the support, as cobalt ions adsorbed onto the surface of $MoS_2$ crystallites, and in tetrahedral sites in the

$\gamma$–$Al_2O_3$ lattice [8]. Therefore, these HDS catalysts contain multiple phases, few of which may actually be involved in catalytically important roles.

The complexity of these industrial catalysts has made it difficult to understand the surface chemistry of adsorbed reactants, intermediates, and other probe molecules. Many investigations have been conducted using transition metal single crystals or thin films of catalytically active materials as models of catalyst surfaces, such that one or few structural phases dominate. Through the use of modern surface science techniques and the adsorption of various probe molecules, relationships between HDS activity and catalyst composition or structure, as well as the elucidation of reaction mechanisms, may be obtained more directly than is possible for powdered or pelletized catalysts. The use of single crystals or thin films can also reduce the complexities caused by the pore structure associated with conventional catalysts, allowing the active surface area of the metal to be more readily measured. However, it is crucial that the single crystals or thin films used exhibit catalytic activity or no conclusions relating either surface structure to catalytic activity or those concerning reaction mechanisms can be obtained.

Somorjai *et al.* investigated Mo(100) single crystals [9–12] and metal foils [13] as model catalysts for thiophene HDS. They reported that the Mo(100) single crystal catalyzes thiophene HDS and that the product distribution is similar to the distribution obtained over unsupported $MoS_2$. Therefore, they concluded that these metal surfaces are suitable substrates for model studies of HDS catalysts.

Other investigators have examined the adsorption and reaction of thiophene on

clean Mo(100) [14], clean and sulfided Mo(110) [15] and W(211) [16], and Pt(111), Pt(100), and Pt(210) [17].

In addition to single metal crystals, thin film structures of catalysts have been investigated. For example, Hayden and Dumesic [18] analyzed the morphology of thin layers of $MoO_3$ and $MoS_2$ on thin films of alumina. McIntyre *et al.* [19–20] examined thin films of cobalt–molybdenum–sulfide supported on alumina and found that they exhibited activity for thiophene HDS.

Several different surface sensitive techniques have been employed to analyze HDS reactions on single metal crystals and thin film structures of catalysts. These have included XPS [17–20], high-resolution electron energy loss spectroscopy (HREELS) [14,17], Auger electron spectroscopy [14–15], thermal desorption and reaction techniques (TDS, TPD, TPR) [14–15,17], electron microscopies [18], and $^{14}C$ and $^{35}S$ radiotracer labelling techniques [10–11].

The majority of the research using surface techniques on transition metal single crystals or thin film structures as model catalyst surfaces for HDS reactions has been conducted under ultra-high vacuum (UHV) conditions ($\leq 10^{-9}$ Torr). There may be several difficulties in extending these data to typical supported HDS catalysts and HDS reactions which operate at high pressures [21]. For example, weakly bound species, which may be important as reaction intermediates, may not remain adsorbed at low pressures. In addition, metal single-crystal surfaces do not properly represent the surface of a metal sulfide catalyst crystallite. The surface metal cations in a metal

sulfide are not all fully coordinated by sulfur anions, while the metal atoms on the surface of a sulfided single crystal can be fully covered by sulfur. Therefore, a metal sulfide catalyst possesses surface vacancies; a sulfided metal surface does not.

Optical spectroscopies, such as infrared (IR) spectroscopy, are not limited to UHV conditions, and have been used for many years to characterize chemical bonding and reactions at surfaces. However, many materials are limited by low surface areas or low IR transmittance, and have remained uncharacterized by IR techniques. Recent modifications to standard IR methods have increased its surface sensitivity by many orders of magnitude, and have allowed for *in situ* characterization of gas–solid adsorption and reaction processes. The technique of infrared reflection–absorption spectroscopy (IRRAS) was first applied to thin films by Greenler [22] and has since been used to characterize a variety of single crystal metal surfaces and thin film structures during many adsorption processes. Extensive reviews have been given by Darville [23] and Finke [24].

IRRAS is a surface sensitive spectroscopic technique capable of obtaining spectra at submonolayer coverage of species adsorbed on single crystal metal surfaces or other thin film structures, even in the presence of an absorbing gas. The theory is based on the physics of the reflection of light from a smooth metal surface. Upon reflection, the electric field vector of light undergoes a phase change, the magnitude of which depends on the plane of polarization of the incident light. Light polarized perpendicular to the plane of incidence ($I_s$) undergoes an electric field shift of 180 degrees, independent of

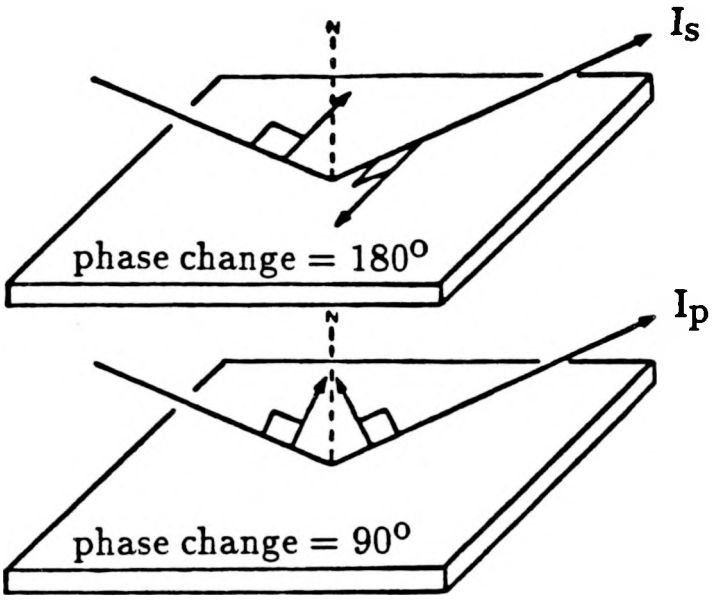


Figure 1. Illustration of the phase change of polarized light upon reflection from a metal surface [24]

the angle of incidence. A node exists in the electric field at the surface due to the destructive interference of the incident and reflected light. The electric field vector of light polarized parallel to the plane of incidence ($I_p$) changes phase by up to 90 degrees, depending on the incident angle. The normal components of the incident and reflected rays interfere constructively, resulting in an oscillating electric field at the surface in the normal direction. Therefore, samples on the surface that have vibrational modes normal to the surface absorb $I_p$ preferentially, resulting in an enhancement of these modes. These relationships are illustrated in Figure 1.

The sensitivity of the technique depends on the reflectivity of the substrate and varies as a function of the refractive index and the film thickness [25]. The most commonly used metals have been Pt, Pd, Ni, Cu, and Ag. These metals exhibit the largest reflectivity values in the IR range, and result in the greatest enhancement of the electric field at the surface.

*In situ* studies of adsorbing gases on metal single crystals or thin film structures require the ability to differentiate between the sample and the ambient gas phase. The availability of Fourier transform infrared spectrometers (FTIR) and the addition of modulation techniques have resulted in large increases in the sensitivity of the basic electric field enhancement (*i.e.*, the ability to discriminate between the absorption of the sample and the ambient gas phase). The highest sensitivity is realized when the signal is modulated such that the final spectrum is represented by the ratio of the intensity difference ($I_p - I_s$) to the intensity sum ($I_p + I_s$) [26].

IRRAS has been used almost exclusively for the case of adsorbates on thin film or metal surfaces. However, the use of thin film structures can extend the applicability of IRRAS to many non-metals. The presence of a highly reflecting metal under a thin film of a catalytic material can enhance and orient the electric field, making it possible to examine adsorbed molecules on the catalyst surface. As demonstrated by Finke [24,27], the presence of a very thin film on a reflecting surface does not significantly decrease the normal component of the electric field at the surface. Layers are considered to be optically thin when $d/\lambda < 10^{-4}$, where $d$ is the film thickness and $\lambda$ is

the wavelength of the radiation. For IR radiation, $d/\lambda < 10^{-4}$ for films that are several hundred Ångströms thick.

Finke [24] has reported on polarization–modulation Fourier transform infrared spectroscopy (PM–FTIRRAS) investigations of several products and intermediates in the catalytic formation of maleic anhydride from $C_4$ hydrocarbons, using $MoO_3$ thin films deposited on palladium. Due to the low surface area of the catalytic thin film, he concluded that the use of UHV techniques and *in situ* formation of catalytically active thin film structures would be required to "activate" (or "clean") a higher percentage of the surface sites for the adsorption of reactants, intermediates, or other probe molecules.

This section reports the design, construction, and preliminary testing of such a UHV PM–FTIRRAS chamber, capable of obtaining IRRAS spectra under conditions ranging from atmospheric pressure to UHV conditions, along with the associated optical components and gas feed system. Although UHV conditions are not required for the IRRAS technique, they may provide "ideal" surfaces in terms of cleanliness and available surface sites. These surfaces may then be used to obtain information on catalytically important adsorption interactions and possible reaction mechanisms involved at gas–solid interfaces.

# EXPERIMENTAL DESIGN

## Standard Spectrometer

A Nicolet 60SX FTIR spectrometer was modified to perform the IRRAS experiments. The spectrometer is controlled by a dedicated Nicolet computer which operates the optics bench and is responsible for data collection, manipulation, and storage. A diagram of the optical path of the standard spectrometer is presented in Figure 2, with a description of the components given in Table 1.

## Modifications for PM–FTIRRAS

No major changes were made to the standard optics bench. Most additions to the optical system were mounted on an external table adjacent to the FTIR. The standard sample compartment was used to accommodate the polarization–modulation (PM) optics. The IR beam was polarized at a 45 degree angle with respect to the sample by a silicon substrate Brewster's angle polarizer (Harrick Scientific, model PTD–E1R). The plane of polarization was modulated about the 45 degree angle by a zinc selenide photoelastic modulator (PEM) (Hinds International, series II), operated at a frequency of 37 kHz.

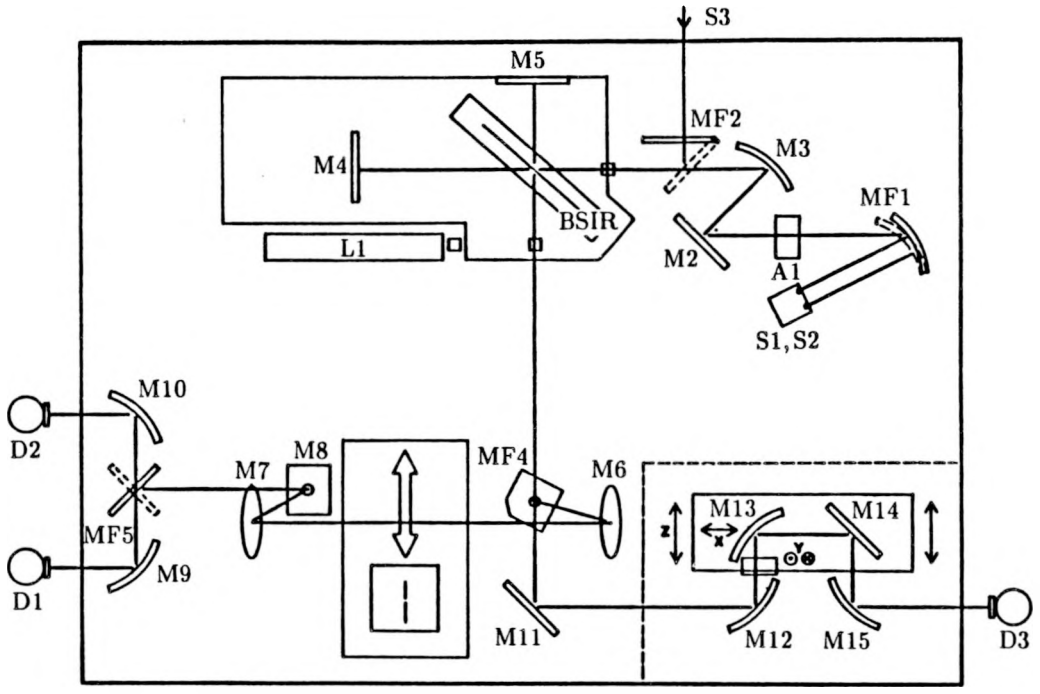


Figure 2. Diagram of the optical layout of a Nicolet 60SX Fourier transform infrared spectrometer [24]

This corresponded to changing the plane of polarization from parallel ($I_p$) to perpendicular ($I_s$) to the plane of incidence at 74 kHz. The IR beam followed the normal beam path of the spectrometer upon leaving the sample compartment. The final focusing mirror, M9, was replaced by a flat mirror (Melles Griot) so that a collimated beam left the optics bench (Figure 2).

The PM–FTIRRAS cell, optics, and IR detector were mounted on an external table constructed of 0.25-in aluminum sheet. Rubber pads were placed under the legs of the table to reduce building vibrations. The external beam path is illustrated in

Table 1. Symbols used in schematic of FTIR optical components (Figure 2)

| | | | |
|---|---|---|---|
| S1 | standard glowbar source | MF4 | moving flat mirror to microbeam compartment |
| S2 | standard tungsten-halogen source | M6 | sample focussing off-axis parabolic mirror, 237 mm EFL |
| S3 | optional source | M7 | sample collection off-axis parabolic mirror, 237 mm EFL |
| MF1 | computer controlled source selection mirror, 208 mm EFL | M8 | flat mirror |
| A1 | computer controlled aperature | MF5 | 2-position computer controlled detector selection flat mirror |
| M2 | flat mirror | M9,M10 | detector condensing off-axis parabolic mirrors, 64 mm EFL |
| M3 | collimating off-axis parabolic mirror, 208 mm EFL | D1,D2,D3 | pre-aligned detector positions |
| MF2 | moving flat mirror to external source | M11 | flat mirror |
| BSIR | infrared/laser beamsplitter | M12 | microbeam condensing off-axis parabolic mirror, 64 mm EFL |
| M4 | interferometer moving mirror | M13 | Z-axis microbeam computer controlled focussing off-axis parabolic mirror, 64 mm EFL |
| M5 | interferometer fixed mirror | M14 | X-axis microbeam computer controlled flat mirror |
| L1 | reference laser | M15 | detector condensing off-axis parabolic mirror, 64 mm EFL |

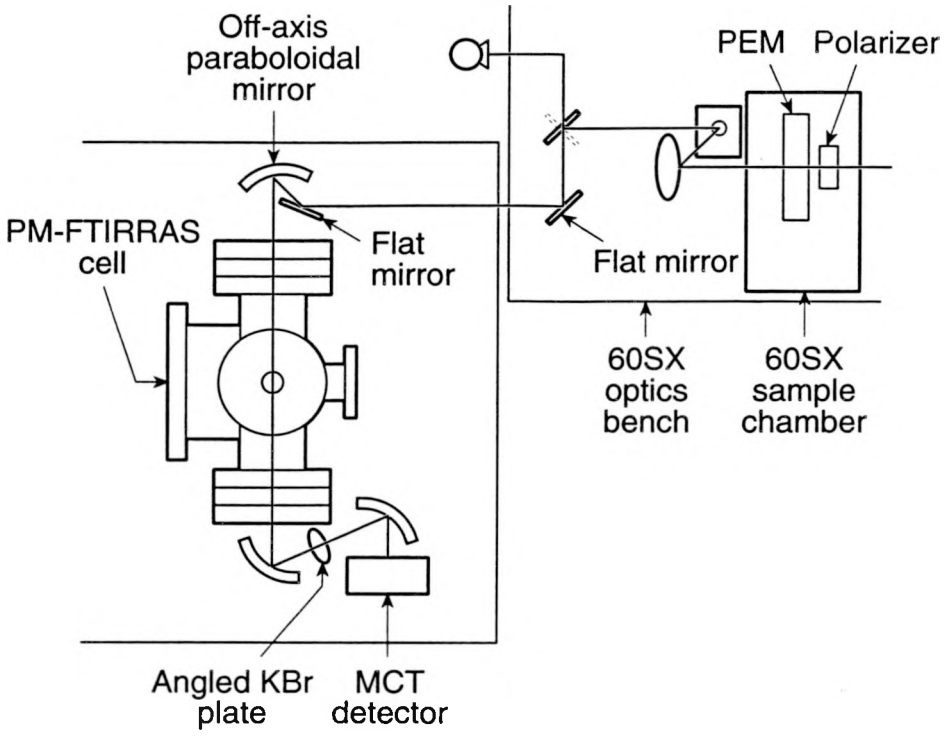


Figure 3. Optical layout for the PM–FTIRRAS external components

Figure 3. A flat mirror (Melles Griot, 3 × 3 in) was used to raise the beam height and to provide the proper angle of incidence (60 degrees) onto the first focusing mirror. Off-axis parabolodial mirrors (Melles Griot, d = 203.2 mm) were used to focus the beam on the sample and were installed on mirror mounts which were aligned by three ultra-fine adjustment screws (Newport Research Corporation). The mirror mounts and the IR detector were mounted on variable-height stands and translation stages (Newport Research Corporation) which allowed alignment of the IR beam along the entire optical path. The beam was focused on the sample at an angle of incidence of 83 degrees from the surface normal, recollimated, passed through a KBr compensation plate to correct for

optical dichroism [26], and sent to a liquid-nitrogen cooled mercury–cadmium–telluride (MCT) detector.

## Signal Handling Electronics

A full description of the electronic processing involved in the IRRAS technique has been provided previously [24,27] and will only be summarized here. A schematic of the demodulation circuit is shown in Figure 4.

The MCT detector signal consisted of the standard interferogram along with another interferogram, several orders of magnitude smaller, centered at the modulation frequency. As described previously, the highest sensitivity is realized when the final spectrum consists of the ratio of the intensity difference ($I_p - I_s$) to the intensity sum ($I_p + I_s$). The signal from the detector was split into two paths, referred to as the numerator and the denominator. The numerator signal was sent to a band pass filter (EG&G PAR, model 5011F), centered at the modulation frequency of the PEM, which effectively removed the large interferogram at the low frequencies. This was necessary to prevent the signal from saturating the dynamic range of the next component of the signal path, a lock-in amplifier (EG&G PAR, model 5207). The lock-in amplifier used as its reference a signal originating from the PEM. The lock-in output was proportional to the intensity difference ($I_p - I_s$) and was further filtered before being combined with the denominator signal.

The denominator signal was amplified in order to control the magnitude of the

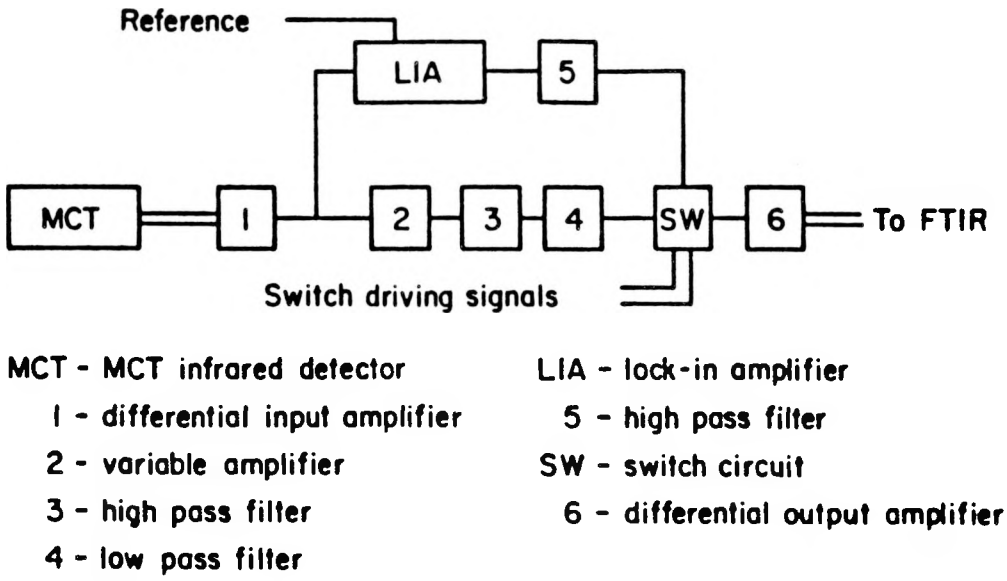


Figure 4. PM–FTIRRAS signal demodulation circuit [24]

ratio $(I_p - I_s)/(I_p + I_s)$ by a variable gain amplifier (1–100 times). The denominator signal was filtered through high- and low-pass filters, and was combined with the numerator signal at the switch circuit.

The switch circuit allowed the numerator and denominator signals to be collected and stored simultaneously, and ensured that the first data point (and all subsequent odd points) was always from the denominator, while all even data points were from the numerator. This arrangement allowed the spectrometer to average multiple scans to improve the signal-to-noise ratio of the final spectrum.

Through the use of computer software [24], the combined interferogram was

divided into two interferograms: one from the even data points and one from the odd data points. The resulting interferograms were mathematically demodulated by Fourier transform and converted into single beam spectra.

## PM–FTIRRAS Cell

The UHV chamber designed for the PM–FTIRRAS studies is illustrated in Figure 5. The cell was constructed of stainless steel. All flanges were sealed using copper gaskets.

Special ports to accommodate KBr windows (International Crystal Laboratories, 49 mm diameter, 6 mm thick) were designed in a manner similar to those reported by Hollins and Pritchard [28]. The window lies in a recess in a modified 4.5-in stainless-steel UHV flange and is retained by an outer clamping flange (Figure 6). Vacuum seals are provided by Viton O-rings. The outer O-ring seal between the flanges prevents the UHV-side O-ring from exposure to atmospheric pressure and permits the inner space between the O-rings to be evacuated through the 0.25-in stainless-steel tube welded into the side of the middle flange. This differential pumping was essential for UHV performance of the chamber and was provided through a vacuum manifold evacuated by a roughing pump (Alcatel, model 2004A).

The window-seat recess was designed to be slightly deeper than the thickness of the KBr window to ensure that the window is pressed upon only by the O-rings. A slotted retaining ring was incorporated on the UHV side of the window to avoid the

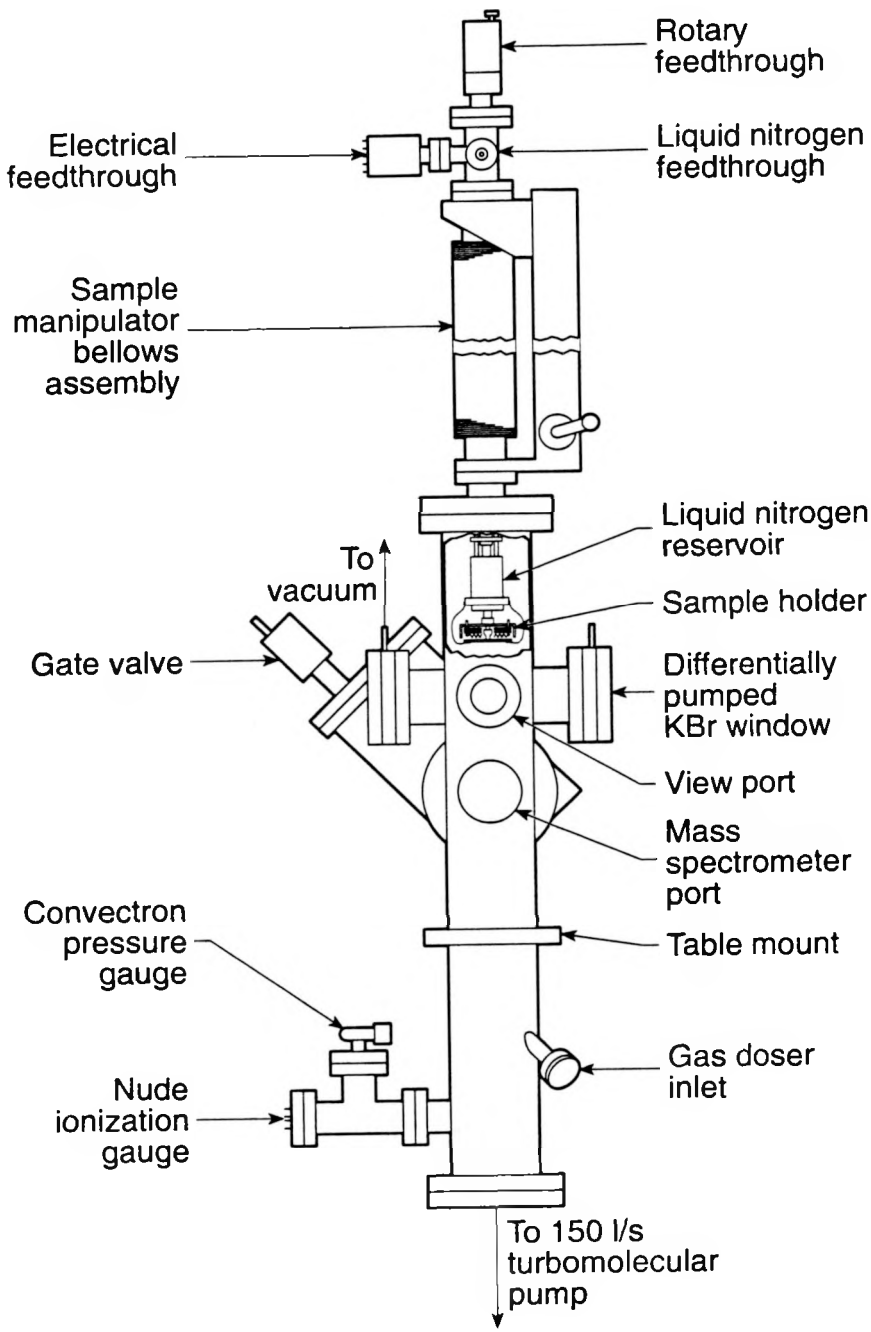


Figure 5. PM–FTIRRAS UHV cell

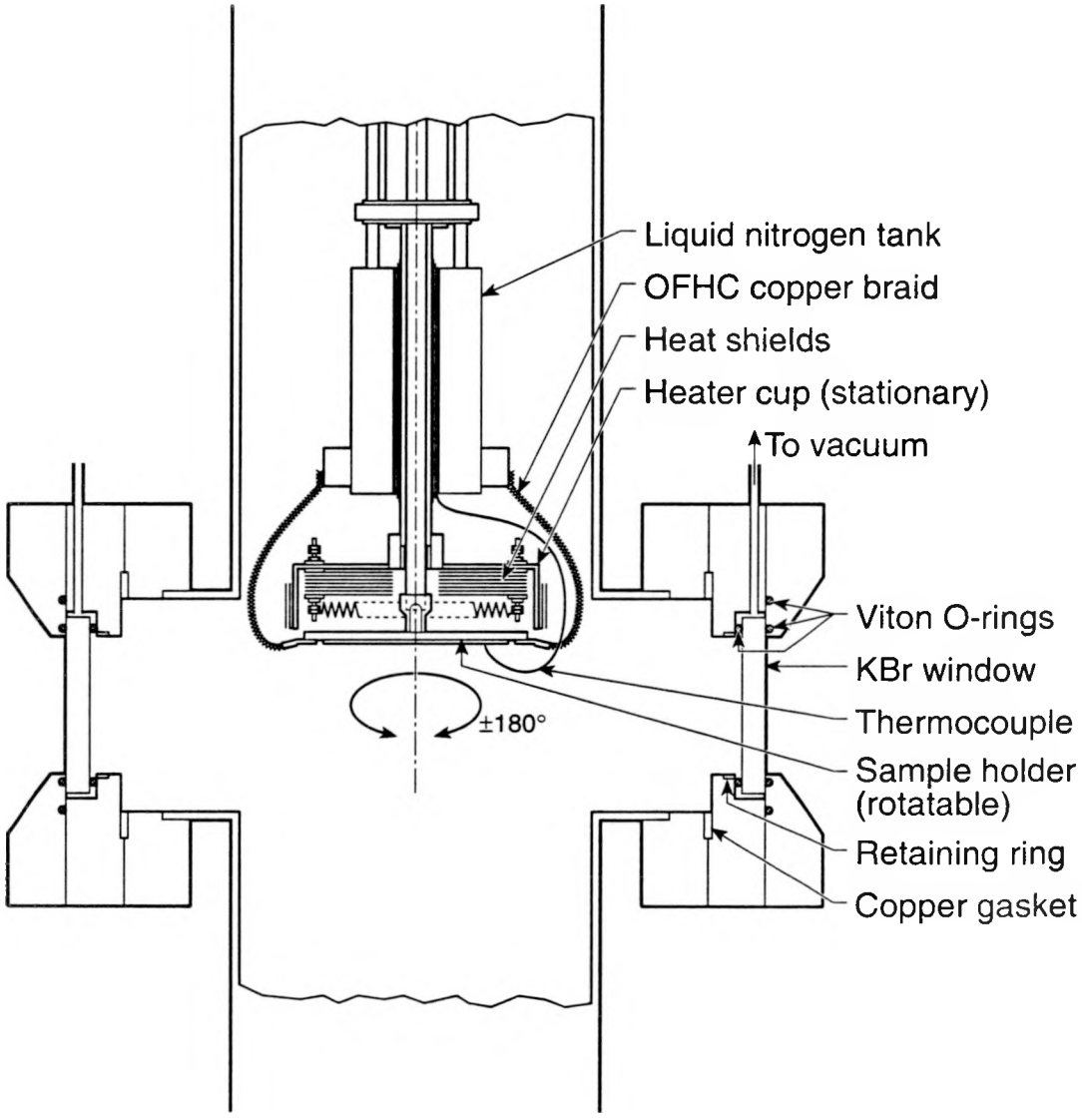


Figure 6. Detail of the differentially-pumped window and sample holder assemblies

possibility of trapping any pockets of gas that may slowly leak into the vacuum chamber from a normal O-ring groove.

The sample was attached to a rotatable ($\pm$180 degrees) sample holder by two small hold-down screws with stainless-steel clips and pointed "down" into the incoming IR beam or reactant gas (Figure 6). The sample is heated by a tantalum wire radiation heater incorporated in a circular housing at the back of the sample. The shallow housing contains multiple radiation shields to maximize the radiated power to the back of the sample. The heating stage was controlled by a programmable temperature controller (Eurotherm, model 818P). The temperature of the sample was monitored by a thermocouple attached to the face of the sample holder. Temperatures in excess of 600°C could be obtained.

Cooling of the sample is possible using a liquid nitrogen cooling system. The cooling unit is composed of a liquid nitrogen feed-through collar, a liquid nitrogen reservoir, and OFHC copper braid (Figure 5 and Figure 6). The liquid nitrogen reservoir is mounted near the sample stage. A short section of OFHC copper braid is attached between the reservoir and the sample stage. The low temperature performance of the sample holder is limited by the length of the copper braid, the conduction heat transfer between the stage and supporting probe, and the area of the sample. In general, it is possible to obtain a minimum temperature of approximately −168°C.

The sample holder is attached to a bellows XY sample manipulator (UHV Instruments, Inc., model 2500–275–25). The manipulator provides $\pm$180 degree

rotation for the sample and vertical (Y) travel of up to 25 in. The sample manipulator also houses the necessary electrical, liquid nitrogen, and rotary feed-throughs (Figure 5).

Figure 5 also illustrates several auxiliary ports attached to the chamber. A viewport was incorporated in order to aid in sample alignment. A port for attachment of a mass spectrometer was provided such that the mass analyzer probe could be placed close to the sample surface. Ports located near the bottom section of the cell were added for the installation of pressure gauges and a gas feed assembly. The entire chamber was attached directly to an adjacent chemical vapor deposition (CVD) system [29], and could be isolated by closing the gate valve.

## Vacuum and Gas Feed Systems

The vacuum system consisted of a 150 l/s turbomolecular pump (Leybold Turbovac, model TMP 150) backed by a rotary vane roughing pump (Leybold Trivac, model D8A). Differential pumping for the KBr windows and gas feed system was provided by an Alcatel (model 2004A) roughing pump. Base pressures of $10^{-7}$ Torr could be routinely obtained without baking out the chamber.

Pressure measurement was accomplished using a thermal conductivity gauge (Granville–Phillips, model Convectron) and a nude ionization gauge (Granville–Phillips). The gauges were controlled by a Granville–Phillips series 307 vacuum gauge controller.

Gas samples were admitted to the chamber through a differentially-pumped

cosine-emitter gas doser, designed to enhance the flux of gas molecules at the surface of the sample without increasing the background pressure in the chamber. The gas doser assembly in shown in Figure 7. The rate of gas effusion is controlled by a 2-$\mu$m stainless-steel orifice (Buckbee–Mears Company) compression mounted between two stainless-steel gaskets within a 0.25-in Cajon VCR fitting. Gas collimation at the sample surface was provided by a cosine emitter, constructed of 0.125-in stainless-steel tubing. A very thin stainless-steel foil (0.0015 in) was braised onto the end of the tube, and a small hole (0.0135 in) was drilled in the center of the foil cap.

Control of the gas flow to the gas doser was regulated by the pressure in a stainless-steel gas manifold. The pressure in the manifold was measured by a thermoconductivity pressure gauge (Granville–Phillips, model Convectron). Differential pumping was provided by the same vacuum manifold system used for differentially pumping the KBr window assembly. Nupro bellows valves (model SS–4H–TH3) were used to isolate the vacuum and gas feed lines to the doser.

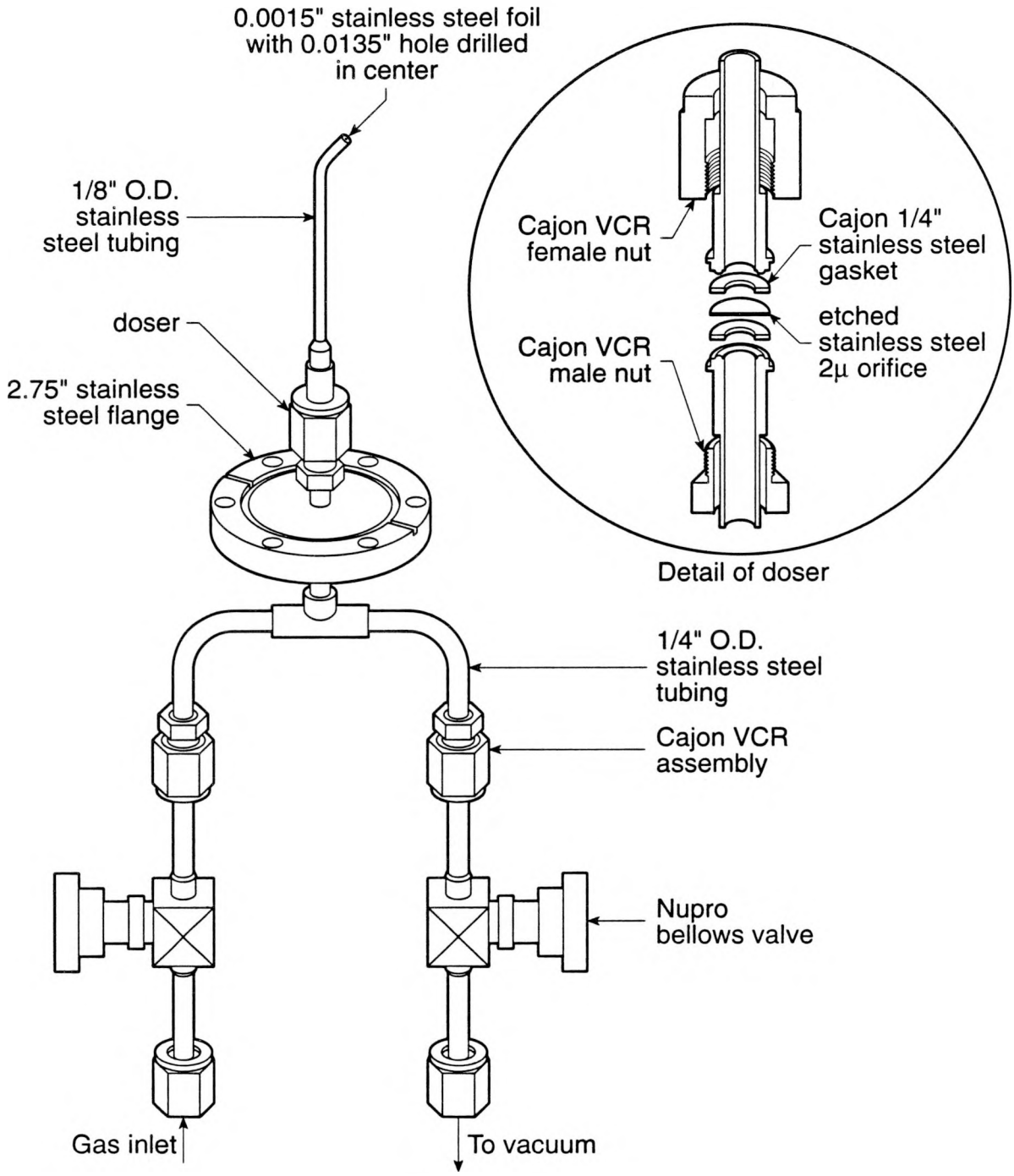


Figure 7. UHV gas doser assembly

# EXPERIMENTAL METHODS

## Thin Film Preparation

To demonstrate the operation of the UHV PM–FTIRRAS system, a thin film of palladium and thin film structures consisting of poly(methyl methacrylate) (PMMA) deposited on silicon–copper thin films were used. These samples were used in previous PM–FTIRRAS investigations where their preparation and characterization have been described in detail [24,27]. Therefore, their preparation will only be summarized here.

Thin films of the reflecting metals were prepared by an electron-beam evaporation apparatus in a bell-jar system under high vacuum conditions. Films were deposited to a thickness of approximately 1200 Å. A palladium film was evaporated onto a 2-in diameter silicon wafer (Monsanto). For the silicon–copper thin film structures, copper was deposited first onto a thin microscope cover glass (22 × 50 mm, 0.2mm thick) (Fisher Scientific, Inc.). Silicon was then evaporated onto the copper film to a thickness of approximately 200 Å. Thin films of PMMA were prepared by a spin-coating technique from both 0.25 and 1.0 wt% solutions of PMMA in chloroform. The resulting PMMA films were approximately 250 and 1000 Å thick, respectively.

## General PM–FTIRRAS Operation

A list of the Nicolet 60SX parameter settings used for the PM–FTIRRAS evaluation is given in Table 2. Spectra were collected at 4-$cm^{-1}$ resolution. The mirror velocity (VEL) was optimized to approximately 0.200 cm/s to allow the 400–4000 $cm^{-1}$ range to pass through the lock-in amplifier [24]. The low- (LPS) and high-pass (HPS) filters were bypassed to inhibit smearing of the numerator and denominator signals before they were split into individual interferograms. The 60SX FTIR has a method of comparing a newly acquired scan with the summed file from previous scans in order to sort out shifted or otherwise different scans that were due to vibrations of the optics bench or changes in the sample. In PM–FTIRRAS, a shift of the interferogram by a single data point would result in the mixing of the numerator and denominator signals.

Table 2. 60SX FTIR parameter settings for UHV PM–FTIRRAS evaluation

| Parameter | Setting | Description |
|---|---|---|
| VEL | 60 | 0.203 cm/s |
| NDP | 4096 | 4-$cm^{-1}$ resolution |
| HPS | 0 | bypassed |
| LPS | 0 | bypassed |
| COR | HI | high correlation |
| NSD | 400 | number of scans |
| APT | BL | fully open |

Accordingly, the correlation value (COR) was set as high as possible. The aperature in the beam path (APT) was fully opened to maximize the intensity of the infrared beam at the sample and the detector.

The alignment of the mirrors and sample in the optical path was crucial to obtain high quality spectra. The highly reflective sample acted as a mirror and was included in the optical alignment process. The focusing mirrors were mounted at a distance of 8 in horizontally from the center of the sample and 1 in below the sample height. This arrangement gave an angle of incidence of approximately 83 degrees. The first step in the optimization procedure was to maximize the signal at the MCT detector through alignment of all the mirrors in the optical path, including the sample.

In order to maximize the signal-to-noise ratio in the final spectra, the electronic additions to the spectrometer also had to be optimized. To obtain the maximum signal at the output of the lock-in amplifier, the reference signal from the PEM was adjusted to be in phase with the modulating detector signal. This phase adjustment was performed using the lock-in amplifier with the amplitude of the PEM set to the level to be used in the experiments (5000 nm). The phase was adjusted to null the lock-in output signal. As the output decreased, the full scale sensitivity of the lock-in was decreased in order to fine-tune the zeroing of the signal. A highly reflective sample was present in the sample holder and the KBr compensation plate was normal to the IR beam during this process. The phase was then changed by 90 degrees. The KBr compensation plate was tilted in order to null the lock-in output again. This procedure set the phase adjustment

correctly, which could be verified by changing the phase by 90 degrees and observing a null in the output.

## Gas Doser Operation

Operation of the gas doser was evaluated using He, Kr, and CO. A pressure of approximately 20 Torr of each gas was admitted into the gas manifold. The IRRAS cell was maintained at a pressure of approximately $1 \times 10^{-7}$ Torr. To expose the sample to gas, the gas inlet bellows valve on the doser assembly was opened simultaneously as the vacuum bellows valve was closed. Pulses of 10-s duration were dosed at 40-s intervals. The partial pressure of the adsorbate entering the chamber was measured using a UTI 100C closed-ion source quadrupole mass spectrometer interfaced to a Hewlett–Packard Vectra ES computer through a UTI SpectraLink (model 100) module. At the end of each pulse, the vacuum valve was opened as the gas inlet valve was closed.

## General Procedures

The polycrystalline thin film of palladium was loaded into the PM–FTIRRAS cell. The chamber was evacuated to $10^{-7}$ Torr and the sample was heated to 150°C for 16 h. The sample was cooled to room temperature and a reference PM–FTIRRAS spectrum of the palladium film was acquired. The sample was lowered to within 1 in of the gas doser outlet where it was exposed to CO for approximately 30 Torr-s. The sample was returned to its original position by raising the sample holder with the sample

manipulator and another PM–FTIRRAS spectrum was collected. The chamber was back-filled with CO to a pressure of approximately 20 Torr and the sample was scanned once more.

The thin film structures of PMMA/silicon/copper were analyzed at atmospheric pressure and under high-vacuum conditions. The 1000 Å PMMA film was placed into the chamber. An unenhanced reflection spectrum was collected at atmospheric pressure using 400 scans and 4-$cm^{-1}$ resolution without using polarized radiation or modulation techniques. This spectrum was ratioed to a reference spectrum of a 200 Å thin film of silicon on 1200 Å of copper acquired under the same conditions. Finally, 400 scans of the 1000 Å of PMMA on the silicon–copper thin film structure were collected using the full PM–FTIRRAS technique.

PM–FTIRRAS spectra of the 250 Å PMMA film were obtained at atmospheric pressure and at $10^{-7}$ Torr using the same collection time (400 scans) and resolution (4-$cm^{-1}$). A reference spectrum of the silicon–copper thin film structure was also collected.

# RESULTS AND DISCUSSION

The response of the mass spectrometer to several pulses of CO through the gas doser assembly is presented in Figure 8. An approximate square pulse shape is detected, indicating the "on/off" characteristic of the gas doser. The PM–FTIRRAS chamber pressure was approximately $1 \times 10^{-7}$ Torr and did not increase upon addition of the CO pulses. Since the mass analyzer probe was located further from the doser outlet than the actual sample, the response at the sample surface is probably even more ideal than is illustrated in Figure 8. The other gases tested displayed similar characteristics.

The exit orifice in the cosine-emitter gas doser assembly was designed to have a very small length-to-diameter ratio (approximately 0.1). The angular distribution of gas emitted from such orifices has been thoroughly investigated. Collimation with small length-to-diameter ratios ($<<$ 1) provides molecular exit angles with near-cosine exit flux of gases [30]. Maximum surface coverage is obtained at a distance from the sample equal to one-half the sample diameter [31].

The PM–FTIRRAS spectrum of CO adsorbed on palladium is shown in Figure 9.

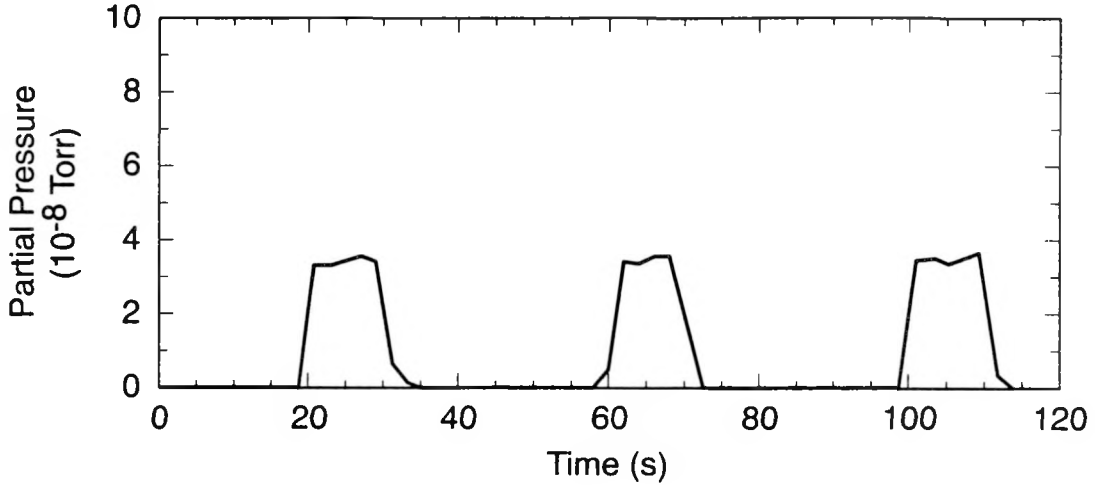


Figure 8. Mass spectrometer response to pulses of CO from the cosine-emitter gas doser assembly

A reference spectrum of the palladium film is included. This spectrum represents CO adsorbed with approximately 20 Torr in the chamber. No adsorbed CO bands were detected at $10^{-7}$ Torr. It is assumed that the absence of CO bands at low pressure is related to a lack of sufficient adsorption sites, due to partial contamination of the palladium surface as a result of the age of the film (approximately 2 years). The bands at 2162 $cm^{-1}$ have been assigned to linearly bonded CO and the band at 2114 $cm^{-1}$ to the CO adsorbed between two surface palladium atoms in a bridged configuration. These bands are at higher wavenumbers than those reported of 2070 and 1957 $cm^{-1}$

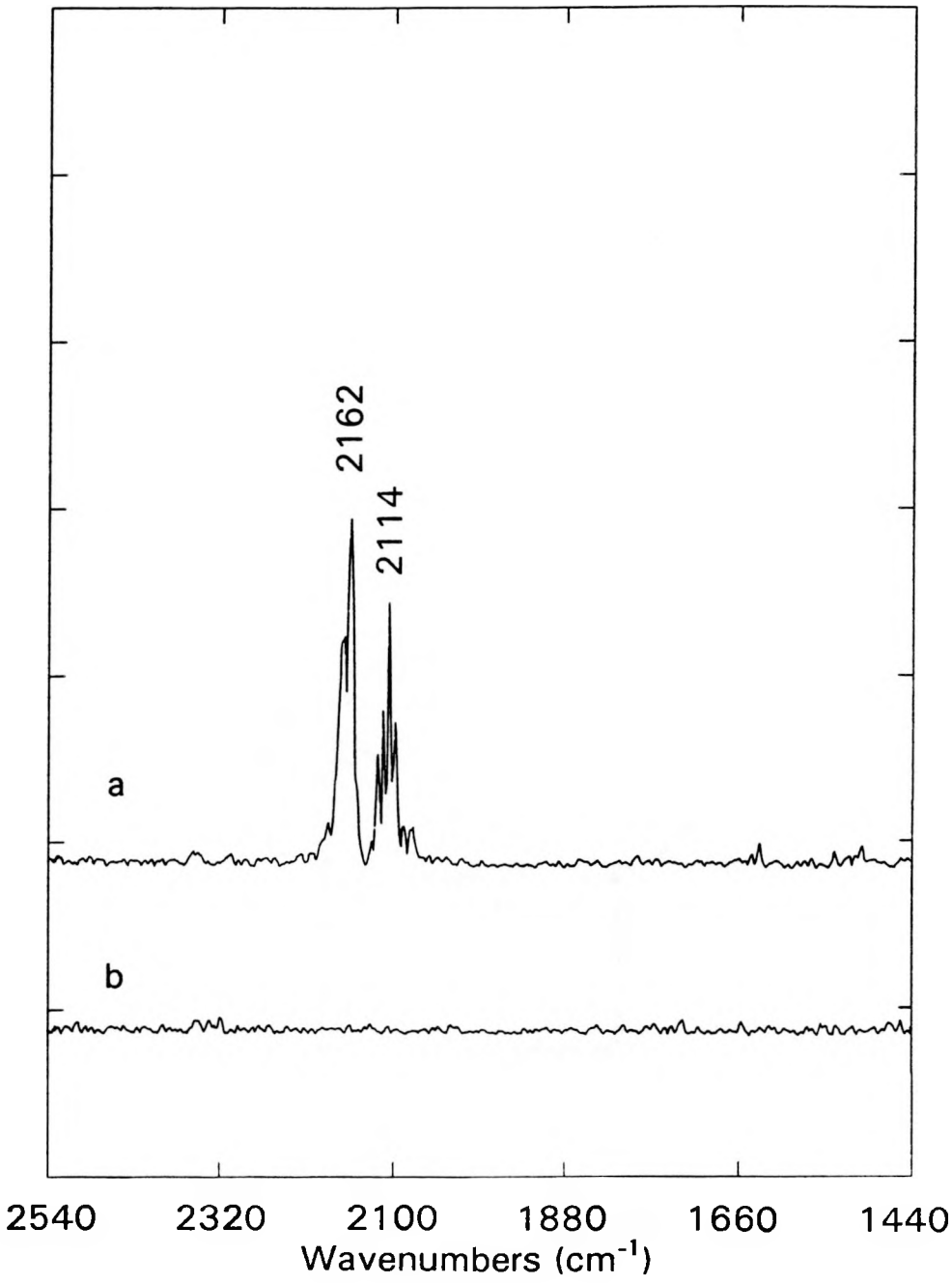


Figure 9. PM–FTIRRAS spectra of (a) CO adsorbed on palladium film, (b) bare palladium film

obtained under similar conditions [24]. However, it has been determined that bands due to CO adsorbed on palladium shift to higher wavenumbers, by as much as 100 $cm^{-1}$ or more, as the surface coverage is increased [32].

The CO bands also exhibit some fine structure components evident as small narrow peaks. Several possibilities exist which may explain the apparent peak splitting. For example, Allara *et al.* [33–34] reported that reflection–absorption spectra may be distorted relative to transmission spectra with significant changes occurring in peak maxima. These changes are due, in part, to the contribution of the refractive index to the reflectivity of the sample, coupled with the rapid changes in the refractive index in the region of an absorption band (anomalous dispersion effects). Therefore, theoretical calculations predict the possibility of band splitting.

Other possibilities for the peak splitting include miscancellation of gas phase water, incomplete cancellation of gas phase CO, or some other artifact due to the age of the film. The preparation of fresh films of palladium would be required to perform further adsorption experiments to better understand these unexpected absorption bands.

The infrared throughput of the PM–FTIRRAS system was also evaluated using the highly reflective palladium film. Optimization of the optical path alignment resulted in an interferogram signal of approximately 5.3 V peak-to-peak amplitude. With the MCT detector attached directly to the standard 60SX spectrometer, a signal of about 6.8 V is obtained. Therefore, considering the increased number of reflections and the

longer optical path length associated with the UHV PM–FTIRRAS apparatus, very little signal intensity is lost.

The spectra of the 1000 Å film of PMMA on a silicon–copper thin film structure are presented in Figure 10. For the unenhanced reflection spectrum (Figure 10a), a small infrared band at 1737 $cm^{-1}$ is the only indication of the PMMA film on the surface. The sharp negative peaks in the range of 1500–1560 $cm^{-1}$ represent incomplete cancellation of gas-phase water when ratioed against the silicon–copper thin film structure reference spectrum.

In contrast, the PM–FTIRRAS spectrum of the 1000 Å film demonstrates sharp and intense infrared bands in the wavenumber range between 2000 and 600 $cm^{-1}$. Although the range above 2000 $cm^{-1}$ indicated bands due to C–H bond stretching, the C=O vibrations were much more intense and more readily demonstrate the relative sensitivity of the PM–FTIRRAS technque. The absorption bands matched those of other published values and were of the same relative intensity [24,27]. In addition, the incomplete cancellation of the gas-phase water bands, present in the other spectrum, was corrected, even though the entire beam path was open to air. This figure clearly demonstrates the increased sensitivity of the PM–FTIRRAS technique, and provides evidence that the UHV PM–FTIRRAS system performance is comparable to that of a previously reported apparatus [24,27].

To further demonstrate the sensitivity of the technique, a thinner film of PMMA was investigated. Figure 11 displays the PM–FTIRRAS spectra for the 250 Å film of

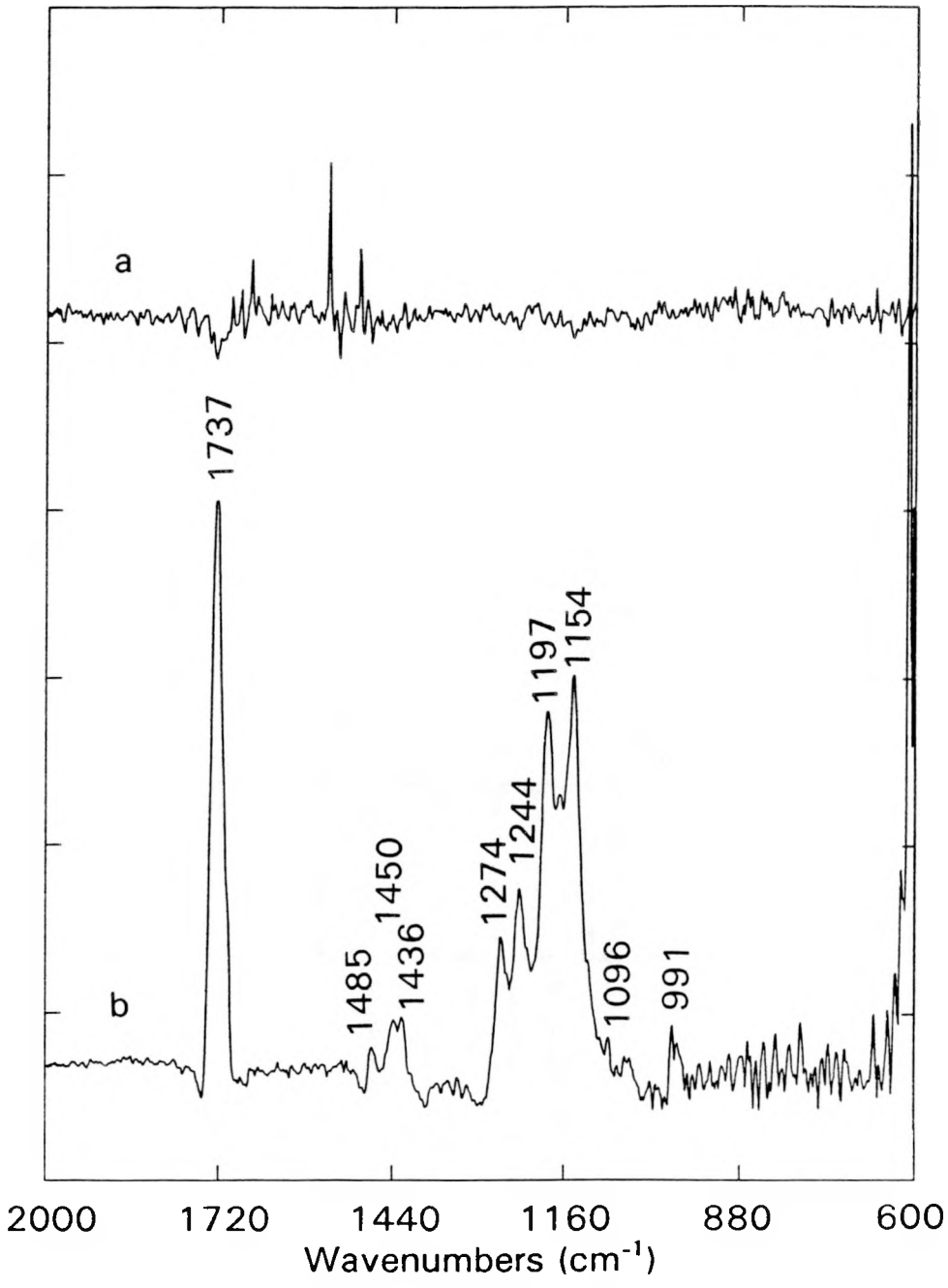


Figure 10. Spectra of 1000 Å PMMA film on silicon–copper substrate: (a) unenhanced reflection spectrum, (b) PM–FTIRRAS spectrum

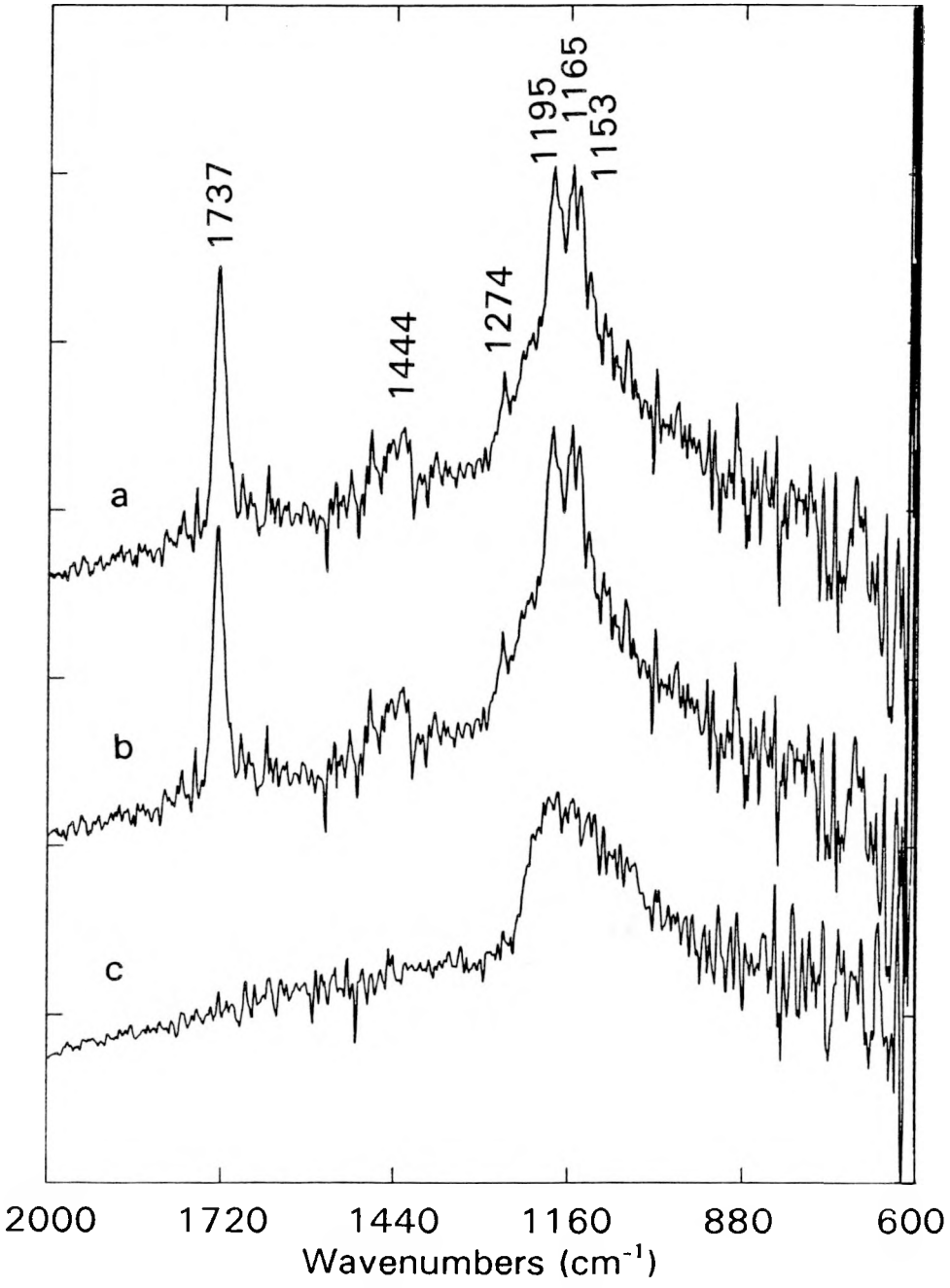


Figure 11. PM–FTIRRAS spectra of: (a) 250 Å PMMA film on silicon–copper substrate at $10^{-7}$ Torr, (b) same film at atmospheric pressure, (c) silicon–copper substrate

PMMA on the silicon–copper thin film structure. Most of the bands present in the 1000 Å film are still resolved in the 250 Å film. These spectra also compare favorably with previously reported 250 Å PMMA films [24,27]. A reference spectrum of the silicon–copper substrate is also included. The broad absorption band in the reference spectrum near 1100 $cm^{-1}$ was assigned to Si–O bonds, due to the incorporation of small amounts of oxygen in the silicon film [24,27].

Spectra of the 250 Å films of PMMA were collected at $10^{-7}$ Torr (Figure 11a) and atmospheric pressure (Figure 11b) to observe the effect, if any, of vibrations due to the operation of the vacuum system during collection. As illustrated in Figure 11, the spectra are essentially identical, indicating that vacuum system vibrations have a negligible effect on the quality of the PM–FTIRRAS spectra.

With the successful demonstration of the operation of the UHV PM–FTIRRAS system, the potential exists for studying adsorption on a variety of substrates. Infrared spectroscopy has been used extensively to characterize the molecules adsorbed on catalyst surfaces. However, many catalyst systems do not lend themselves to standard transmission IR studies, due to low surface areas or high absorption of IR radiation. PM–FTIRRAS offers an alternative technique to overcome the restrictions of these catalyst systems. Using thin film structures with the catalyst as the top layer avoids the limitations of infrared transmittance and low surface area [24,27]. PM–FTIRRAS also offers the advantage over transmission spectroscopy of analyzing the catalyst surface with regard to the orientation of the adsorbed molecules relative to the surface. It has

been demonstrated in the literature that IRRAS is sensitive enough to analyze monolayer coverages. In addition, *in situ* investigations of adsorption and reaction processes are possible.

It has been difficult to relate investigations conducted under UHV conditions to catalytic reactions, such as HDS, at high pressures. The application of PM–FTIRRAS to catalytic thin film structures, at both UHV and atmospheric pressures, may result in a more fundamental understanding of the relationships between the "ideal" surfaces in UHV technology and actual operating conditions of catalytic and other chemical reaction processes.

# CONCLUSIONS

An IRRAS cell capable of obtaining spectra under conditions ranging from atmospheric pressures to UHV conditions was designed, assembled, and tested. A cosine-emitter gas doser was observed to operate in an ''on/off'' manner without affecting the system background pressure. Comparable results to previous IRRAS studies were obtained for the analysis of the thin film structures, indicating the successful completion of the system.

# ACKNOWLEDGMENTS

This work was conducted through the Ames Laboratory which is operated for the U. S. Department of Energy by Iowa State University under Contract W–7405–Eng–82. This research was supported by the Office of Basic Energy Sciences, Chemical Sciences Division. Many helpful discussions with S. J. Finke are gratefully acknowledged.

# REFERENCES


1. Parham, T. G., and Merrill, R. P., *J. Catal.* **85**, 295 (1984).

2. Clausen, B. S., Topsøe, H., Candia, R., Villadsen, J., Lengeler, B., Als-Nielsen, J., and Christensen, F., *J. Phys. Chem.* **85**, 3868 (1981).

3. Pollack, S. S., Makovsky, L. E., and Brown, F. R., *J. Catal.* **59**, 452 (1979).

4. Schrader, G. L., and Cheng, C. P., *J. Catal.* **80**, 369 (1983).

5. Li, C. P., and Hercules, D. M., *J. Phys. Chem.* **88**, 456 (1984).

6. Zingg, D. S., Makovsky, L. E., Tisher, R. E., Brown, F. R., and Hercules, D. M., *J. Phys. Chem.* **84**, 2898 (1980).

7. Patterson, T. A., Carver, J. C., Leyden, D. E., and Hercules, D. M., *J. Phys. Chem.* **80**, 1700 (1976).

8. Topsøe, H., Clausen, B. S., Candia, R., Wivel, C., and Mørup, S., *J. Catal.* **68**, 433 (1981).

9. Gellman, A. J., Neiman, D., and Somorjai, G. A., *J. Catal.* **107**, 92 (1987).

10. Gellman, A. J., Bussell, M. E., and Somorjai, G. A., *J. Catal.* **107**, 103 (1987).

11. Bussell, M. E., and Somorjai, G. A., *J. Catal.* **106**, 93 (1987).

12. Bussell, M. E., Gellman, A. J., and Somorjai, G. A., *J. Catal.* **110**, 423 (1988).

13. Bussell, M. E., and Somorjai, G. A., *Catal. Lett.* **3**, 1 (1989).

14. Zaera, F., Kollin, E. B., and Gland, J. L., *Surf. Sci.* **184**, 75 (1987).

15. Roberts, J. T., and Friend, C. M., *Surf. Sci.* **186**, 201 (1987).

16. Preston, R. E., and Benziger, J. B., *J. Phys. Chem.* **89**, 5010 (1985).

17. Lang, J. F., and Masel, R. I., *Surf. Sci.* **183**, 44 (1987).

18. Hayden, T. F., and Dumesic, J. A., *J. Catal.* **103**, 366 (1987).

19. McIntyre, N. S., Chan, T. C., and Spevack, P. A., *Appl. Catal.* **63**, 391 (1990).

20. McIntyre, N. S., Chan, T. C., Spevack, P. A., and Brown, J. R., *in* "Advances in Hydrotreating Catalysts" (M. L. Ocelli and R. G. Anthony, Eds.), Vol. 50, p. 187. Elsevier, Amsterdam, 1989.

21. Prins, R., de Beer, V. H. J., and Somorjai, G. A., *Catal. Rev.—Sci. Eng.* **31**, 1 (1989).

22. Greenler, R. G., *J. Chem. Phys.* **44**, 310 (1966).

23. Darville, J., *in* "Vibrations at Surfaces" (R. Caudano, J.-M. Gilles, and A. A. Lucas, Eds.), p. 341. Plenum Press, New York, 1982.

24. Finke, S. J., Ph.D. Dissertation, Iowa State University, Ames, 1988.

25. Greenler, R. G., *J. Vac. Sci. Technol.* **12**, 1410 (1975).

26. Golden, W. G., Dunn, D. S., and Overend, J., *J. Catal.* **71**, 395 (1981).

27. Finke, S. J., and Schrader, G. L., *Spectrochim. Acta* **46A**, 91 (1990).

28. Hollins, P., and Pritchard, J., *J. Vac. Sci. Technol.* **17**, 665 (1980).

29. Cross, J. S., and Schrader, G. L., manuscript in preparation.

30. O'Hanlon, J. F., "A User's Guide to Vacuum Technology—Second Edition." John Wiley and Sons, Inc., New York, 1989.

31. Campbell, C. T., and Valone, S. M., *J. Vac. Sci. Technol. A* **3**, 408 (1985).

32. Ortega, A., Hoffman, F. M., and Bradshaw, A. M., *Surf. Sci.* **119**, 79 (1982).

33. Allara, D. L., Baca, A., and Pryde, C. A., *Macromolecules* **11**, 1215 (1978).

34. Porter, M. D., Bright, T. B., Allara, D. L., and Kuwana, T., *Anal. Chem.* **58**, 2461 (1986).

# SUMMARY AND RECOMMENDATIONS

## Summary

### Chevrel phase HDS catalysts

Chevrel phases possess a rich solid state chemistry which permits the relationships between catalysis and structure, composition, and oxidation state to be examined. The vast majority of Chevrel phases which have been examined have significant catalytic activity for thiophene HDS. However, there are substantial differences in relative activities of the Chevrel phases. An important factor affecting catalytic activity may be structurally dependent. Highly active large cation Chevrel phases permit little cation delocalization, which results in extended catalyst stability.

An advantageous aspect of these Chevrel phases is the reduced (relative to $Mo^{4+}$) oxidation state of molybdenum. The Chevrel phases, having formal oxidation states which can be varied continuously between +2 and +2.67, allow direct preparation of reduced molybdenum oxidation states for catalytic activity and selectivity measurements.

It was possible to relate catalyst activity to the formal oxidation state of

molybdenum for the lead–lutetium Chevrel phases: thiophene HDS activity is associated with the reduced molybdenum oxidation state, apparently reaching a maximum between $Mo^{2+}$ and $Mo^{4+}$. It was also possible to relate catalytic activity to the $O_2$ and NO chemisorption data: the same reduced molybdenum species which display the greatest activity for thiophene HDS also exhibit the greatest uptake of $O_2$ and NO.

It is not possible to separate fully the structural and chemical (oxidation state) factors to get a single and generalized correlatable parameter to catalytic activity. The chemistry of conventional HDS catalysts and the kinetics of the heterogeneously catalyzed HDS reactions are too complex to be expected to depend on only a single physico-chemical property. However, based on this work with Chevrel phases, it seems likely that reduced (relative to $Mo^{4+}$) molybdenum species play an important role in HDS mechanisms.

**UHV PM–FTIRRAS system**

The gas doser assembly was found to operate in an ''on/off'' manner without affecting the system background pressure. The optical throughput of the infrared signal was not significantly diminished by additional external optics and the UHV chamber itself. Vibrations due to vacuum system operation have negligible effects on the quality of the spectra collected. Comparable results with previous IRRAS studies were obtained for the analysis of the thin film structures, indicating the successful completion of the system.

## Recommendations for Future Research

### Chevrel phase HDS catalysts

1. Other Chevrel phases should be surveyed to determine their HDS activity. In particular, Chevrel phases incorporating partial substitution of the chalcogen or molybdenum may provide a better means of controlling the molybdenum formal oxidation state to observe its role in catalytic activity.

2. An investigation of model nitrogen-containing compounds is recommended. A $NiMo_3S_4$ ($Ni_2Mo_6S_8$) phase has been proposed as the active material in Ni–Mo/$\gamma$–$Al_2O_3$ catalysts for hydrodenitrogenation (HDN) reactions [109]. It would be interesting to see if the Chevrel phases exhibit HDN activity analogous to their HDS activities. Further information concerning the active phases in industrial catalysts may be obtained.

3. Since thiophene and benzothiophene are only model sulfur-containing feeds, investigations with more industrially relevant feedstocks, such as heavy-gas-oils, should be undertaken to determine if Chevrel phases possess sufficient activity to be useful as industrial catalysts.

4. The Chevrel phases are low surface area materials. To become industrially attractive, high surface area materials would be required. It may be possible

to prepare supported Chevrel phases by some of the different synthesis methods reported in the literature. For example, Chevrel phases have been prepared from the hydrogen reduction of $M_p(NH_4)_qMo_3S_9$ precursor salts [101]. Deposition of these salts onto a high surface area support and subsequent reduction, may provide for a method of supporting Chevrel phases. In addition, impregnation of $\gamma-Al_2O_3$ with aqueous solutions of ammonium heptamolybdate and lead nitrate has been reported [110]. Reduction of the resulting material with $H_2$ and $H_2S$ at high temperatures may lead to the formation of supported Chevrel phases.

5. Thin films of Chevrel phases can be prepared by sputter deposition techniques. These thin films could be used to obtain more detailed information of the surface chemistry of adsorbed reactants, intermediates, and other probe molecules through surface sensitive analytical techniques.

**UHV PM–FTIRRAS system**

1. PM–FTIRRAS offers an alternative method for the examination of catalyst systems through the use of thin film structures. Using a catalyst, such as a Chevrel phase or $MoS_2$ material, as the top layer of thin film structures avoids the limitations of low throughput and low surface area. The resulting films could also be oriented so that the top surface of the film comprised a

single crystal plane, allowing information concerning the catalytic properties of individual crystal faces to be obtained.

2. The incorporation of mass spectrometry can add greatly to the information available by the correlation of the presence of adsorbed molecules with the product distribution. Temperature programmed desorption studies can also be performed, resulting in an increased understanding of possible reaction mechanisms. Simultaneous PM–FTIRRAS and mass spectroscopy of adsorbed reactants, intermediates, and other probe molecules may provide considerable new insights into the relationships between the "ideal" surfaces in UHV technology and actual operating conditions of catalytic and other chemical reaction processes.

## ADDITIONAL REFERENCES


1. Schuman, S. C., and Shalit, H., *Catal. Rev.* **4**, 245 (1970).

2. *Oil and Gas Journal* **89**(10), 25 (1991).

3. Gates, B. C., Katzer, J. R., and Schuit, G. C. A., "Chemistry of Catalytic Processes." McGraw–Hill, New York, 1979.

4. Weisser, O., and Landa, S., "Sulphide Catalysts, Their Properties and Applications." Permagon Press, Oxford, 1973.

5. Schuit, G. C. A., and Gates, B. C., *AIChE J.* **19**, 417 (1973).

6. Mitchell, P. C. H., *in* "Catalysis (Specialist Periodical Report)" (C. Kemball, Ed.), Vol. 1, p. 204. The Chemical Society, London, 1977.

7. Massoth, F. E., *in* "Advances in Catalysis" (D. D. Eley, H. Pines, and P. B. Weisz, Eds.), Vol. 27, p. 265. Academic Press, New York, 1978.

8. Grange, P., *Catal. Rev.–Sci. Eng.* **21**, 135 (1980).

9. Furimsky, E., *Catal. Rev.–Sci. Eng.* **22**, 371 (1980).

10. Ratnasamy, P., and Sivasanker, S., *Catal. Rev.–Sci. Eng.* 22, 401 (1980).

11. Mitchell, P. C. H., *in* "Catalysis (Specialist Periodical Report)" (C. Kemball and D. A. Dowden, Eds.), Vol. 4, p. 175. Royal Society of Chemistry, London, 1980.

12. Zdražil, M., *Appl. Catal.* **4**, 107 (1982).

13. Massoth, F. E., and MuraliDhar, G., *in* "Proceedings of the Climax Fourth International Conference on Chemistry and Uses of Molybdenum" (H. F. Barry and P. C. H. Mitchell, Eds.), p. 343. Climax Molybdenum Co., Ann Arbor, MI, 1982.

14. Vrinat, M. L., *Appl. Catal.* **6**, 137 (1983).

15. Topsøe, H., and Clausen, B. S., *Catal. Rev.–Sci. Eng.* **26**, 395 (1984).

16. Topsøe, H., Clausen, B. S., Topsøe, N.-Y., and Pedersen, E., *Ind. Eng. Chem. Fundam.* **25**, 25 (1986).

17. Topsøe, H., and Clausen, B. S., *Appl. Catal.* **25**, 273 (1986).

18. Zdražil, M., *Catal. Today* **3**, 268 (1988).

19. Prins, R., de Beer, V. H. J., and Somorjai, G. A., *Catal. Rev.–Sci. Eng.* **31**, 1 (1989).

20. Speight, J. G., "The Desulfurization of Heavy Oils and Residua." Marcel Dekker, New York, 1981.

21. Maksimov, Yu. V., Kushnerev, M. Ya., Dumesic, J. A., Nechitailo, A. E., and Fridman, R. A., *J. Catal.* **45**, 114 (1976).

22. Aksenov, V. S., Kamyanov, V. F., *in* " Organic Sulfur Chemistry" (R. Kh. Freidina and A. E. Skorova, Eds.), p. 201. Permagon Press, New York, 1981.

23. Thompson, C. J., *in* "Organic Sulfur Chemistry" (R. Kh. Freidina and A. E. Skorova, Eds.), p. 9. Permagon Press, New York, 1981.

24. Donati, E. E., *Adv. Catal.* **8**, 39 (1956).

25. Fitz, C. W., Jr., and Rase, H. F., *Ind. Eng. Chem. Prod. Res. Dev.* **22**, 40 (1983).

26. Gishti, K., Iannibello, A., Marengo, S., Morelli, G., and Titarelli, P., *Appl. Catal.* **12**, 381 (1984).

27. Hopkins, P. D., and Meyers, B. L., *Ind. Eng. Chem. Prod. Res. Dev.* **22**, 421 (1983).

28. Chianelli, R. R., and Daage, M., *in* "Advances in Hydrotreating Catalysts" (M. L. Ocelli and R. G. Anthony, Eds), Vol. 50, p. 1. Elsevier, Amsterdam, 1989.

29. O'Young, C.-L., Yang, C.-H., DeCanio, S. J., Patel, M. S., and Storm, D. A., *J. Catal.* **113**, 307 (1988).

30. Li, C. P., and Hercules, D. M., *J. Phys. Chem.* **88**, 456 (1984).

31. Zingg, D. S., Makovsky, L. E., Tisher, R. E., Brown, F. R., and Hercules, D. M., *J. Phys. Chem.* **84**, 2898 (1980).

32. Patterson, T. A., Carver, J. C., Leyden, D. E., and Hercules, D. M., *J. Phys. Chem.* **80**, 1700 (1976).

33. Parham, T. G., and Merrill, R. P., *J. Catal.* **85**, 295 (1984).

34. Clausen, B. S., Topsøe, H., Candia, R., Villadsen, J., Lengeler, B., Als-Nielsen, J., and Christensen, F., *J. Phys. Chem.* **85**, 3868 (1981).

35. Pollack, S. S., Makovsky, L. E., and Brown, F. R., *J. Catal.* **59**, 452 (1979).

36. Schrader, G. L., and Cheng, C. P., *J. Catal.* **80**, 369 (1983).

37. Topsøe, H., Clausen, B. S., Candia, R., Wivel, C., and Mørup, S., *J. Catal.* **68**, 433 (1981).

38. Wivel, C., Candia, R., Clausen, B. S., Mørup, S., and Topsøe, H., *J. Catal.* **68**, 453 (1981).

39. Delannay, F., Haeussler, E., and Delmon, B., *J. Catal.* **66**, 469 (1980).

40. Lipsch, J. M. J. G., and Schuit, G. C. A., *J. Catal.* **15**, 179 (1969).

41. Schuit, G. C. A., and Gates, B. C., *Amer. Inst. Chem. Eng. J.* **19**, 417 (1973).

42. Voorhoeve, R. J. H., and Stuiver, J. C. M., *J. Catal.* **23**, 228, 243 (1971).

43. Farragher, A. L., and Cossee, P., *in* "Proceedings, 5th International Congress on Catalysis, Palm Beach, 1972" (J. H. Hightower, Ed.), p. 1301. North-Holland, Amsterdam, 1973.

44. Delmon, B., *Bull. Soc. Chim. Belg.* **88**, 979 (1979).

45. Delmon, B., *React. Kinet. Catal. Lett.* **13**, 203 (1980).

46. Zabala, J. M., Mainil, M., Grange, P., and Delmon, B., *React. Kinet. Catal. Lett.* **3**, 285 (1975).

47. Topsøe, N.-Y., and Topsøe, H., *J. Catal.* **84**, 386 (1983).

48. Topsøe, H., Candia, R., Topsøe, N.-Y., and Clausen, B. S., *Bull. Soc. Chim. Belg.* **93**, 783 (1984).

49. Harris, S., *Chem. Phys.* **67**, 229 (1982).

50. Harris, S., *Polyhedron* **5**, 151 (1986).

51. Harris, S., and Chianelli, R. R., *J. Catal.* **86**, 400 (1984).

52. Harris, S., and Chianelli, R. R., *J. Catal.* **98**, 17 (1986).

53. Duchet, J. C., van Oers, E. M., de Beer, V. H. J., and Prins, R., *J. Catal.* **80**, 386 (1983).

54. de Beer, V. H. J., Duchet, J. C., and Prins, R., *J. Catal.* **72**, 369 (1981).

55. Vissers, J. P. R., de Beer, V. H. J., and Prins, R., *J. Chem. Soc., Faraday Trans. I* **83**, 2145 (1987).

56. Bouwens, S. M. A. M., van der Kraan, A. M., de Beer, V. H. J., and Prins, R., *J. Catal.* **128**, 559 (1991).

57. Bouwens, S. M. A. M., Vissers, J. P. R., de Beer. V. H. J., and Prins, R., *J. Catal.* **112**, 401 (1988).

58. Massoth, F. E., and Kibby, C. L., *J. Catal.* **47**, 300 (1977).

59. Hall, W. K., and Lo Jacono, M., *in* " Proceedings, 6th International Congress on Catalysis, London, 1976" (G. C. Bond, P. B. Wells, and F. C. Tompkins, Eds.), Vol. I, p. 245. The Chemical Society, London, 1977.

60. Tauster, S. J., Pecoraro, T. A., and Chianelli, R. R., *J. Catal.* **63**, 515 (1980).

61. Nag, N. K., *J. Catal.* **92**, 432 (1985).

62. Valyon, J., and Hall, W. K., *J. Catal.* **84**, 216 (1983).

63. Valyon, J., and Hall, W. K., *J. Catal.* **92**, 155 (1985).

64. Millman, W. S., Segawa, K.-I., Smrz, D., and Hall, W. K., *Polyhedron* **5**, 169 (1986).

65. Laine, J., Severino, F., Cáceres, C. V., Fierro, J. L. G., and López Agudo, A., *J. Catal.* **103**, 228 (1987).

66. Peri, J. B., *J. Phys. Chem.* **86**, 1615 (1982).

67. Delgado, E., Fuentes, G. A., Hermann, C., Kunzmann, G., and Knözinger, H., *Bull. Soc. Chim. Belg.* **93**, 735 (1984).

68. Delvaux, G., Grange, P., and Delmon, B., *J. Catal.* **56**, 99 (1979).

69. Alstrup, I., Chorkendorff, I., Candia, R., Clausen, B. S., and Topsøe, H., *J. Catal.* **77**, 397 (1982).

70. McIntyre, N. S., Chan, T. C., Spevack, P. A., and Brown, J. R., *Appl. Catal.* **63**, 391 (1990).

71. Vissers, J. P. R., Groot, C. K., van Oers, E. M., de Beer, V. H. J., and Prins, R., *Bull. Soc. Chim. Belg.* **93**, 813 (1984).

72. Bouwens, S. M. A. M., Prins, R., de Beer, V. H. J., and Koningsberger, D. C., *J. Phys. Chem.* **94**, 3711 (1990).

73. Voorhoeve, R. J. H., *J. Catal.* **23**, 236 (1971).

74. Konings, A. J. A., Valster, A., de Beer, V. H. J., and Prins, R., *J. Catal.* **76**, 466 (1982).

75. Thakur, D. S., and Delmon, B., *J. Catal.* **91**, 308 (1985).

76. Duben, A. J., *J. Phys. Chem.* **82**, 348 (1978).

77. McCarty, K. F., and Schrader, G. L., *in* "Proceedings, 8th International Congress on Catalysis, Berlin, 1984" (E. Ertl, Ed.), Vol. IV, p. 427. Dechema, Frankfurt-am-Main, 1984.

78. McCarty, K. F., and Schrader, G. L., *Ind. Eng. Chem. Prod. Res. Dev.* **23**, 519 (1984).

79. McCarty, K. F., Anderegg, J. W., and Schrader, G. L., *J. Catal.* **93**, 375 (1985).

80. McCarty, K. F., Ph.D. Dissertation, Iowa State University, Ames, 1985.

81. McCarty, K. F., and Schrader, G. L., *J. Catal.* **103**, 261 (1987).

82. Huckett, S. C., Angelici, R. J., Ekman, M. E., and Schrader, G. L., *J. Catal.* **113**, 36 (1988).

83. Ekman, M. E., Anderegg, J. W., and Schrader, G. L., *J. Catal.* **117**, 246 (1989).

84. Schrader, G. L., and Ekman, M. E., *in* "Advances in Hydrotreating Catalysts" (M. L. Ocelli and R. G. Anthony, Eds.), Vol. 50, p. 41. Elsevier, Amsterdam, 1989.

85. Kareem, S. A., and Miranda, R., *J. Molec. Catal.* **53**, 275 (1989).

86. Chevrel, R., Sergent, M., and Prigent, J., *J. Solid State Chem.* **3**, 515 (1971).

87. Yvon, K., *in* "Current Topics in Materials Science" (E. Kaldis, Ed.), Vol. 3, p. 53. North-Holland, Amsterdam, 1979.

88. Fischer, Ø., and Maple, M. B., *in* "Topics in Current Physics" (Ø. Fischer and M. B. Maple, Eds.), Vol. 34, p. 1. Springer-Verlag, Berlin, 1982.

89. Chevrel, R., and Sergent, M., *in* "Topics in Current Physics" (Ø. Fischer and M. B. Maple, Eds.), Vol. 34, p. 25. Springer-Verlag, Berlin, 1982.

90. Yvon, K., *in* "Topics in Current Physics" (Ø. Fischer and M. B. Maple, Eds.), Vol. 34, p. 87. Springer-Verlag, Berlin, 1982.

91. Chevrel, R., Potel, M., Sergent, M., and Prigent, J., *Ann. Chim. Fr.* **7**, 92 (1982).

92. Chevrel, R., Gougeon, P., Potel, M., and Sergent, M., *J. Solid State Chem.* **57**, 25 (1985).

93. Chevrel, R., Hirrien, M., and Sergent, M., *Polyhedron* **5**, 87 (1986).

94. Peña, O., and Sergent, M., *Prog. Solid St. Chem.* **19**, 165 (1989).

95. Yvon, K., and Paoli, A., *Solid State Comm.* **24**, 41 (1977).

96. Flükiger, R., and Baillif, R., *in* "Topics in Current Physics" (Ø. Fischer and M. B. Maple, Eds.), Vol. 34, p. 113. Springer-Verlag, Berlin, 1982.

97. Tarascon, J. M., Waszczak, J. V., Hull, G. W., DiSalvo, F. J., and Blitzer, L. D., *Solid State Comm.* **47**, 973 (1983).

98. Schollhorn, R., Kumbers, M., and Besenhard, J. O., *Mater. Res. Bull.* **12**, 781 (1977).

99. Tarascon, J. M., DiSalvo, F. J., Murphy, D. W., Hull, G. W., Rietman, E. A., and Waszczak, J. V., *J. Solid State Chem.* **54**, 204 (1984).

100. Nanjundaswamy, K. S., and Gopalakrishnan, J., *J. Solid State Chem.* **68**, 188 (1987).

101. Nanjundaswamy, K. S., Vasanthacharya, N. Y., Gopalakrishnan, J., and Rao, C. N. R., *Inorg. Chem.* **26**, 4286 (1987).

102. Banks, C. K., Kammerdiner, L., and Luo, H., *J. Solid State Chem.* **15**, 271 (1975).

103. Przysłupski, P., Horyń, R., Szymaszek, J., and Greń, B., *Solid State Comm.* **28**, 869 (1978).

104. Zhao, B. R., Ohtaki, R., Luo, H.-L., and Flesner, L. D., *Thin Solid Films* **110**, 185 (1983).

105. Hertel, G. B., Orlando, T. P., and Tarascon, J. M., *J. Appl. Phys.* **61**, 4829 (1987).

106. Webb, R. J., and Goldman, A. M., *J. Vac. Sci. Technol. A* **3**, 1907 (1985).

107. Webb, R. J., Goldman, A. M., Kang, J. H., Maps, J., and Schmidt, M. F., *IEEE Trans. Magn.* **MAG–21**, 835 (1985).

108. Hinode, H., Yamamoto, S., Wakihara, M., and Taniguchi, M., *Mater. Res. Bull.* **20**, 611 (1985).

109. Simpson, H. D., *in* "Advances in Hydrotreating Catalysts" (M. L. Ocelli and R. G. Anthonty, Eds.), Vol. 50, p. 133. Elsevier, Amsterdam, 1989.

110. Miranda, R., and Kareem, S. A., *Catal. Lett.* **1**, 217 (1988).

111. Kilanowski, D. R., Ph.D. Dissertation, University of Delaware, Wilmington, 1979.

# ACKNOWLEDGMENTS

I would like to thank Dr. Glenn Schrader for providing the opportunity and means to conduct this research project. I would also like to thank Mr. Jim Anderegg for collecting the XPS spectra, and for the many helpful discussions required to sort it all out.

I consider myself to be very fortunate to have had the opportunity to form friendships with many outstanding colleagues throughout the years. I am particularly indebted to SJF and JSC for all of their help in getting me out of the "Blue Room." Special thanks also to EMU. I wish everyone the best for their futures and hope the good times will continue.

I am grateful to my family for their encouragement and support. Thanks, Mom and Dad, for believing in me. I am especially thankful to my daughter, Merissa, for coming along at the perfect time to help me keep things in their proper perspective. Mostly, I would like to thank my wife, Sandie, for her patience, endurance, and unfailing support. We made it!

This work was performed at the Ames Laboratory under Contract W–7405–ENG–82 with the U. S. Department of Energy. The United States government has assigned the DOE Report number IS–T 1412 to this dissertation.

# APPENDIX A. SAMPLE CALCULATIONS

This appendix provides details of the hydrodesulfurization, hydrogenation, and chemisorption activity calculations.

## Hydrodesulfurization and Hydrogenation

### Calibration of reactor system

**Gas flows** The composition and flow rate of all gases fed to the reactor were electronically controlled by mass flow controllers (Tylan, model FC–260). The flow rates were calibrated using a 100-ml bubble flow meter with the outlet gas vented at ambient temperature and pressure. The measured flow rate displayed a very linear response with respect to controller setting over the entire range of each mass flow controller.

**Thiophene and benzothiophene** The thiophene and benzothiophene flow rates from the syringe pump were calibrated by measuring the time required to deliver a known volume of liquid from the syringe. An average of at least three measurements was obtained for each compound. For example, using the 7 ml/h range of the syringe

pump with a 1-ml syringe, an average thiophene flow rate of 0.0847 ml/h was obtained, which corresponds to $2.98 \times 10^{-7}$ mole/s, assuming a thiophene density of 1.06494 g/ml. Similarly, an average flow rate for benzothiophene of 0.0847 ml/h, or $2.01 \times 10^{-7}$ mole/s was determined, using the same conditions, assuming a benzothiophene density of 1.1484 g/ml.

**Detector calibration** Peak areas were determined by digital integration and converted to molar compositions through the use of component FID relative response factors. From these values, the concentration of component $i$ in a mixture is given by:

$$N_i = \frac{N_s}{f_i} \times \frac{A_i}{A_s}$$

where $N_i$ = moles of component $i$,

$N_s$ = moles of standard $s$,

$f_i$ = molar response factor of component $i$ relative to standard $s$,

$A_i$ = peak area of component $i$, and

$A_s$ = peak area of standard $s$.

By definition, $f_s$ is unity. For the thiophene HDS and 1-butene HYD investigations, 1-butene was taken to be the standard, and the relative response factor of thiophene, $f_T$, was determined to be 0.864 [80]. The response factors of all $C_4$ hydrocarbons were assumed to be equal [80]. For the benzothiophene HDS experiments, ethylbenzene was

chosen as the standard. Ethlybenzene and benzothiophene have essentially identical response factors [111]; therefore, they were taken to be equivalent.

**HDS activities**

The conversion of thiophene to desulfurized hydrocarbons is defined as:

$$\text{conversion } (\%) = \frac{\Sigma A_{C4}}{\frac{A_T}{f_T} + \Sigma A_{C4}} \times 100$$

where $A_{C4}$ and $A_T$ are the measured peak areas of the $C_4$ hydrocarbons (1-butene, butadiene, *cis*-2-butene, *trans*-2-butene, and *n*-butane) and thiophene, respectively, and $f_T$ is the thiophene relative response factor. Due to their extremely low concentrations or complete absence, isobutene and $C_3$ hydrocarbons were neglected in the conversion calculations.

The conversion of benzothiophene to ethlybenzene was calculated as:

$$\text{conversion } (\%) = \frac{A_E}{A_B + A_E} \times 100$$

where $A_E$ and $A_B$ represent the peak areas of ethylbenzene and benzothiophene, respectively.

The empty reactor converted 0.3% of thiophene to desulfurized products; this value was subtracted from the conversion data before calculation of the HDS activities.

The hydrodesulfurization activities were calculated from the inlet flow of thiophene or benzothiophene and the conversion level as:

$$\text{HDS activity} = \frac{\dot{N}_i \times \text{conversion}(\%)}{W \times S \times 100} \text{ mole/s•m}^2$$

where $\dot{N}_i$ = molar flow rate of thiophene ($2.98 \times 10^{-7}$ mole/s) or benzothiophene ($2.01 \times 10^{-7}$ mole/s) into the reactor,

$W$ = weight of catalyst (g), and

$S$ = surface area of catalyst ($m^2/g$).

**HYD activities**

The conversion of 1-butene to *n*-butane was calculated as:

$$\text{conversion } (\%) = \frac{A_{n\text{-}B}}{\Sigma A_{C4}} \times 100$$

where $A_{n\text{-}B}$ is the peak area of *n*-butane and $A_{C4}$ is the peak area of the $C_4$ hydrocarbons (1-butene, butadiene, *cis*-2-butene, *trans*-2-butene, and *n*-butane). The empty reactor produced 0.06% *n*-butane from 1-butene. This value was subtracted before calculating the HYD activities.

In the calculation of the 1-butene HYD activities, it was assumed that the 1-butene–hydrogen pulses exhibited plug-flow behavior in passage through the reactor [80]. The molar flow rate of these pulses then becomes the molar flow rate of the helium carrier gas through the catalyst bed. The carrier gas flow rate of 21.6 ml/min

(22°C, 1 atm) and 1.2 mol% mixture of 1-butene in hydrogen corresponds to a 1-butene flow rate ($\dot{N}_{1\text{-}B}$) of:

$$\dot{N}_{1\text{-}B} = \frac{0.012 \times 21.6 \text{ ml/min} \times 1 \text{ atm}}{82.057 \frac{\text{atm ml}}{\text{mole K}} \times 295 \text{ K}} \times \frac{1 \text{ min}}{60 \text{ s}} = 1.78 \times 10^{-7} \text{ mole/s.}$$

The HYD activities were then calculated from a relationship analogous to the HDS activities:

$$\text{HYD activity} = \frac{\dot{N}_{1\text{-}B} \times \text{conversion}(\%)}{W \times S \times 100} \text{ mole/s•m}^2.$$

## Chemisorption

The amount of chemisorbed $O_2$ or NO ($N_c$) was calculated by the equation:

$$N_c \text{ (}\mu\text{mole)} = N_p\left(n - \frac{\Sigma A_i}{A_s}\right)$$

where $N_p$ is the number of moles of $O_2$ or NO in a pulse, $n$ represents the number of pulses, $A_i$ equals the peak area of the non-adsorbed $O_2$ or NO in injection $i$, and $A_s$ is the peak area obtained from the calibration pulses.

The empty reactor adsorbed 0.045 $\mu$mole $O_2$ and 0.049 $\mu$mole NO. These values were subtracted from the initial chemisorption data.

# APPENDIX B. SUPPLEMENTAL X-RAY POWDER DIFFRACTION PATTERNS

This appendix contains the X-ray powder diffraction patterns of: $La_{1.2}Mo_6S_8$ (Figure B.1), $Dy_{1.2}Mo_6S_8$ (Figure B.2), $Lu_{1.2}Mo_6S_8$ (Figure B.3), $Lu_{0.4}Pb_{0.67}Mo_6S_8$ (Figure B.4), and $PbMo_6S_8$ (Figure B.5).

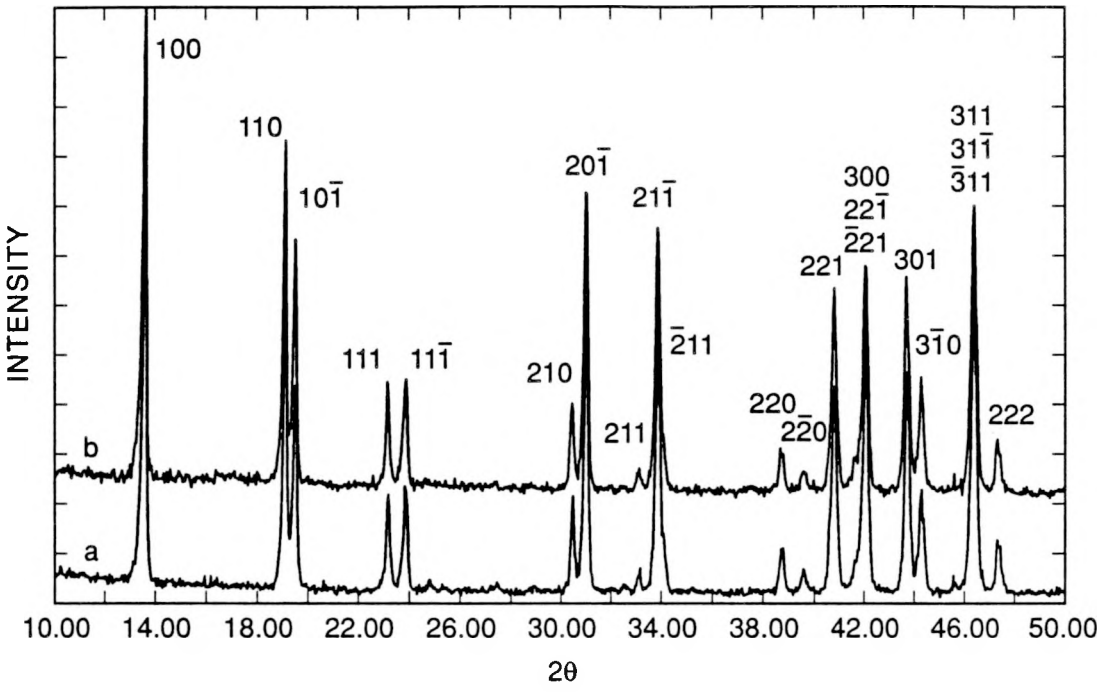


Figure B.1 X-ray powder diffraction pattern of (a) fresh and (b) used (10 h of thiophene reaction) $La_{1.2}Mo_6S_8$ with rhombohedral *hkl* indexes

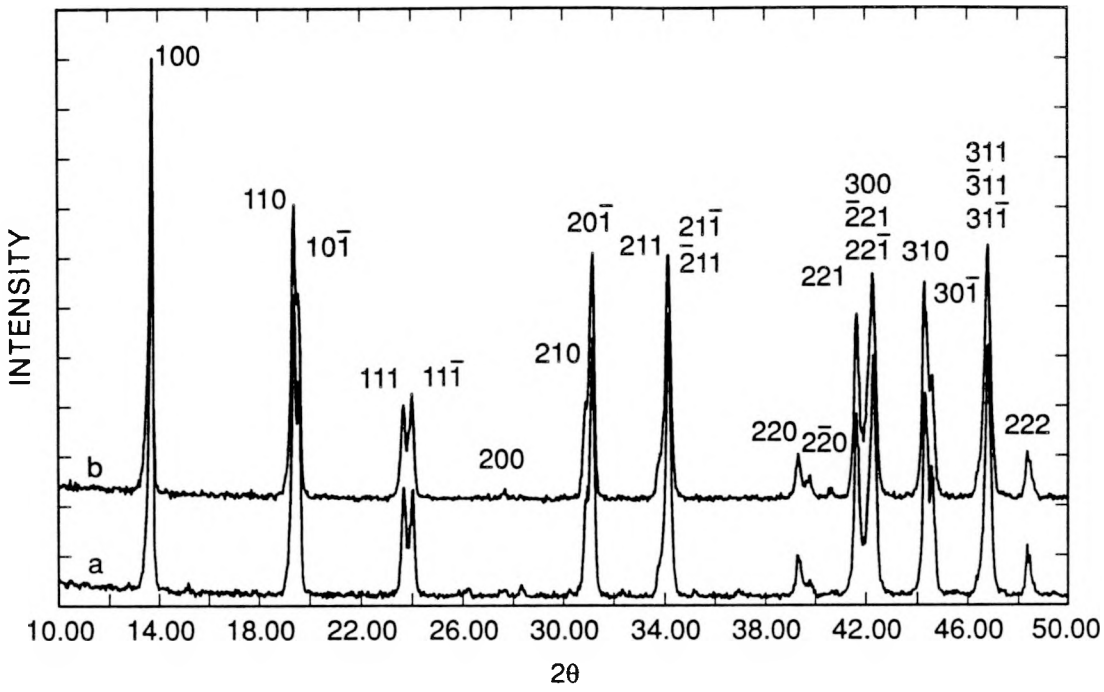


Figure B.2 X-ray powder diffraction pattern of (a) fresh and (b) used (10 h of thiophene reaction) $Dy_{1.2}Mo_6S_8$ with rhombohedral *hkl* indexes

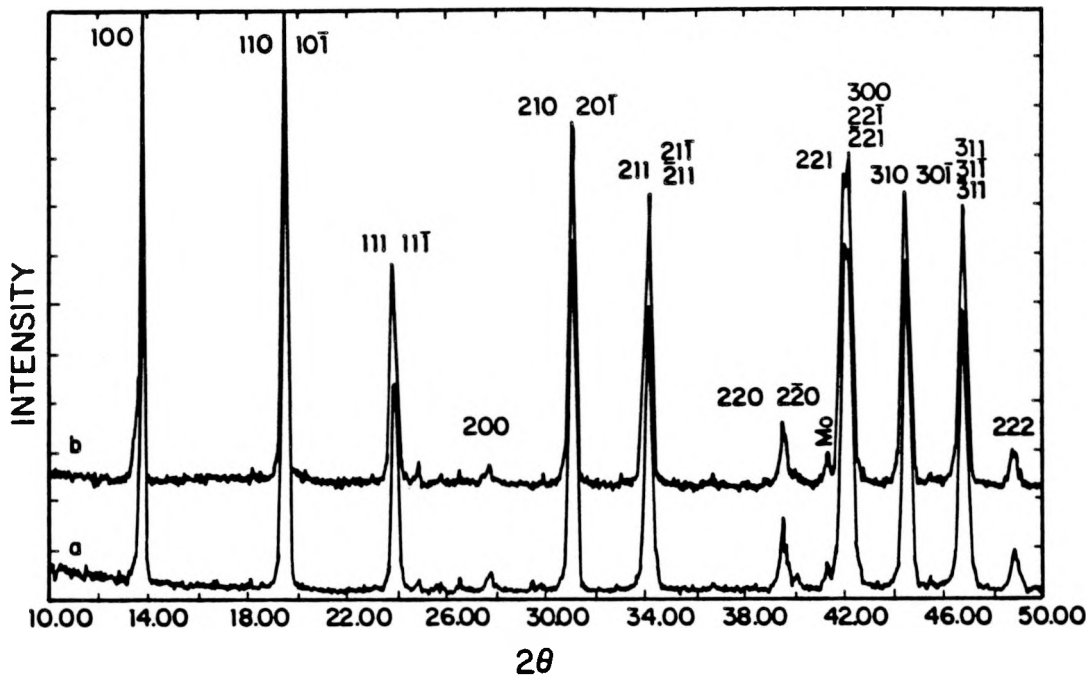


Figure B.3 X-ray powder diffraction pattern of (a) fresh and (b) used (10 h of thiophene reaction) $Lu_{1.2}Mo_6S_8$ with rhombohedral *hkl* indexes

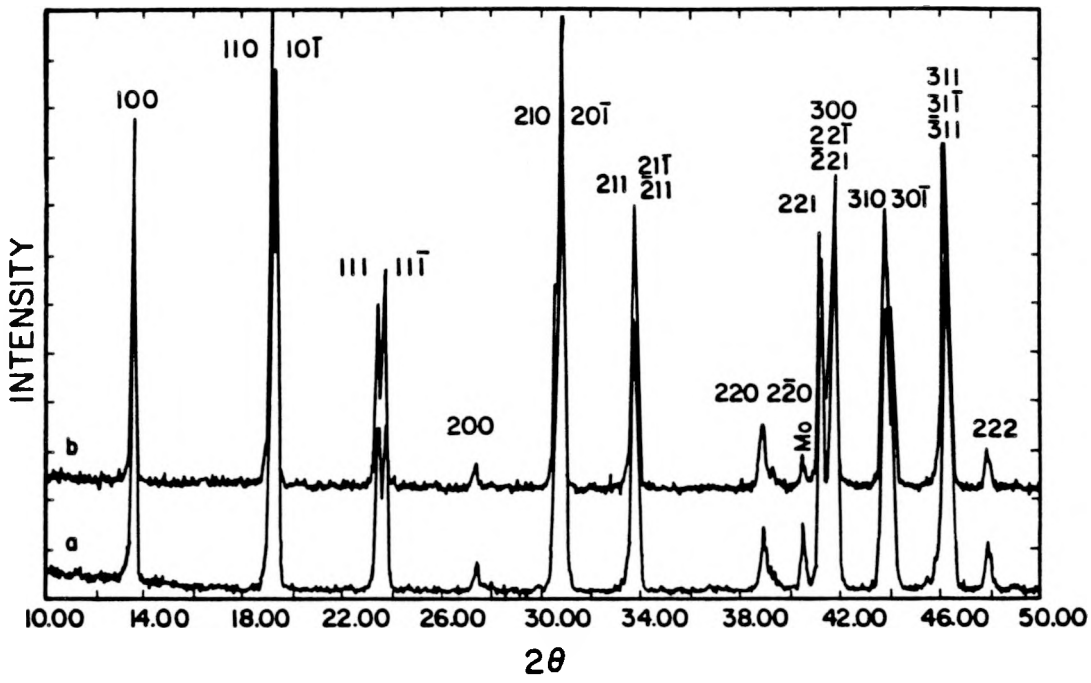


Figure B.4 X-ray powder diffraction pattern of (a) fresh and (b) used (10 h of thiophene reaction) $Lu_{0.4}Pb_{0.67}Mo_6S_8$ with rhombohedral *hkl* indexes

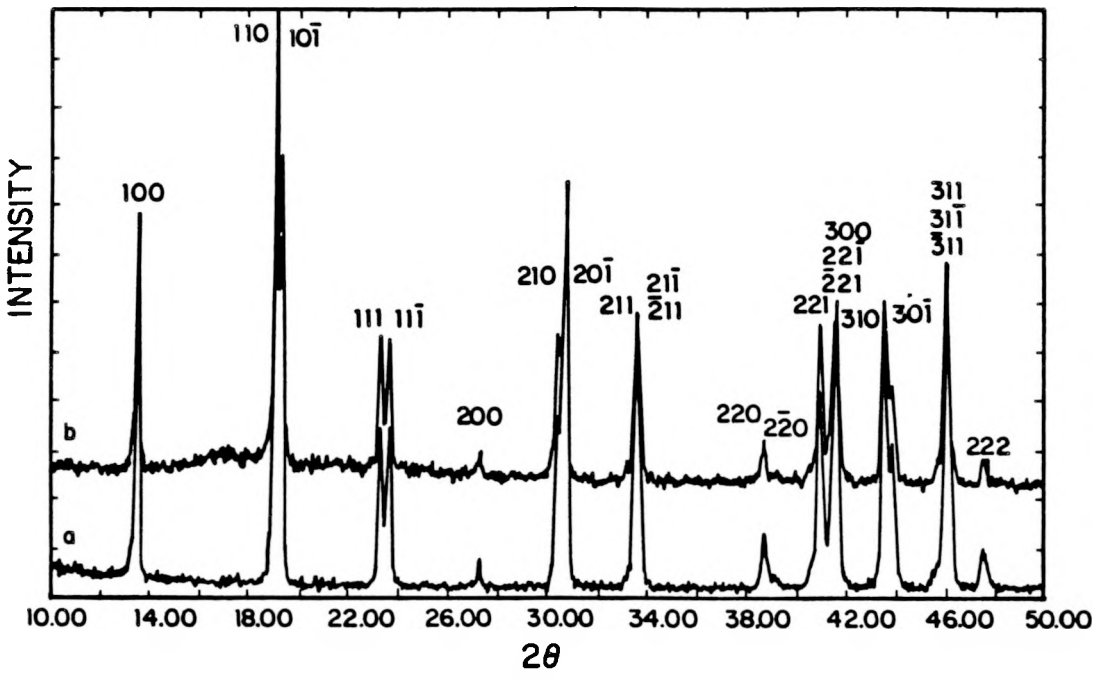


Figure B.5 X-ray powder diffraction pattern of (a) fresh and (b) used (10 h of thiophene reaction) $PbMo_{6.2}S_8$ with rhombohedral *hkl* indexes